

Alma Mater Studiorum – Università di Bologna

DOTTORATO DI RICERCA IN  
INGEGNERIA STRUTTURALE ED IDRAULICA

Ciclo XXIV

**Settore Concorsuale di afferenza:** 08/B2 – SCIENZA DELLE COSTRUZIONI

**Settore Scientifico disciplinare:** ICAR 08

COMPARISON BETWEEN ANALYTICAL AND NUMERICAL METHODS  
FOR THE ASSESSMENT OF MASONRY ARCH BRIDGES:  
CASE STUDY OF CLEMENTE BRIDGE ON SAVIO RIVER

**Presentata da:** VERONICA BARTOLOMEO

**Coordinatore Dottorato**

CHIAR.MO PROF. ING. ERASMO VIOLA

**Relatore**

PROF. ING. LUCIO NOBILE

**Corelatore**

ING. CRISTINA GENTILINI

**Esame finale anno 2012**



## **ABSTRACT**

This research has focused on the study of the behavior and of the collapse of masonry arch bridges. The masonry arch bridges are standing from hundreds of years and can be considered one of the oldest subjects of scientific research. Despite this, it can be difficult to analyze their behavior for all the uncertainties related to the analysis of the materials in existing structures. The latest decades have seen an increasing interest in this structural type, that is still present and in use, despite the passage of time and the variation of the transport means. Several strategies have been developed during the time to simulate the response of this type of structures, although even today there is no generally accepted standard one for assessment of masonry arch bridges.

The aim of this thesis is to compare the principal analytical and numerical methods existing in literature on case studies, trying to highlight values and weaknesses. The methods taken in exam are mainly three: i) the Thrust Line Analysis Method; ii) the Mechanism Method; iii) the Finite Element Methods. The Thrust Line Analysis Method and the Mechanism Method are analytical methods and derived from two of the fundamental theorems of the Plastic Analysis, while the Finite Element Method is a numerical method, that uses different strategies of discretization to analyze the structure. Every method is applied to the case study through computer-based representations, that allow a friendly-use application of the principles explained. A particular closed-form approach based on an elasto-plastic material model and developed by some Belgian researchers is also studied.

To compare the three methods, two different case study have been analyzed: i) a generic masonry arch bridge with a single span; ii) a real masonry arch bridge, the Clemente Bridge, built on Savio River in Cesena. In the last case, a detailed historic analysis has been conducted together with laboratory tests to determine the mechanical characteristics of masonry arches.

In the analyses performed, all the models are two-dimensional in order to have results comparable between the different methods taken in exam. The different methods have been compared with each other in terms of collapse load and of hinge positions.





# Table of Contents

## Chapter 1. State of the Art

1.1	<i>Sommario</i> .....	3
1.2	<i>Classic Theories</i> .....	4
1.3	<i>Jacques Heyman and the “Safe Theorem”</i> .....	5
1.4	<i>Plastic Limit Analysis</i> .....	11

## Chapter 2. Methods and Models For Analysis of Masonry Arches

2.1	<i>Sommario</i> .....	15
2.2	<i>Classification of the methods for the assessment of masonry arches</i> .....	17
2.3	<i>Thrust Line Analysis Method</i> .....	19
2.4	<i>Mechanism Method</i> .....	25
2.5	<i>Finite Element Method</i> .....	30
2.6	<i>Elasto-Plastic Model</i> .....	39
2.A	<i>Annex: Bresse’s equations with the replacement of <math>N(\theta)</math> and <math>M(\theta)</math> formulations</i> .....	49

## Chapter 3. Application to a Generic Masonry Arch Bridge

3.1	<i>Sommario</i> .....	61
3.2	<i>A Generic Arch Subjected to a Vertical Concentrated Load</i> .....	62
3.3	<i>Archie-M and Ring</i> .....	64
3.4	<i>Finite Element Method</i> .....	68
3.5	<i>Elasto-Plastic Model</i> .....	72
3.6	<i>Comparison between Results</i> .....	78

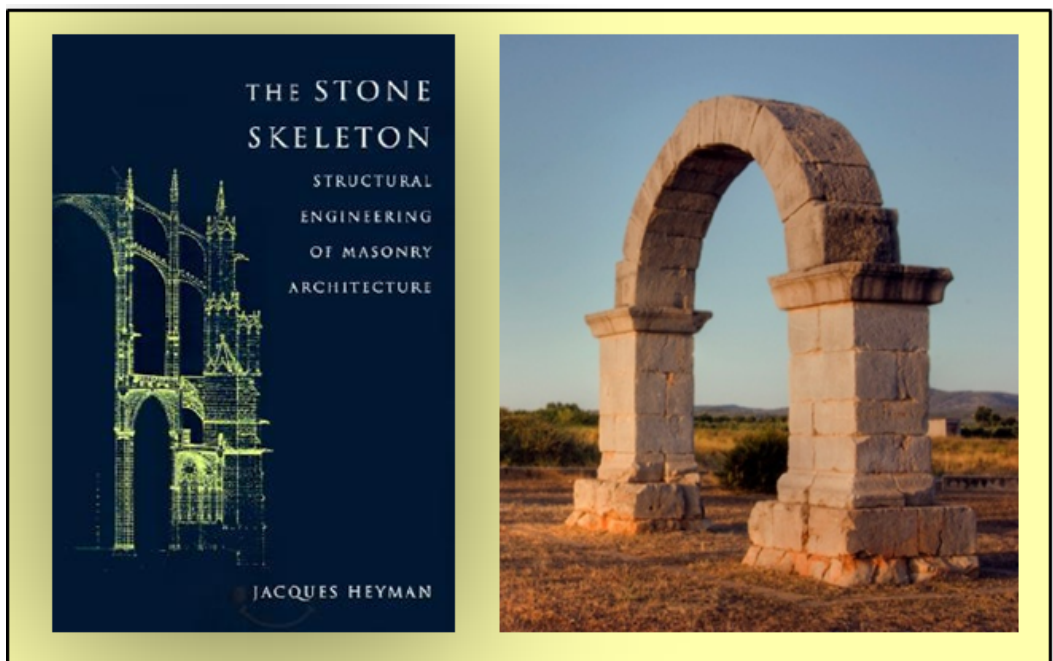
## **Chapter 4. Case Study of Clemente Bridge**

4.1	<i>Sommario</i> .....	83
4.2	<i>A Bridge, a Symbol: a brief description</i> .....	85
4.3	<i>Historical Notes</i> .....	87
4.4	<i>Analysis of Constructive Techniques</i> .....	95
4.5	<i>Analysis of materials</i> .....	102
4.6	<i>Comparison between the different methods</i> .....	108
4.A	<i>Annex: Post war Documentation</i> .....	117
4.B	<i>Annex: On Site Photos</i> .....	129
4.C	<i>Annex: Results of laboratory tests on samples taken on site</i> .....	135
 <b>Conclusions</b> .....		139
 <b>References</b> .....		145

## Chapter 1

# State of the Art

---





## 1.1 SOMMARIO

*“Arco non è altro che una fortezza causata da due debolezze, imperochè l’arco negli edifici è composto di due quarti di circolo, i quali quarti circoli ciascuno debolissimo per sé desidera cadere e oponendosi alla ruina l’uno dell’altro, le due debolezze si convertono in un’unica certezza.”*

Leonardo da Vinci

L’approccio classico per determinare la stabilità dei ponti ad arco risale alla teoria di Pippard e Ashby, ulteriormente sviluppata negli anni 60 dal Prof. Heyman. Questa teoria assume che la muratura: i) non abbia resistenza a trazione; ii) abbia un’infinita resistenza a compressione; iii) non avvenga rottura per scorrimento. Il meccanismo di collasso dell’arco è quindi identificato dalla progressiva formazione di quattro cerniere, che coincidono con i punti in cui la curva delle pressioni è tangente all’intradosso o all’estradosso dell’arco. Il meccanismo per formazione di cerniere non è l’unico possibile per l’arco<sup>1</sup>, ma studi sperimentali<sup>2</sup> dimostrano che è il più probabile in caso di ponti ad arco ben contraffortati. L’analogia tra questo meccanismo di collasso e quello proprio delle strutture metalliche permette di applicare anche alle strutture in muratura i fondamentali teoremi dell’analisi plastica, incluso il “*safe theorem*”.

La ricerca del Prof. Heyman evidenzia quindi che un’analisi di tipo elastico nel caso di strutture in muratura è problematica perché non esiste un unico stato di equilibrio calcolabile. L’analisi limite permette invece di considerare la struttura solo in relazione al suo stato ultimo, utilizzando pochi parametri materiali e trascurando lo stato di tensione iniziale.

---

<sup>1</sup> Meccanismo di rottura a scorrimento e misto scorrimento-cerniera.

<sup>2</sup> A.W. Hendry, S.R. Davies e R. Royles, *Test on a Stone, Masonry Arch at Bridgemill-Girvan*, Transport and Road Research Lab, Contractor Report 7, UK (1985)

## 1.2 Classic Theories

In his book<sup>3</sup> “*La scienza delle costruzioni e il suo sviluppo storico*”, Edoardo Benvenuto gave us the historical perspective of the first static theories regarding the masonry arch. Between the seventeenth and eighteenth century, the geometric and the empiric rules reported in the ancient treatises were replaced by a real static theory on the stability of the arches. Philippe De La Hire was the first to develop an innovative approach, which remained the same for all the scholars of the eighteenth century. The arch was seen as a series of rigid blocks with well-defined geometry and a specific weight. However his model neglected the friction, which was taken into account by Coulomb’s Model. Since Coulomb's essay (1773) and Mery’s subsequent elaboration (1840), the problem of statics of the masonry arch will have to wait more than a hundred years before being called into question.

Only around the fifties of this century, the problem is taken up and dealt with a more congenial method. Attempts in the twenties to adapt the elastic theory to the masonry arch were not very successful. The weak point of these attempts was to assume the masonry material as elastic and to consider valid the results even if the thrust line was external to the core in some points. The turning point of the fifties is determined by the appearance of the limit design and of its increasing applications to structural analysis. The theorems of limit analysis are admirably suited to the determination of the collapse load of masonry arches.

So nowadays the engineering methods of assessment for arch bridges mainly rely on the pioneering work by Pippard and Ashby<sup>4</sup>(1939) and Pippard<sup>5</sup>(1948). They determined the load required, at a given location, to cause the formation of two additional hinges, and hence a mechanism, in a two hinged arch. These procedures guaranteed that an equilibrium configuration exists for the considered structural model but gave only rough estimates of the limit load. Following their lead and Drucker’s studies, Kooharian published the first modern work on this subject in 1952, which was followed one year later by Onat and Prager’s input. Another milestone was Heyman’s publication in 1966, where he explained for the first time the applicability of ultimate load theory for any masonry loadbearing structure. Heyman’s contributions are so fundamental that is difficult to imagine today the state of the art without his work. In the next paragraph, the fundamental hypotheses at the base of his theory will be explained.

---

<sup>3</sup> Benvenuto E. (1981), *La scienza delle costruzioni e il suo sviluppo storico*, Sansoni, Firenze

<sup>4</sup> Pippard, A.J.S., Ashby, R.J., (1939). *An experimental study of the voussoir arch*, Inst.n Civ. Eng., **10**, 383-403.

<sup>5</sup> Pippard, A.J.S., (1948), *The approximate estimation of safe loads on masonry bridges*, Civil engineer in war, **1**, 365, Inst.n Civ. Eng.rs.

### 1.3 Jacques Heyman and the “Safe Theorem”

#### *Hypothesis on masonry material*

In 1966 Professor Jacques Heyman<sup>6</sup> has introduced some hypotheses for the determination of the admissibility domain of the masonry material. The three assumptions are reasonable approximations, but – as the same Heyman remembers – each is not strictly true and must be protected with reservations. Heyman does not introduce nothing new, but formalizes in a clear way some hypotheses on the material, that formed the basis for the calculation of the arches in the XVIII and XIX century. These assumptions enable Heyman to frame the masonry action in the plastic theory and to formulate the famous *safe theorem*, that will be explained later on. The three hypotheses are: (i) the masonry has no tensile strength; (ii) the masonry has infinite compression strength; (iii) sliding failure doesn’t occur. As regards the first, it is an assumption that does not always adhere to the reality, but it is at safety benefit. It is strictly true only if the masonry is made by dry-stone blocks or with weak mortar: however, in most cases, the adherence between mortar and masonry blocks is negligible because the mortar may decay in time. Therefore, whatever is the ultimate tensile strength of the individual blocks, the masonry may be considered a non resistant tensile material (NRT material).

The hypothesis of infinite compression strength is a valid approximation only if the ratio between the average compression stress and the masonry compression strength is a negligible value compared to the unit. That is, the compression strength is not infinitely great, but if the

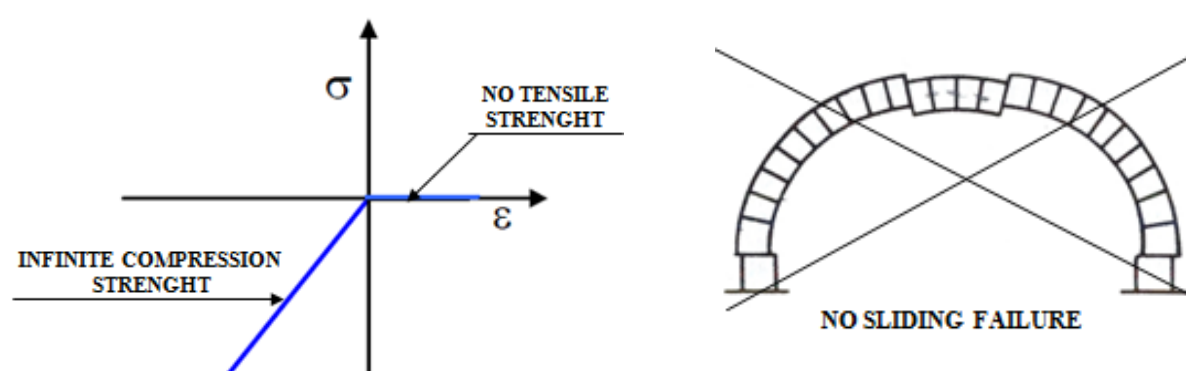


**Figure 1.1** Heyman’s three hypotheses: (i) the masonry has no tensile strength; (ii) the masonry has infinite compression strength; (iii) sliding failure doesn’t occur.

<sup>6</sup> Heyman, J. (1966), *The stone skeleton. Structural Engineering of Masonry Architecture*, University of Cambridge, Cambridge

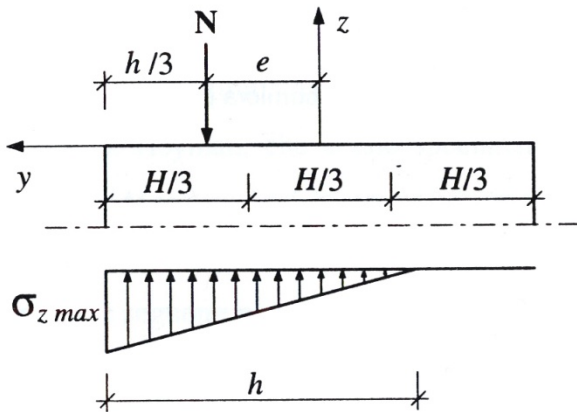


**Figure 1.2: Reduction of the resistant section when the stresses come out of the middle third.**

ratio illustrated is sufficiently small, the hypothesis of infinite compression strength is justified.

However it should pay attention to the rise of stresses concentrations. In fact, when an NRT material is considered, if the stresses come out of the middle third, occurs: (i) a reduction of the resistant section; (ii) a redistribution of the compression stresses; (iii) an increase of the peak values. In normal conditions of exercise, stresses are so low that prevent any phenomena of crushing failure.

The assumption of absence of sliding failure is equivalent to assert that the shear component of the force, which is exercised between two voussoirs, never exceeds the friction between them. In fact, low compression stresses allow to develop high friction forces, that prevent voussoirs from losing cohesion and sliding. The validity of this hypothesis can be verify considering the slope of the thrust line respect to the joints: if the thrust line is perpendicular to the joints, there is no mutual sliding between the voussoirs. Instead, if it forms an angle minor than  $90^\circ$ , the voussoirs tend to slide downwards or upwards.

Concerning Heyman's hypotheses, the collapse mechanism of the arch is then identified by the progressive formation of hinges, that coincide with the points where the thrust line is tangent to the intrados or extrados of the arch. The mechanism for formation of

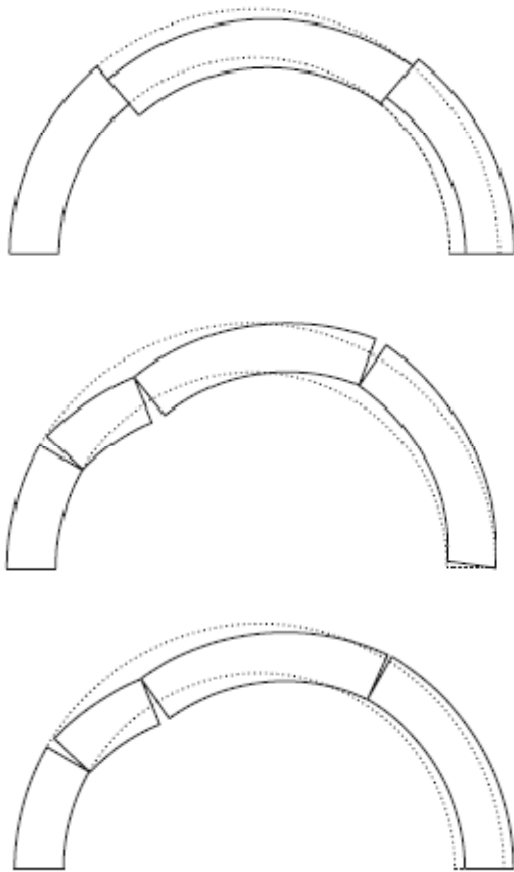


**Figure 1.3 Possible collapse mechanism for the arch: i) a shear mechanism; ii) a hinge-mechanism; iii) a combined shear-hinge mechanism.**



hinges is not the only possible for the arch<sup>7</sup>, but the experimental studies of Hendry (*figure 1.4*) show that it can be considered as the most likely collapse mechanism for arches well buttressed. The analogy between the rotation failure mechanism of the arch and that of the steel frames allows Heyman to apply even to the masonry structures the fundamental theorems of the plastic analysis, including the *safe theorem*.

### ***Safe Theorem***

*“If any equilibrium state can be found, that is, one for which a set of internal forces is in equilibrium with the external loads, and, further, for which every internal portion of the structure satisfies a strength criterion, then the structure is safe.”*

J. Heyman

Concerning Heyman, it is not necessary to find the real equilibrium state to assure arch safety, but only reasonable equilibrium states. This is very important since it is impossible to know the real state because of its ephemeral nature (failure of the foundations, thermal variations, etc.). In this way, it is possible to ensure the safety of the arch working only with the equations of equilibrium and consistency, without making assumptions on the boundary



***Figure 1.4 Hendry's experiment on collapse of real masonry arch bridge***

---

<sup>7</sup> According to Boothby, an arch bridge can collapse as a result of three possible collapse mechanisms: a shear mechanism, a hinge-mechanism and a combined shear-hinge mechanism.

conditions, that would be very difficult to verify. A way to represent the equilibrium equations is the thrust line, that shows the distribution of internal forces under a given load.

As demonstrates Gerstner<sup>8</sup>, the masonry arch is a structure statically indefinite, so there are endless lines of thrust, that satisfy the balance. In 1800s, the debate was just focused on the research of the real thrust line: i) for Moseley,<sup>9</sup> it was the one that minimizes the horizontal thrust in the keystone; ii) for Winkler<sup>10</sup>, it was the one that diverges the less possible from the axis line of the arch. The safe theorem allows to remedy the vagueness connected to the true thrust line location between infinite number of possibilities: an arch is safe simply if a thrust line can be drawn inside his thickness. So Heyman's approach can be defined in equilibrium approach. A safe arch, just checked by the safe theorem, will not collapse whatever is the movement induced in the abutments, provided that: i) the movements are little; ii) the equilibrium equations are not changed; iii) the whole geometry of the arch is not distorted.

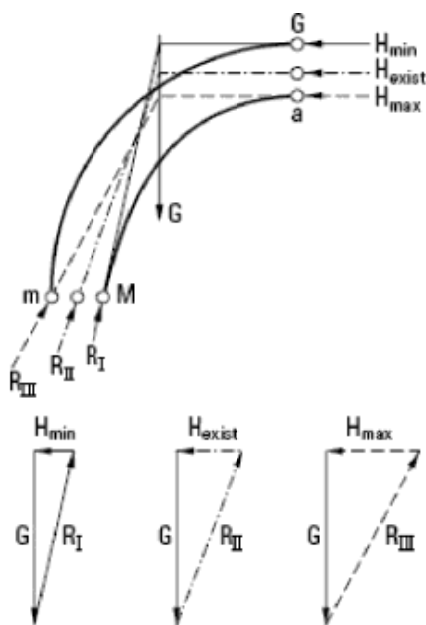


Figure 1.5 Moseley's determination of the thrust line

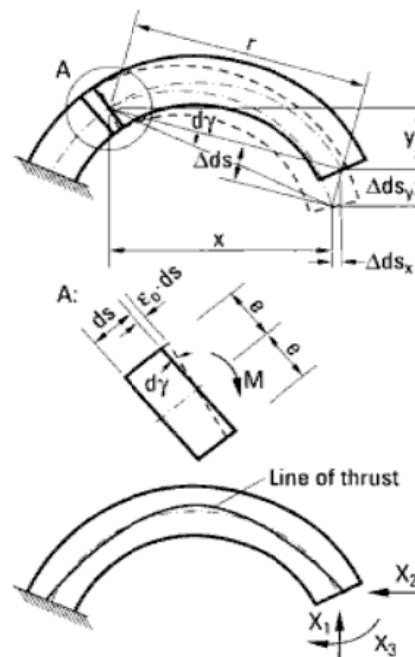


Figure 1.6 Winkler's determination of the thrust line

## Limit States

The thrust line has not to go out of the masonry thickness: to this end, it is interesting to

<sup>8</sup> Gerstner F.J. von (1831-1834), *Handbuch der Mechanik*, J. Spurny, Prague

<sup>9</sup> Moseley H. (1833), *On a new principle in statics, called the Principle of least pressure*, The London and Edinburgh Philosophical Magazine and Journal of Science, vol. 3, pp. 285-288

<sup>10</sup> Winkler E. (1867), *Die Lehre von der Elastizität und Festigkeit*, Dominicus, Prague

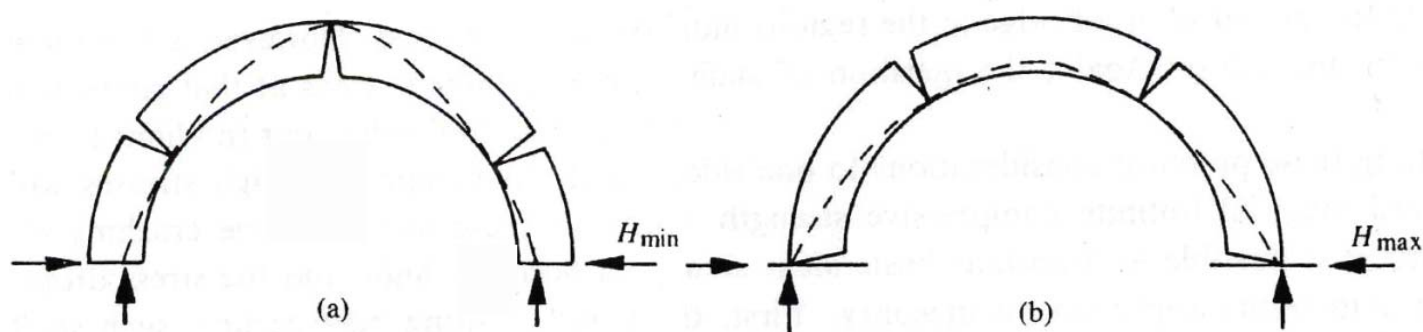


Figure 1.7 J. Heyman. (a) Minimum abutment thrust. (b) Maximum abutment thrust.

study its two extreme positions, that represent two states still in equilibrium. In fact, when the thrust line touches the lower or the upper boundary of the arch, the masonry finds itself at the limit of the admissible states region and the eccentricity is such that promotes the formation of hinges. In particular, in the two extreme conditions, the thrust line gives the location of three hinges that open: in this way, the value of the horizontal abutment thrust can be calculated.

In the two extreme positions of the thrust line, the horizontal abutment thrust will be: a) minimum; b) maximum. The minimum horizontal thrust will be obtained when the arch acts on the environment: for example, after removing the centering that supports the masonry, an arch will thrust on the abutments and these one will open slightly. In minimum thrust state, or passive state, the thrust line will have the greatest rise and the smallest clear span; it will touch the extrados at the key and intrados at the back. The maximum horizontal thrust will be obtained when the environment acts on the arch: for example, when two abutments move closer to each other, the arch span diminishes. In state of maximum thrust state, or active state, the thrust line will have the smallest rise and the greatest clear span; it will touch the extrados at the crown and the intrados down. Three hinges will open if one is at the key; on the contrary, four hinges form.

It is important to know the two extreme positions of the thrust line, because the real thrust of the arch can't be calculated, but the upper and the lower limits can be fixed.

### Collapse

The collapse of a masonry arch does not involve an absence of strength, but rather a loss of stability. In fact the collapse takes place when a thrust line can't be found within the arch boundaries. The crisis is connected with the formation of a fourth hinge, that transforms the stable arch in an unstable mechanism of collapse. The four hinges open in alternating way in the

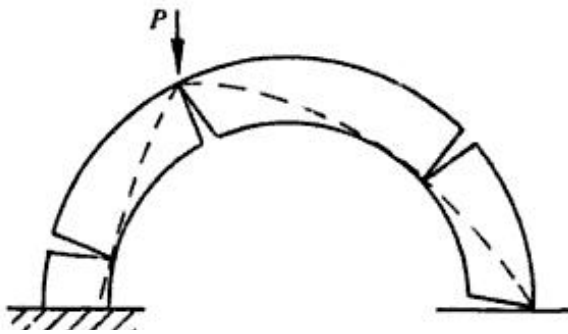


*Figure 1.8 An additional point load generate the fourth hinge*

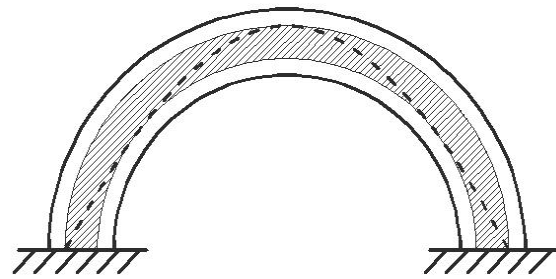


*Figure 1.9 Geometry Safety factor of 2*

intrados and in the extrados, following a pattern that is function of the arch shape and the working loads. In case of symmetrical load, a fifth hinge can open, but generally slight geometrical failings make the structure to behave asymmetrically. A masonry arch has to support two main types of loads: i) the self weight; ii) the additional loads. The additional point loads have a thrusting nature and can cause collapses because their action move the thrust line out of the arch, generating the fourth hinge. Then they implicate meaningful changing of shape. On the contrary, the self weight is the resistant load of every masonry structure and opposes every mechanism of collapse.

### **Stability Check**

The catenary is the arch true shape. Arches with other shape stand up because catenaries are included in their thickness. The thrust line shape is the mathematical catenary if the self weight is equally distributed around the arch. There is a minimum thickness of semicircular arch that just contains a catenary. The limit arch has exactly this minimum thickness and is in unstable equilibrium. The ratio between the real arch thickness and the limit arch one defines the safety factor, that is of geometric nature. Heyman suggests 2 as safe practical value: that is, if you're able to draw a thrust line in the middle half of the arch, the arch is safe. So the thrust line can be perceived as an index of the stability condition of the arch.

## 1.4 Plastic Limit Analysis

The research of Professor Heyman highlights that an elastic analysis is problematic for masonry structures because there isn't a unique calculable equilibrium state. On the contrary, the limit analysis allows to consider the structure only in relation to its ultimate state, using few material parameters and neglecting the initial stress state. Some of the principal methods for the assessment of masonry arch bridges are based on the fundamental theorems of Limit Analysis, that now will be explained.

A summary of the basic rules that apply in the theory of plasticity can be found in the work of Horne<sup>11</sup> (1979). In the context of masonry arches, there are fundamentally three main considerations to apply the theorems of plastic limit analysis: i) the internal actions must be in equilibrium with the external loads; ii) there must be a sufficient number of hinge to transform the structure into a mechanism; iii) the maximum stresses must be less than or equal to the material strength.

The three fundamental theorems of plastic analysis can be stated in simplified form as:

- **Static or lower bound theorem.** If the equilibrium and yield conditions are everywhere satisfied, then the load factor  $\lambda_l$  is less than or equal to the failure load factor  $\lambda_p$ ;
- **Kinematic or upper bound theorem.** If the equilibrium and the mechanism conditions are everywhere satisfied, then the load factor  $\lambda_u$  is greater than or equal to the failure load factor  $\lambda_p$ ;

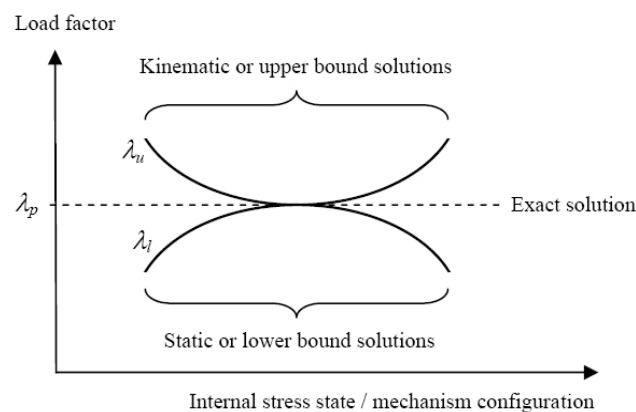


**Figure 1.10** *The relationship between upper and lower bound solutions*

<sup>11</sup> Horne, M.R. 1979. Plastic theory of structures, 2nd edition, Oxford: Pergamon Press.

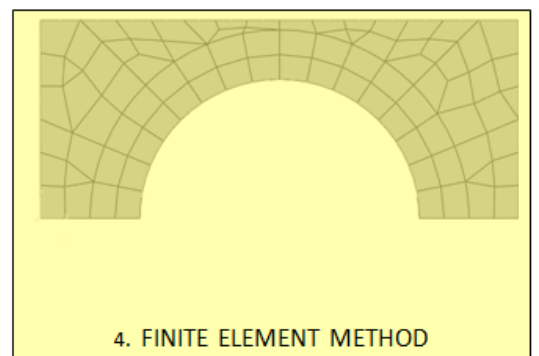
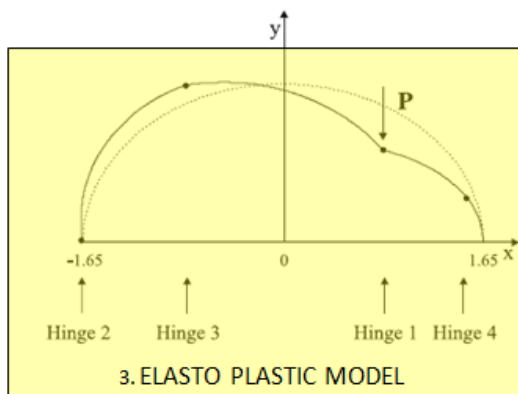
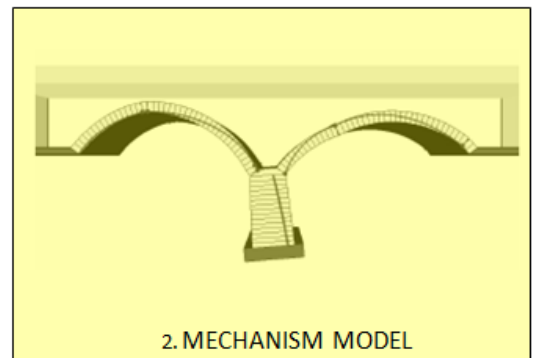
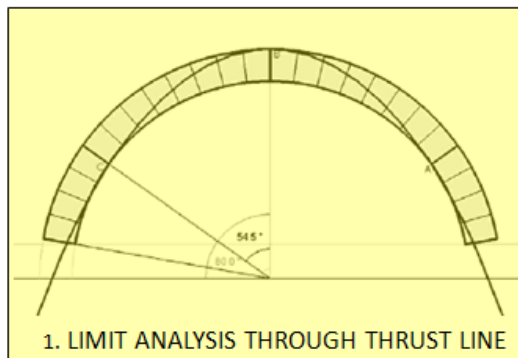
- **Uniqueness theorem.** If the internal stress state is such that the three conditions of equilibrium, mechanism, and yield are satisfied then that load factor is the collapse load factor  $\lambda_p$ .

The relationship between upper and lower bound solutions is illustrated in *figure 1.10*.

Chapter 2

## Methods and Models For Analysis of Masonry Arches

---







## 2.1 SOMMARIO

*“If any equilibrium state can be found, that is, one for which a set of internal forces is in equilibrium with the external loads, and, further, for which every internal portion of the structure satisfies a strength criterion, then the structure is safe.”*

Jacques Heyman

La teoria di Heyman ha dato vita nel tempo a diversi modelli. Infatti il “*safe theorem*” unito alla teoria della funicolare può essere utilizzato per sviluppare strategie computazionali per l’analisi di strutture in muratura, come è stato fatto da Block<sup>1</sup> e da Oschendorf. Ai fini della sicurezza è quindi necessario solo poter disegnare una plausibile curva delle pressioni all’interno dello spessore dell’arco. Tra i programmi di analisi basati su questa metodologia, si trova Archie-M sviluppato dalla Obvis<sup>2</sup>, che indica graficamente una possibile curva delle pressioni per qualsiasi regime di carico. Anche se lo scopo di Archie-M è solo quello di dimostrare se un determinato ponte ad arco possa sopportare o meno un dato carico, si può stimare il carico di collasso variando il moltiplicatore di carico fino a quando la curva delle pressioni tocca il bordo dell’arco e si forma un numero sufficiente di cerniere.

Nell’analisi limite, si può poi utilizzare un modello discreto e idealizzare l’arco come un assemblaggio di blocchi rigidi. Nel 1978 Livesley fu il primo ad adottare modelli discreti per l’analisi limite di strutture in muratura. Partendo da un modello discreto, si può inserire poi all’interno del modello una resistenza a compressione finita, ridefinendo il dominio di rottura non lineare di sforzo normale e momento. Generalmente è conveniente assumere che i blocchi siano rigidi e modellare tutte le rotture nei contatti tra i blocchi. Tra i programmi di analisi basati su questa metodologia, si trova LimitState Ring<sup>3</sup>, che utilizza appunto tecniche di analisi plastica, avvalendosi di modelli discreti. Il programma usa un’ottimizzazione matematica, che permette di identificare lo stato limite ultimo, determinando la percentuale di “*live load*”, che porterà al collasso.

Un altro metodo usato per descrivere il comportamento strutturale dei ponti ad arco in muratura è il Metodo degli Elementi Finiti. Si parte da un approccio completamente diverso. Adottando diverse strategie di discretizzazione, come micro-modellazione o macro-modellazione, si divide la struttura in una serie di elementi finiti. Si può effettuare un’analisi

---

<sup>1</sup> P. Block, *Equilibrium systems. Studies in Masonry Structure*, Thesis of master of Science in Architecture Studies, MIT, Boston (2005)

<sup>2</sup> Obvis Ltd., [www.obvis.com](http://www.obvis.com)

<sup>3</sup> LimitState Ltd., [www.limitstate.com](http://www.limitstate.com)

non lineare, assegnando particolari leggi costitutive al materiale. I risultati includono la massima sollecitazione e l'analisi della deformabilità. Il Metodo degli Elementi Finiti rappresenta lo strumento più versatile per l'analisi numerica di problemi strutturali. Tuttavia nel caso di muratura storica, la particolare natura del materiale deve portare a prestare maggior attenzione all'applicazione di questo metodo.

In questo lavoro è stato adottato anche un modello elasto-plastico, sviluppato da alcuni ricercatori belgi<sup>4</sup>. Alla base di questo modello elasto-plastico, ci sono le tre equazioni di equilibrio di un concio infinitesimo di arco in direzione radiale, tangenziale e alla rotazione. Sia per il peso che per il carico esterno vengono scritte espressioni analitiche in funzione dell'angolo e della posizione sulla curva. Sostituendo tutte le variabili nelle equazioni di equilibrio, si ottengono equazioni differenziali di secondo ordine. Risolvendo le equazioni differenziali, si determinano le espressioni analitiche delle forze interne, espressioni che includono tre costanti di integrazione. Per trovare una soluzione univoca per le forze interne nell'arco, bisogna quindi introdurre le condizioni al contorno: in questo caso si adottano le equazioni di Bresse<sup>5</sup>. Noti gli spostamenti in entrambi i sostegni, queste equazioni possono essere usate per determinare le tre costanti di integrazione. In questo modello, vengono introdotte anche le proprietà del materiale, ovvero della muratura. Restando nell'ipotesi di assenza di resistenza a trazione, si studiano le varie distribuzioni possibili delle sollecitazioni. Sul diagramma dato dalla combinazione tra sforzo normale e momento, il confine della zona elasto-fragile-plastica corrisponde ad una distribuzione plasto-fragile. Finché le combinazioni di sforzo normale e momento in ogni sezione dell'arco rimangono all'interno della curva limite plasto-fragile, l'arco riesce a sopportare il carico senza formazione di cerniere. Quando si aumenta ulteriormente il carico, a un certo punto ci si trova sulla curva limite del dominio ed è in questo momento che si forma la prima cerniera plastica. Questa procedura viene ripetuta fino a quando le cerniere plastiche arrivano a un numero tale che l'intero sistema può deformarsi sotto carico permanente costante.

---

<sup>4</sup> A. Audenaert, H. Peremans and W.P. De Wilde, *Static determination of the internal forces and displacement in arch bridges*, The masonry society Journal, 22 (1), 2004, pp. 97-109

<sup>5</sup> M. Bresse, *Cours de Mécanique Appliquée*, Paris, Imprimerie de Gauthier-Villar, 1859

## 2.2 Classification of the methods for the assessment of the masonry arches

Structural analysis is a general term describing the operations to represent the real behavior of a construction. The analysis can be founded on mathematical models created on theoretical bases or on physical models tested in laboratory. In both cases, the models try to individuate the load carrying capacity of the structure, identifying the stress state, the strain and the internal forces distribution of the entire structure or of its parts. Besides for arch structures, the models try to indicate the failure mode and the location of plastic hinges.

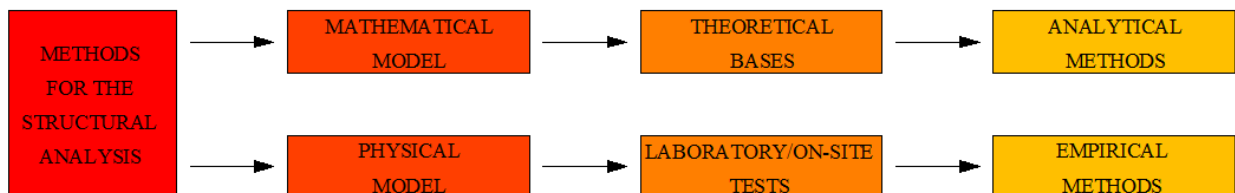


*Figure 2.1 Methods of load carrying capacity assessment*

In this chapter, analytical methods for the structural analysis of the masonry arch bridges are treated. In literature there are many types of theoretical methods that can be used. These methods can be divided into different categories concerning their origin, scope, applicability and approximation level.

As previously seen, about the three fundamental structural criteria<sup>6</sup>, it is the stability that governs the life of the masonry arches because the average medium stresses are low and the strains are negligible. So the most important methods for the evaluation of masonry arch bridges are derived from Heyman's theories and from the fundamental theorems of the Plastic Analysis. They are: i) the thrust line analysis method; ii) the mechanism method.

The Thrust Line Analysis Method is based on the lower bound theorem or "safe" theorem and defines the limits for the thrust line location. It uses a static approach and defines the limit load, that ensure the equilibrium of the arch bridge analyzed. On the contrary, the Mechanism Method is based on the upper bound theorem and studies the number of plastic hinges needed to transform the arch in a mechanism. In this case, the stability of the arch is analyzed with regards to a kinematic approach. Both the methods are valuable: due to their different bases, the first one underestimates the structure strength, while the second overestimates it.

<sup>6</sup> strength, stiffness and stability

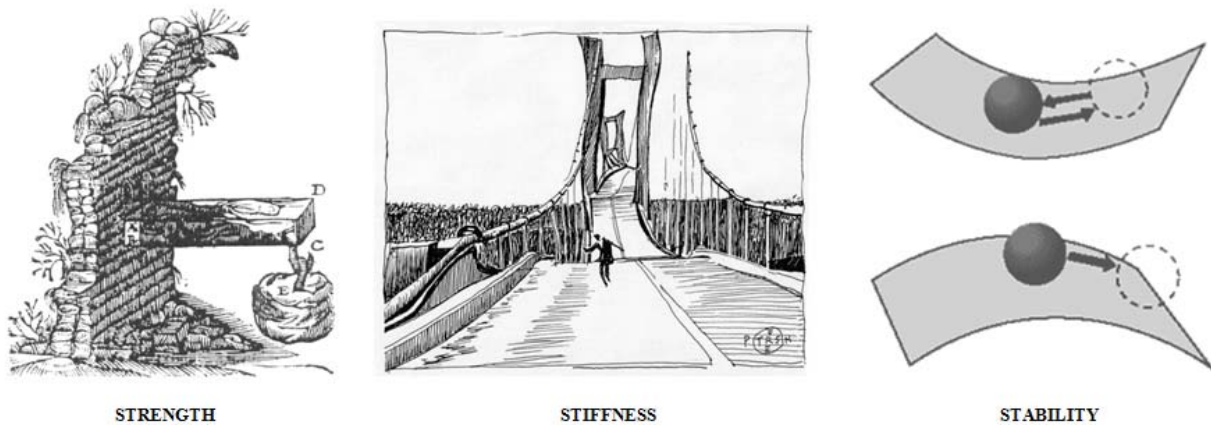


**Figure 2.2 Representation of the three fundamental structural criteria: Strength, Stiffness and Stability**

Another method used to describe the structural behavior of the masonry arch bridges is the Finite Element Method. It starts from a completely different approach. Adopting different strategies of discretization, as micro-modeling or macro-modeling, the structure can be divided in a series of finite elements. Non linear analysis can be performed, assigning particular constitutive laws to the material. The results include the maximum stress and deformability analysis. The Finite Element Method represents the most versatile tool for the numerical analysis of structural problems. However in the case of historic masonry, the peculiar nature of material leads to pay particular attention to the application of this method.

In the next paragraphs, these methods will be described more specifically. In particular, there will be presented the material models that can be used. At the end of every paragraph there will be introduced the most common computer-based representations connected to each method. These computerized approaches allow a friendly-use application of the principles explained. Depending on the used method, they enable to obtain various output including the load carrying capacity.

The last paragraph of this chapter will deal with a particular closed-form approach developed by some Belgian researchers in the last years. This method is based on the fundamental theorems of limit analysis and is used to determine the critical points with a relatively small modeling effort. To assure the stability of the masonry arch bridges, a model based on equilibrium equations and compatibility conditions is first developed. Next, the material properties are added to determine the formation of the hinges.

## 2.3 Thrust Line Analysis Method

This general method analyzes the arch stability, evaluating the location of the thrust line inside the cross section. The thrust line represents the *locus* of points along the arch through which the resultant forces pass. If all the arch voussoirs have the same size, the line of thrust has almost the shape of an inverted catenary.

*“As hangs the flexible, so but inverted will stand the rigid arch.”* wrote Robert Hooke in 1675. *“None but the catenaria is the figure of a true and legitimate arch.”* completed Gregory twenty years later, in 1697. These quotes describe the mechanics of the arch in a brief, but precise way. *Figure 2.3* shows a simple example used by Heyman (1982) to explain this concept: a weightless string subjected to three forces. The funicular polygon inverted represents the thrust line.

The thrust line may be located at the middle of the section or very close to the edge. It depends from the resultant of inertial forces in a given cross section. If no moment and transverse force occur into the arch, the thrust line coincides with the centre-line of the section. In the other cases, the thrust line departs from the arch centre-line and so it is important to define the distance between the thrust line and the center of the mass, i.e. the eccentricity  $e$  (*figure 2.4*).

The thrust line method analyzes the location and the slope of the thrust line inside the cross section through two parameters. The first one is the eccentricity of the forces resultant, that describes the location of the thrust line in the cross section. The

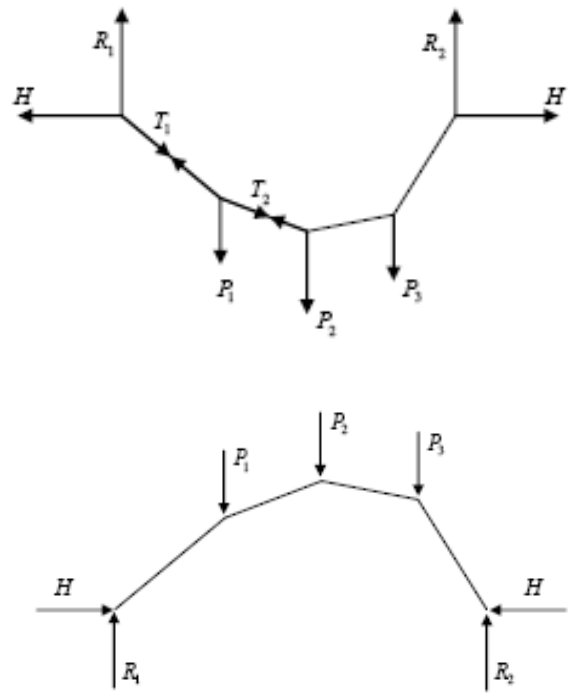


**Figure 2.3 Inverted funicular polygon and the Thrust Line**

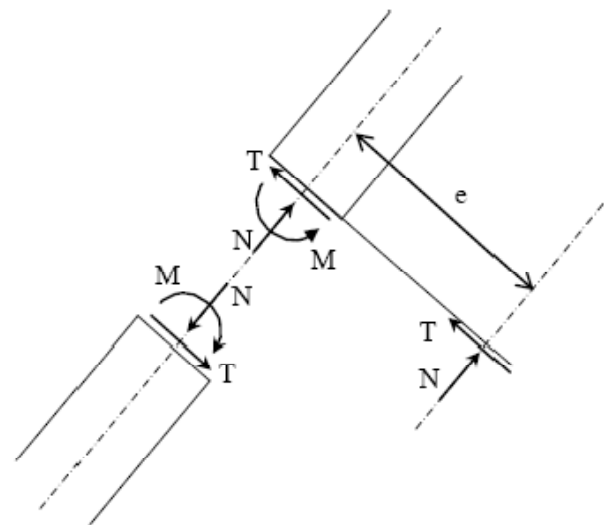


**Figure 2.4 The eccentricity  $e$**

eccentricity is easy to calculate because it is a function of the normal force  $N$  and the bending moment  $M$  acting in the considered cross-section. The second important parameter is the relation between normal force  $N$  and shear force  $T$ , that defines the slope of the thrust line. Calculation of thrust line location can be performed using the equilibrium equation or by solving a linear programming problem.

So every thrust line is a possible equilibrium solution. Unfortunately the masonry arch is not a statically determinate structure and this solution is not unique. There are infinite possible lines of thrust. The equilibrium equations are not sufficient to obtain the inner forces.

The thrust line analysis method defines the load carrying capacity by limiting the zone where the resultant force can be positioned. This method presents some variants which differ from each other by the size of the limits. The limits depends on the theory and the material model assumed. The main approaches will be described below.

### **Middle Third Rule**

The first variant of this method is also the most ancient. The Middle Third Rule is anticipated by Thomas Young<sup>7</sup> in 1817, worked out by Claude-Louis Navier<sup>8</sup> in 1826 and applied to masonry arch by William Rankine<sup>9</sup> in 1858. This rule states that the thrust line must lie within the middle third of the cross section, that is it must lie within the kern to avoid any tensile stresses. The eccentricity is defined as:

$$e = \left| \frac{M}{N} \right| \leq \frac{d}{6}$$

This criterion is based on the elastic theory. Until the forces resultant remains within the kern, there are only compressive stresses. When the force passes the middle third, the section undergoes also tensile stresses (*figure 2.5*). However it is assumed that the masonry has not tensile strength, so in this case the section is not contributing entirely. Cracks may occur and this is wanted to avoid.

The middle third rule is extremely safe approach in the determination of the collapse load. It is very difficult to satisfy because of this rigorous limit. It can be reach only: i) if it is

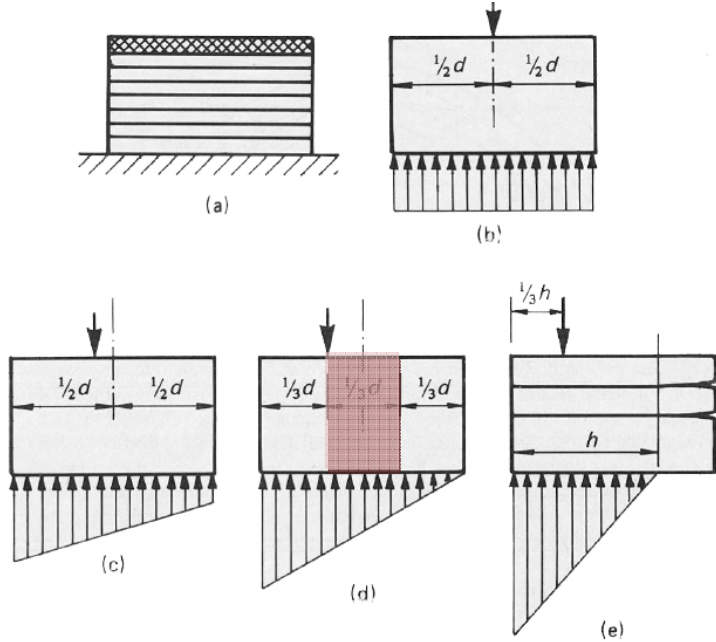
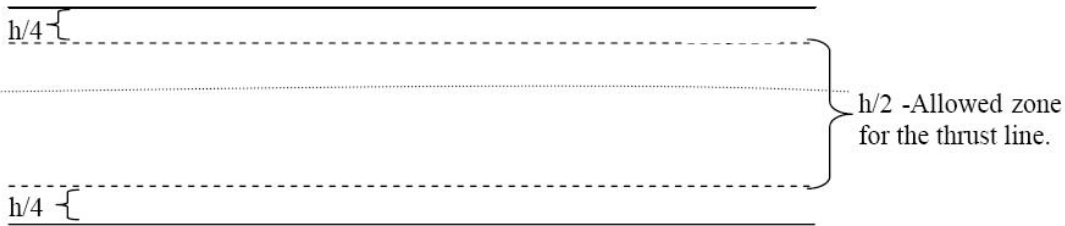
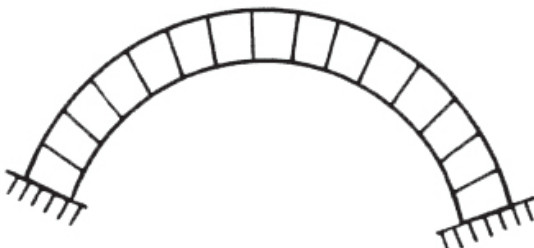
---

<sup>7</sup> Thomas Young, Article in the *Supplement to the fourth edition of the Encyclopaedia Britannica* (1817).

<sup>8</sup> Navier 1826. *Résumé des Leçons données à L'École des Ponts et Chaussées, sur l'application de la mécanique à l'établissement des constructions et des machines*. Paris.

<sup>9</sup> Rankine, W. J. M. 1858. *A Manual of Applied Mechanics*. London: Charles Griffin.

**FIGURE 2.5 THRUST LINE ANALYSIS METHOD**

MIDDLE THIRD RULE	 <p style="text-align: center;">Heyman (1982). A pile of stone subjected to a compressive force.</p>
MIDDLE HALF RULE	
HEYMAN'S RULE	

considered in the design phase; ii) if the dead loads dominate considerably over live loads.

### **Middle Half Rule**

The difficulty to satisfy the previous criteria has led to apply a less conservative version of this method, that is the middle half rule. This approach increases the limits for the thrust line. In this case, the thrust line should lie within the central half of the arch section (*figure 2.5*). The eccentricity is defined as:

$$e = \left| \frac{M}{N} \right| \leq \frac{d}{4}$$

### **Heyman's Rule**

Another variant of the thrust analysis method is proposed by Jacques Heyman<sup>10</sup>, as seen in the first chapter. With *the safe theorem*, he assumes that an arch is safe simply if a thrust line can be drawn inside his thickness. An arch will collapse only if the thrust line reaches the arch edge at least in four points, converting the arch into a mechanism. This rule is surely the less conservative than the other because the whole cross section become the allowed zone for the thrust line. This can be expressed as:

$$e = \left| \frac{M}{N} \right| \leq \frac{d}{2}$$

This approach includes an important assumption concerning the masonry behavior. An infinite compression strength is attributed to the masonry material. This enables the thrust line to stay at the edge of the cross section. The assumption is not realistic, but this method can be considered a good method to use because in the majority of the masonry arch bridges the stress level are quite low respect to the masonry compressive strength.

All the variant of the thrust analysis method can be summarized by the Heyman's concept of "geometric safety factor", just explained in the first chapter. For example the masonry arches that satisfy the middle third rule have a geometric safety factor equal to three.

---

<sup>10</sup> Jacques Heyman, *The Stone Skeleton*, Cambridge University Press, Cambridge, 1966



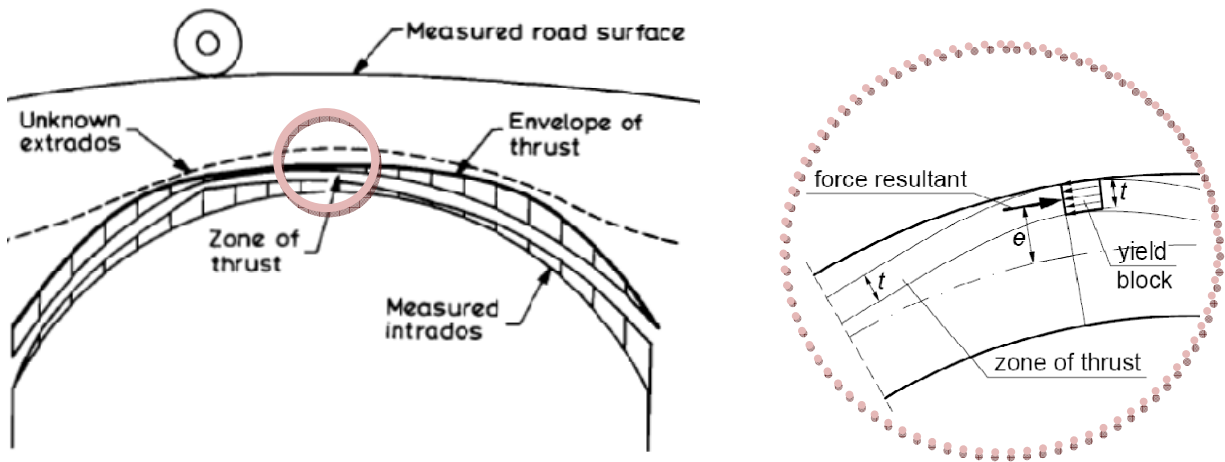


Figure 2.6 Harvey. The thrust zone.

### Thrust Zone Analysis Method

A method very similar to the thrust line method is the thrust zone method developed by Bill Harvey in 2001. It is based on an elasto-plastic model and considers a finite compressive strength that doesn't allow the thrust line to stay at arch edge. A rectangular "yield block" is created around the force resultant. The force resultant is positioned in the middle of the rectangular area, at  $t/2$  (figure 2.6). The height of the yield block is a function of the normal force  $N$ , the strength material  $f_c$  and the thickness of the arch  $B$  and can be calculated as:

$$t = \frac{N}{f_c \cdot B}$$

### Computer Based Application: Archie-M

Thrust line analysis together with Heyman's safe theorem can be used to elaborate computational strategies for the structural analysis of masonry arch bridges. For example, in 2006 Philip Block<sup>11</sup> has developed an interactive computational procedure, that uses the thrust lines to clearly visualize the forces within the masonry and to predict possible collapse modes. The program lets the user to change the arch geometry, analyzing the different locations that can be assumed by the thrust line.

Between the specialized analysis programs based on this method, there is also Archie-M

<sup>11</sup> Block, P., Ciblac, T. and Ochsendorf, J. 2006. Real-time limit analysis of vaulted masonry buildings, *Computers & Structures*, 84(29-30), p. 1841-1852.

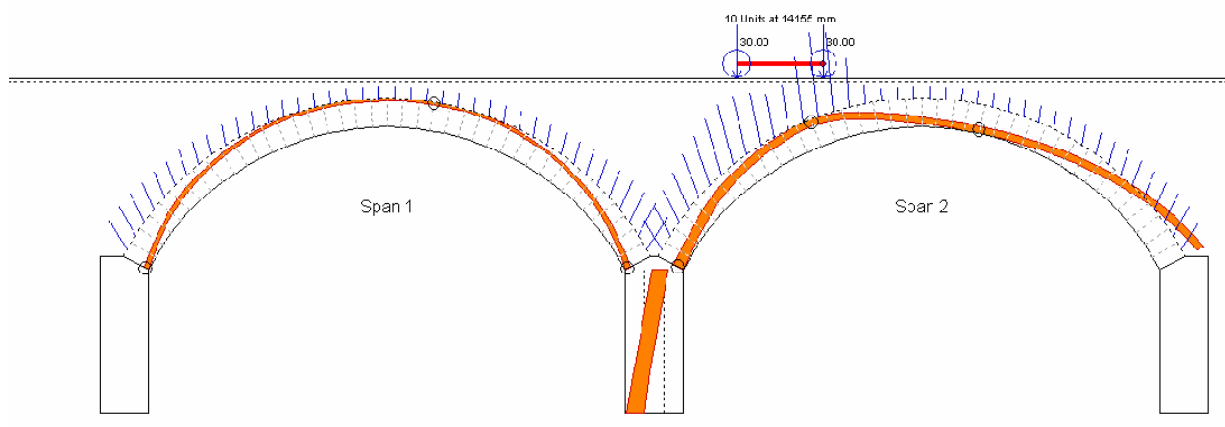


**Figure 2.7 Typical output of Archie-M (Obvis)**

developed by Harvey and OBVIS Ltd<sup>12</sup> in 2001. Archie-M is a computer program, that analyzes multi-span arch bridges together with supports and backfill. It carries out a form of equilibrium analysis. That is to say it determines whether an arch will remain stable, without first considering how it will deform under load. In fact the software uses the thrust line analysis combined with a thrust zone to model the masonry finite crushing strength. In practice the program is based on the thrust zone analysis method.

Calculations are carried out on a static scheme of a three hinges arch. The hinge positions are chosen as the most likely for the given load pattern. The program is easy to use because it shows graphically the position of a potential thrust-line and the formed hinges for any given loading regime (*figure 2.7*). Until the thrust zone is within the cross section of the arch at every point, the structure is safe. When the thrust zone begins to touch the arch edge in a fourth point, a mechanism is created and the collapse state is reached.

Although the aim of Archie-M is to demonstrate whether an arch bridge can withstand a given load or not, the collapse load can be estimate by varying the load value until a sufficient number of hinges is formed.

The program provides also the internal forces and the thrust zone position for each arch segment. The live load is distributed through the fill with a sine shape. The backfill is modeled as a continuous body that spreads the load and provides both active and passive soil pressure.

<sup>12</sup> Obvis Ltd., [www.obvis.com](http://www.obvis.com)

## 2.4 Mechanism Method

The Mechanism Method is a kinematical method, based on the upper bound approach. This method belongs to the plasticity theory and was firstly used for steel structures. Later Heyman<sup>13</sup> has applied it to masonry arch. The term *mechanism* refers to the possibility of structure to move in accordance to internal and external constraints. This Method assumes that a masonry arch becomes a mechanism when at least four plastic hinges open. Many experimental tests confirm this hypothesis. However position of hinges is unknown.

First step is to assume the possible position of four hinges. In a simplified analysis with only a concentrated force on the arch, the first three hinges can be assumed to be located under the load and at the springing. It's reasonable to hypothesize hinges A and C on the intrados and hinges B and D on the extrados (*figure 2.8*). The concentrated force  $W$  is applied on the arch with no dispersion through the fill. Self weights  $V_i$  include the weights of the backfill blocks and of the corresponding arch segment. The four unknowns are the reaction forces of the two abutments  $H$ ,  $V_a$ ,  $V_b$  and the failure load  $W$ . The problem can be solved with the moment equilibrium equations at the hinges or with the equations of virtual works. In the first case, four equilibrium equations can be derived around the hinges and solved, giving the four unknowns. In the second case, the structure collapses if the total virtual work for at least one of the mechanisms allowable is positive.

In order to find the best mechanism, it is necessary to repeat the analysis for each

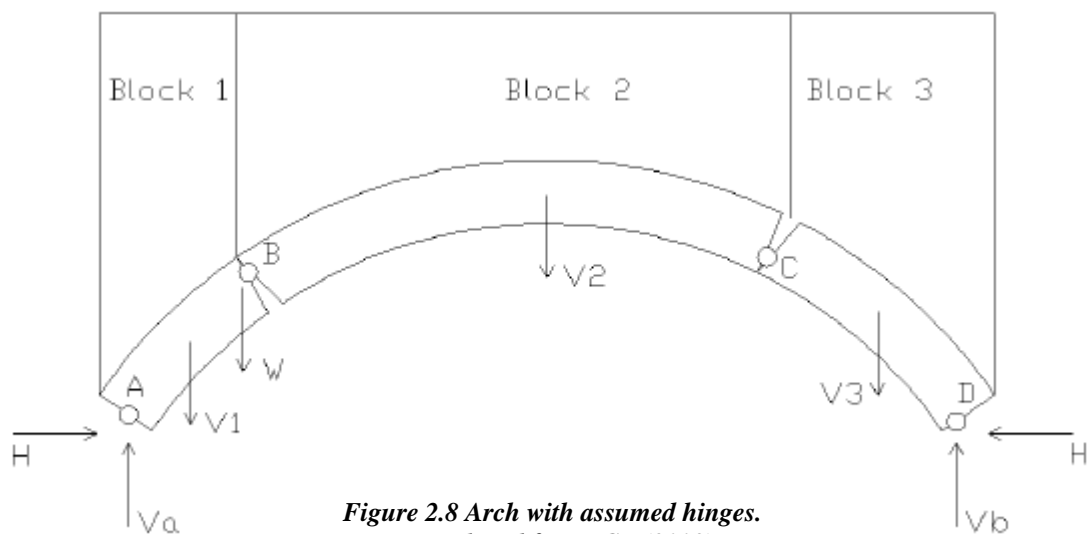


*Figure 2.8 Arch with assumed hinges.  
Reproduced from ICE (2008)*

<sup>13</sup> Heyman, J., *The masonry arch*, Ellis Horwood, 1981

possible load position and adopt the lowest result. The process remains simple and may be undertaken with a hand calculator, but it is much more convenient to use a programmable machine. A linear algorithm with a target function minimizing the live load factor can be adopted. In this way the most probable mechanism mode is found automatically.

There are some variants of this method that differ from each other concerning the geometry and the material model. Here two variants will be exposed. In the first case it is considered a rigid material model characterized by infinite compression strength, while in the second case a rigid-perfectly plastic material is taken into account. In both cases, the material is considered homogeneous and no tensile resistant.

### Rigid Blocks

A type of analysis using the mechanism method is the rigid block analysis. It is presented by Livesley<sup>14</sup>, that pioneered in 1978 the development of discrete limit analysis models for masonry structures. Livesley found a solution for the equilibrium condition and the mechanism conditions described by Heyman, using the linear programming.



*Figure 2.9 From the real arch to the rigid block model*

<sup>14</sup> Livesley R.K. (1978), *Limit analysis of structures formed from rigid blocks*, International Journal for Numerical Method in Engineering, 12, pp. 1853-1871.

This theory simplifies the masonry arch as an assemblage of plane blocks, that are infinitely rigid and have an infinite strength. The division into these blocks is regular, but doesn't respect necessarily the actual number of units of the original arch. Usually the blocks are slightly larger than the physical ones because the mortar joints are not explicitly modeled. The blocks can be also extremely larger than the actual ones in order to reduce the computational effort. In this case it must be careful that the discretization does not affect the expected mode of response. As checked experimentally, the number of blocks to obtain a sufficiently exact solution is about forty.

At the collapse, the blocks can either slide or rotate. The blocks movement can be calculated using the minimal energy for global deformation.

### Rigid-Plastic Blocks

An important extension of Livesley's rigid block analysis has been made by Gilbert<sup>15</sup> in 1998. As no real material can sustain infinite compressive stresses, this variant of the mechanism method assumes a finite compressive strength, redefining the failure domain of normal stress and moment (*figure 2.11*). Also in this case, the failures are modeled in the contacts between the blocks, but the explained assumption constrains the

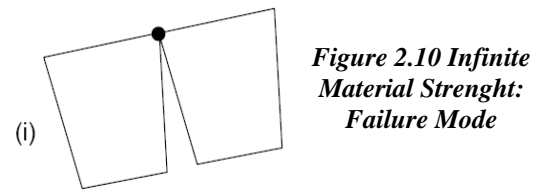


**Figure 2.10 Infinite Material Strength: Failure Mode**

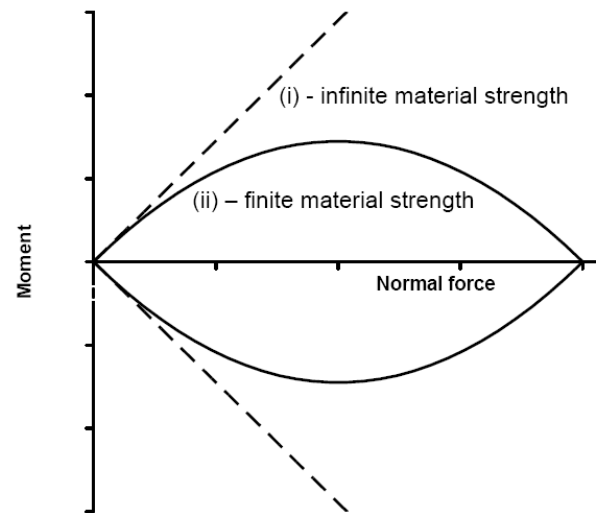


**Figure 2.11 Failure Domains for different material strength**

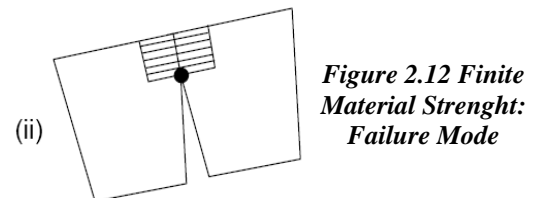


**Figure 2.12 Finite Material Strength: Failure Mode**

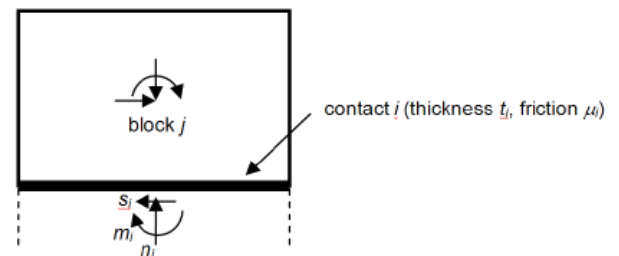


**Figure 2.13 Stress Block**

<sup>15</sup> Gilbert, M. (1998): *On the analysis of multi-ring brickwork arch bridges*. Proceedings of 2<sup>nd</sup> International Arch Bridges Conference, Venice, pp. 109-118.

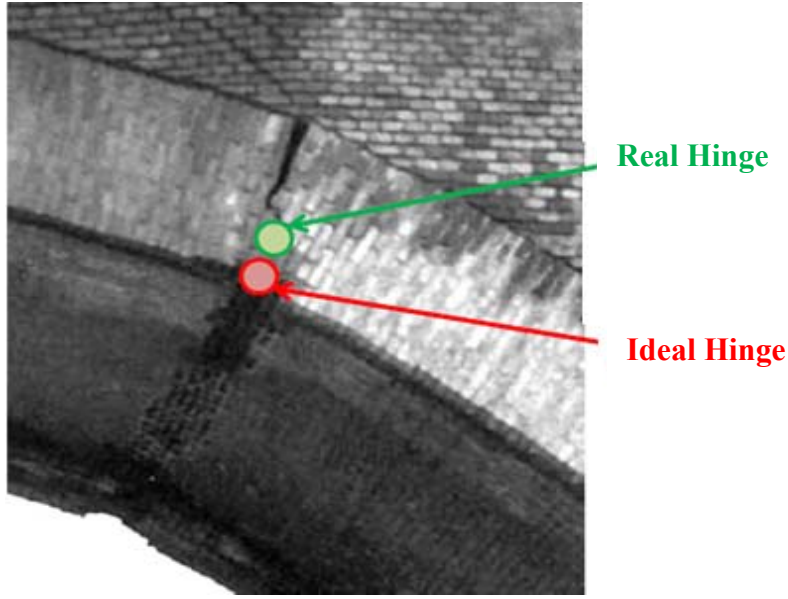


*Figure 2.14 From the real arch to the rigid block model*

hinges not to stay on the arch edges. (figure 2.12). In this way, the rotation point is brought back inside the arch, that behaves as it would have a lower thickness (figure 2.13). In the proximity of the hinges, the compressive force is carried by a rectangular stress block lying at the edge of masonry. The finite domain is defined by Gilbert<sup>16</sup> as:

$$\begin{cases} m_i \leq n_i \left( 0.5t_i - \frac{n_i}{2\sigma_{crush} b} \right) \\ m_i \geq -n_i \left( 0.5t_i - \frac{n_i}{2\sigma_{crush} b} \right) \end{cases} \text{ for each contact, } i = 1, \dots, c$$

where  $n_i$  are the normal force,  $m_i$  is the bending moment,  $t_i$  is the arch thickness and  $\sigma_{crush}$  is the compression strength. The passage to a finite compressive strength complicates the computation. In fact it transforms a linear problem to a non linear one. Gilbert solves the question applying an iterative solution, that uses a Linear Programming solver. In this way it is possible to obtain a solution to the global problem and to approximate the constraints as a series of linear constraints. The rigid-plastic block analysis can be considered the basic model for understanding the fundamental behavior of the masonry arches.

<sup>16</sup> Gilbert, M. (2001), RING home page, <http://www.shef.ac.uk/ring>

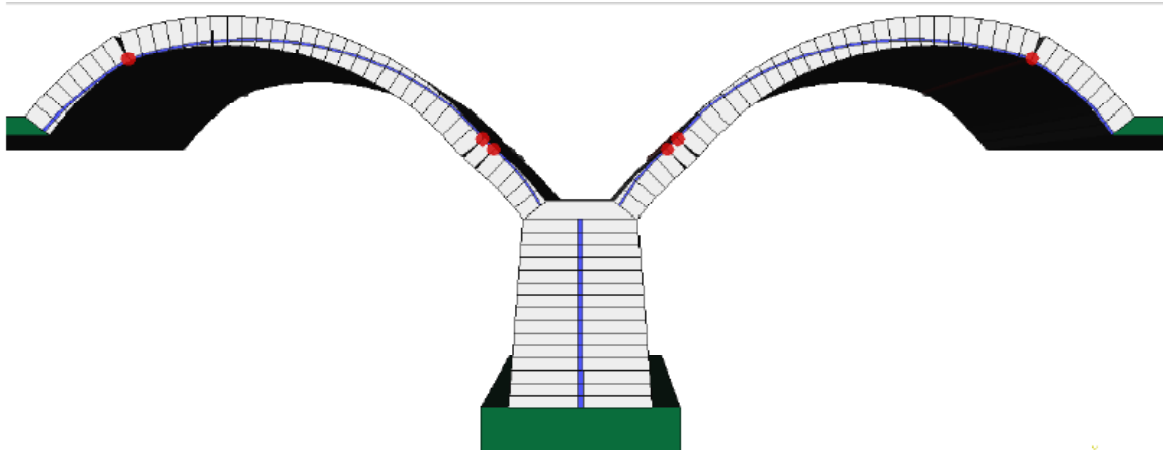


*Figure 2.15 Typical output of Ring(LimitState)*

### **Computer Based Application: Ring**

The two-dimensional rigid-plastic analysis has been inserted by Gilbert and Melbourne into a software called RING, developed by a University of Sheffield spin-off company, LimitState Ltd. The program is able to analyze multi-span masonry arch bridges, built of arch barrels, supports and backfill (*figure 2.15*). A particular feature of this software is the capacity to analyze multi-ring arches enabling separations between the various rings.

The program employs an efficient linear programming technique for the solution of virtual works equations. This mathematical optimization allows to identify the ultimate limit state, determining the percentage of live load, that will lead to the collapse. As a result of the analysis, the minimum adequacy factor for live load is obtained, together with a graphic representation of the thrust line and the failure mode. Exact location of hinges is indicated. The live load is distributed through a Boussinesq distribution with a maximum spread angle. The passive pressure is the only lateral pressure used.

## 2.5 Finite Element Method

Masonry arch bridges can be analyzed also using the Finite Element Method. Today this method can be considered the most general instrument for numerical analysis of structural problems. While the Thrust Line Analysis Method and the Mechanism Method are specific for the analysis of the arch stability, the Finite Element Method gives the possibility to model all the types of structures. In the last twenty years, many researchers have developed different finite element models for materials with low tensile strength, such as masonry. However the current knowledge of masonry mechanics is underdeveloped in comparison with other fields, as concrete and steel. So the Finite Element Method can be applied to the masonry analysis, but with particular attention due to the specific nature of the material.

The base principle of the Finite Element Method is to discretize the continuous structures into a series of partial domains called finite elements, that interact with each other only at certain points called nodes. Through this method, a continuous problem with infinite unknowns is reduced to a discrete problem with a finite number of unknowns. Usually the displacement method is used and the node movements are determinate. Then the actions in the nodes and internal strains can be evaluated using a series of fundamental relationships.

### Masonry Modelling

The discretization of the structure is the first step of this method. While in the frame structures there is a univocal choice, in the masonry structures there are different strategies of discretization. The main reason is due to the particular characteristics of masonry, that is an anisotropic material composed by bricks and mortar. In particular the presence of the mortar is difficult to model.

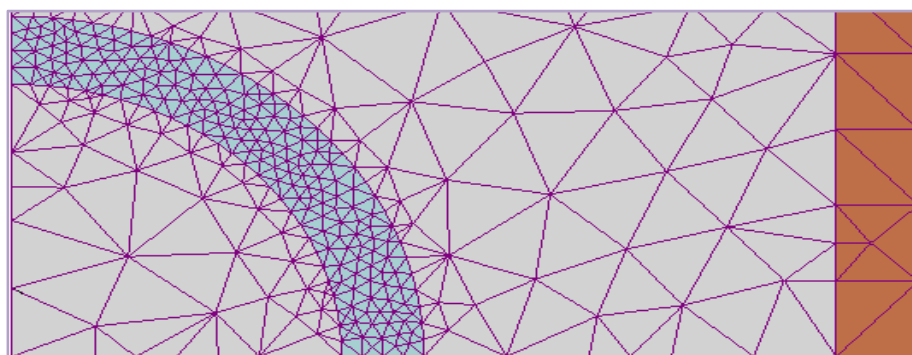


*Figure 2.16 Finite element method*



The key point in the development of accurate stress analyses of masonry constructions is the definition and the use of suitable constitutive laws. Taking into account the heterogeneity of the masonry material, the models proposed in literature can be divided three different classes concerning their grade of definition: i) micro-modeling; ii) multi-scale modeling; iii) macro-modelling.

**Micro-models** simulate each constituent of the masonry material with its own specific constitutive law and failure criteria. Micro-models can be detailed or simplified<sup>17</sup>. In the first case, the unit and the mortar are constituted by continuum elements, while the unit-mortar interface is represented by discontinuous elements (*figure 2.17*). In the second case, mortar and brick/mortar interface are combined in a single discontinuous joint element, so it is possible to consider masonry as a set of elastic blocks bonded together by potential fracture line.

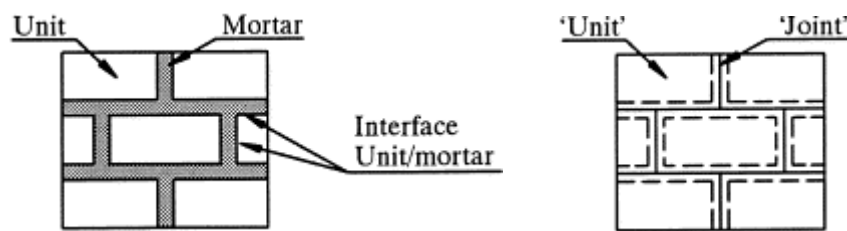


**Figure 2.17** Modelling strategies for masonry: i) detailed micro-modeling; ii) simplified micro-modeling

The mechanical properties of elements that characterize the micro-model can be obtained through experimental tests<sup>18</sup> conducted on the single material components. The principal disadvantage of the micro-models is that requires a highly refined mesh and a great computational effort. In fact both the unit blocks and the mortar beds have to be discretized, obtaining a high number of nodal unknowns. Nevertheless, this model is the most suitable to reproduce laboratory tests.

**Multi-scale models** consider firstly different constitutive laws for the units and the mortar joints; then, a homogenization procedure is performed obtaining a macro-model for masonry which is used to develop the structural analysis. To explain the Multi-scale analysis, the model developed by Brasile<sup>19</sup> is one the most significant. In this case, the strategy is based on an

<sup>17</sup> Lourenco P. B., Computational Strategies for Masonry Structures, PhD thesis, Delft University of Technology, 1996

<sup>18</sup> Compressive test, tension test, bending test..ect

<sup>19</sup> Brasile S. , Casciaro R. , Formica G. , " Multilevel approach for brick masonry walls". *Computer methods in applied mechanics and engineering*, 2007, Vol. 196

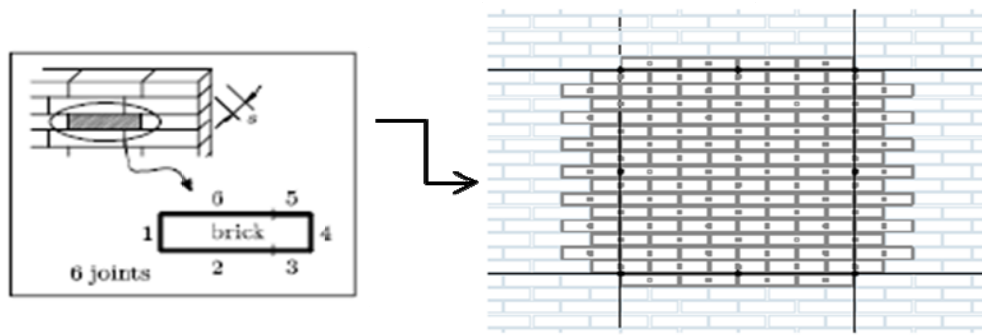


**Figure 2.18 Multi-scale Models**

iterative scheme, which uses simultaneously two different modeling of masonry. The first one is defined at the scale of the local brick and joint and describes their nonlinear mechanical interaction. The second one is defined at the global scale of the wall and looks like an approximation of the previous model. The passage from one scale to another is obtained through an operator, that is able to define the global displacements starting by local ones. Also in this case, the mechanical properties of units and mortar joints are obtained through experimental tests. The principle advantage of the multi-scale model is to derive in a rational way the stress-strain relationship of the masonry, taking into account the mechanical properties of each material component. On the other side, the non-linear homogenization procedure could induce some computational difficulties.

**Macro-model** is also called *homogeneous or continuous model* because it considers the masonry as a smeared continuum (figure 2.19), where there isn't a distinction between the

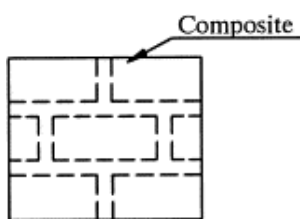


**Figure 2.19 Macro Model**

block and mortar joints. This model treats the masonry as anisotropic composite and uses constitutive laws to define the behavior of the masonry material, i.e. stress-strain relationship. This model could be unable to describe in a detailed way some mechanisms connected to the damage evolution, but it is very effective from a computational point

of view when structural analyses are performed. In fact it's the only method that can be used in presence of a large number of units and joints, without a more expensive computational effort.

In general, the finite element method applied to masonry arch bridges is mainly concentrated on global aspects rather than on local approaches. Today macro models use an isotropic homogenized failure surface similar to those developed for the analysis of concrete structures. Some of the most popular failure surfaces are shown in *Figure 2.20*.

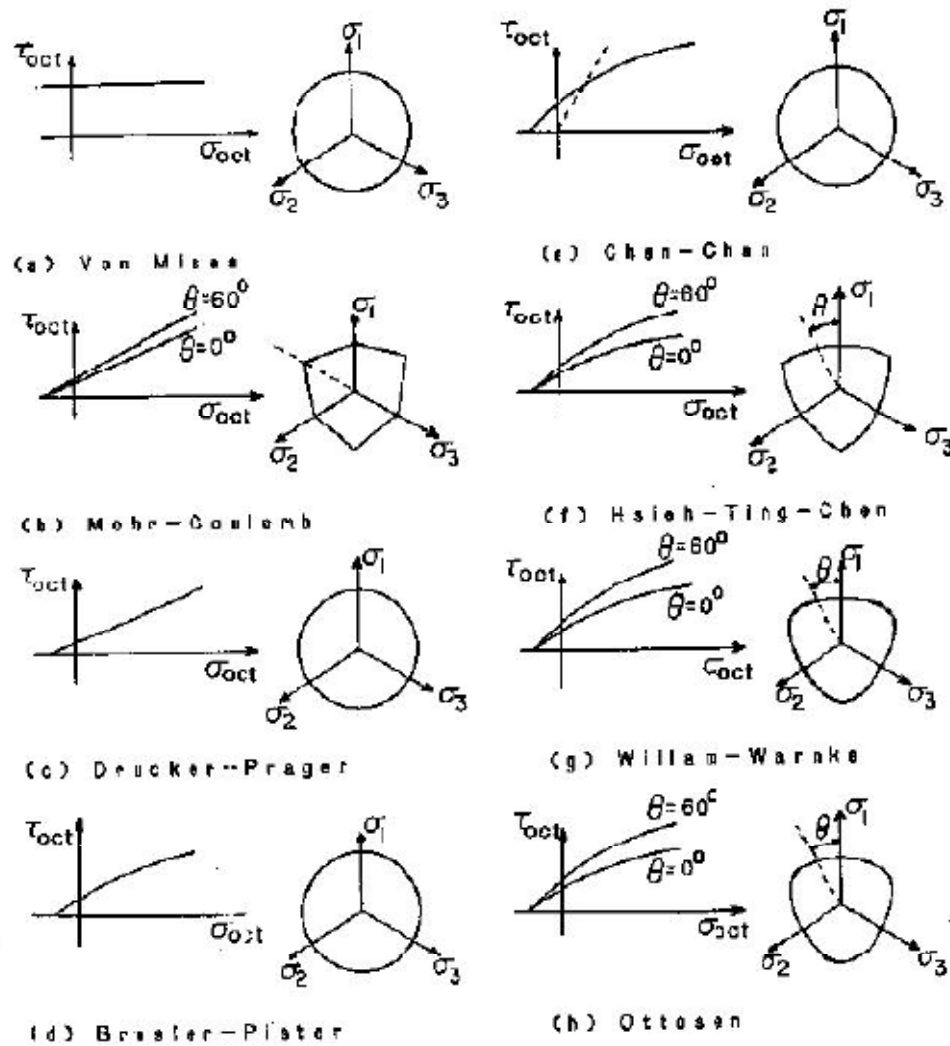
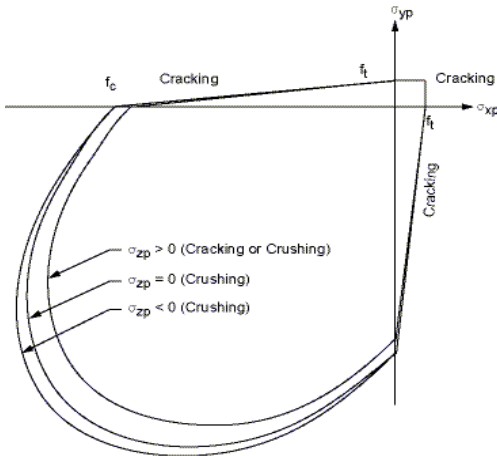


Figure 2.20 Chen. (1985) Failure criteria

The most simplified idea can be given by Rankine criterion, but more refined and more appropriated criteria for concrete-like materials limit surface is determined by William-Warnke criterion.

**William-Warnke Criterion<sup>20</sup>**. It's a criterion that is conceived to describe the concrete, but can also be applied to other brittle materials, as masonry. It is a good criterion, but is complicated because it uses five parameters. Cracking is modeled through an adjustment of the material properties and it is simulated through a "smeared band" of cracks, rather than discrete cracks.

<sup>20</sup> William, K. J., Warnke E. D. (1975). *Constitutive Model for the Triaxial Behavior of Concrete*. Proceedings, International Association for Bridge and Structural Engineering, ISMES. Bergamo, Italy, ISMES. Vol. 19: 174.



**Figure 2.21 William-Warnke Criterion.**  
**Failure domain for plane stress states**

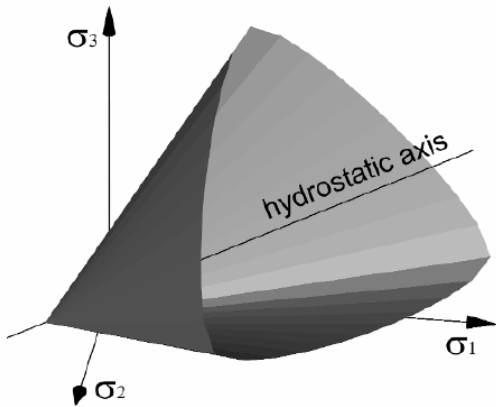


**Figure 2.22 William-Warnke Criterion.**  
**Failure domain for tridimensional stress states**

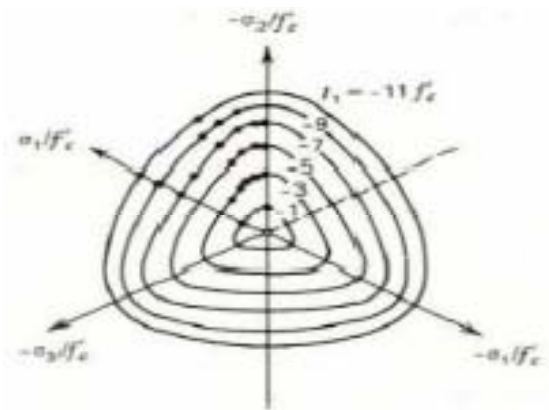


**Figure 2.23 William-Warnke Criterion.**  
**Deviatoric Plane**

The smeared crack model allows the crack opening in three orthogonal directions for every point of integration. The complex behavior of masonry is assumed to be isotropic before cracking and ortotropic after cracking. The failure criterion for a multi-axial stress state is represented by the following relation:

$$\frac{F}{f_c} - S \geq 0$$

Where  $F$  is a function of the principal stress state,  $S$  is the failure surface expressed in terms of the principal stresses and of the five parameters  $f_t$ ,  $f_c$ ,  $f_{cb}$ ,  $f_1$ ,  $f_2$ . In particular  $f_t$  and  $f_c$  are the values of the uniaxial tension strength and the uniaxial compression strength.  $f_{cb}$  is the value of the biaxial compression strength.  $f_1$  and  $f_2$  represent the values of compression strength in presence of a hydrostatic stress state, respectively under biaxial and uniaxial regime. So cracking occurs when the tensile stress exceeds the limit value (Rankine criterion), while the crushing takes place when all of the principal stresses are compressive and exceed the limit value. Failure domain for biaxial and tridimensional stress state are represented in figures 2.21 e 2.22.

The meridians of tension and compression are respectively two paraboles. They are connected by an ellipsoidal surface, passing through the elliptical deviatoric curve as base section.

### Backfill Modelling

Also the backfill can be modeled through additional elements that allow the transfer of loads and passive reactions on the arch barrel. Different constitutive models have been proposed for soils modeling. The differences are based on the shape of the yield surface in the meridian plane, the shape of yield surfaces in the deviatoric stress plane and the use of flow rules. The material of the soil is considered usually nonlinear and is defined by Mohr-Coloumb or Drucker-Prager limit criteria.

**Mohr-Coulomb Criterion.** It is the best known failure criterion in soil mechanics. It is the first type of failure criterion that takes into consideration the effect of the hydrostatic pressure on the strength of granular materials. This criterion states:

$$|\tau| = c - \sigma \cdot \tan \varphi$$

where  $\tau$  is the shear stress,  $\sigma$  is the normal stress<sup>21</sup>;  $c$  and  $\varphi$  are the cohesion and the angle of internal friction. Coulomb's failure surface is an irregular hexagonal pyramid in the principal stress space (figure 2.25).

**Drucker-Prager Criterion**<sup>22</sup>. This criterion, formulated in 1952, represents the major advance in the extension of metal plasticity to soil plasticity. It is the approximate expression

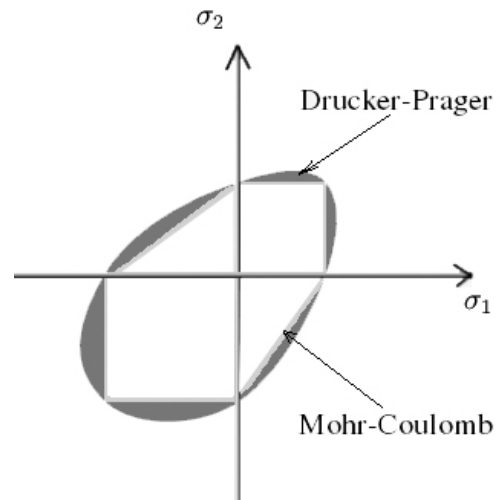


Figure 2.24 Drucker-Prager Criterion. Failure domain for plane stress states

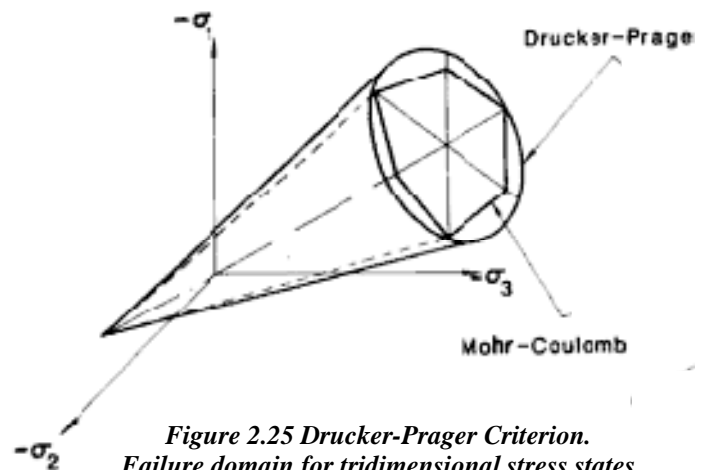


Figure 2.25 Drucker-Prager Criterion. Failure domain for tridimensional stress states

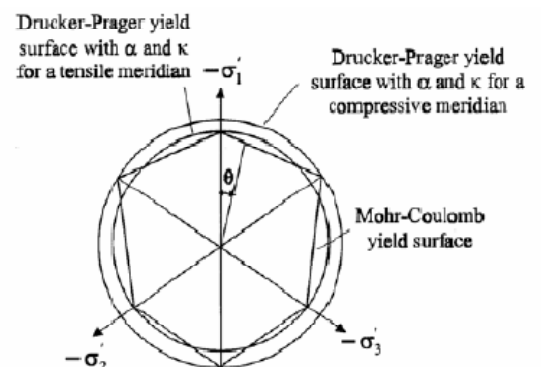


Figure 2.26 Drucker-Prager Criterion. Deviatoric Plane

<sup>21</sup> Compressive stress as a negative quantity and tensile stress as a positive quantity.

<sup>22</sup> Drucker, D. C. and Prager, W. (1952). *Soil mechanics and plastic analysis for limit design*. Quarterly of Applied Mathematics, vol. 10, no. 2, pp. 157–165

of the Mohr-Coulomb criterion. The aim was to overcome the problem of Mohr-Coulomb criterion, that the gradient of the plasticization function was not defined in a univocal way on the pyramid corners. Drucker-Prager Criterion provides as failure surface a cone whose axis is the hydrostatic axis (*figure 2.25*). This cone can be inscribed or circumscribed the hexagonal pyramid of Mohr-Coulomb Criterion, depending on the values of the constants  $\alpha$ ,  $k$ . The failure criterion can be represented by the following relation:

$$f(I_1, J_2) = -\alpha I_1 + \sqrt{J_2} - k = 0$$

where  $I_1$  is the first invariant of the stress tensor,  $J_2$  is the second invariant of deviatoric stress tensor.  $\alpha$  and  $k$  are material constants, determined from experiments. When  $\alpha$  is equal to zero, the Drucker-Prager criterion is reduced to the Von Mises criterion. In fact the first criterion represents an extension of the second one with the addition of the influence of a hydrostatic pressure in failure.

In finite element method, it is more convenient to use Drucker-Prager criterion than Mohr-Coulomb criterion. In fact the Mohr-Coulomb hexagonal failure surface is mathematically convenient only in problems where it is obvious which one of six sides is to be used. If this information is not known in advance, the corners of the hexagon can cause considerable difficulties and give rise to complications in obtaining a numerical solution with the finite element models.

### **Computer Based Application: ANSYS, ABAQUS, DIANA**

Also the finite element method comprises computer-based representations. They are specialized ready-to-use computer programs that can be applied to masonry arches as to other type of structures. Computer FEM systems used to analyze the masonry structures are ABAQUS<sup>23</sup> or DIANA<sup>24</sup> often with self-implemented user codes to these applications. But there are other ones.

For example, in 1999 Ng et al<sup>25</sup> used a FEM commercial package nonlinear, LUSAS<sup>26</sup>, with a two-dimensional model to analyze a series of arch bridges. In this case, masonry is

---

<sup>23</sup> Abaqus FEA (formerly ABAQUS) is a suite of software applications for finite element analysis and computer aided engineering, originally released in 1978. [www.simulia.com](http://www.simulia.com)

<sup>24</sup> [Tnodiana.com](http://Tnodiana.com)

<sup>25</sup> Ng K., Fairfield C., Sibbad A. (1999). *Finite-element analysis of masonry arch bridges*, Proceedings of the Institution of Civil Engineers: Structures and Buildings, Vol. 134, pp. 119-127

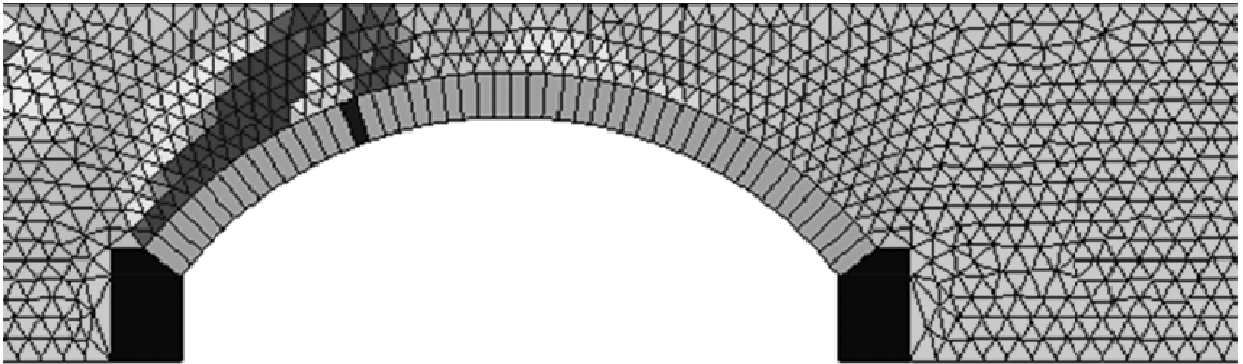


*Figure 2.27 Bidimensional Model*

characterized as Von Mises material with different strengths in tension and compression. The authors study the structure behavior, varying a series of parameters. They conclude that the values of the Young modulus of elasticity can not have effect on the arch collapse.

In 2001 Fanning et al<sup>27</sup> generate three-dimensional nonlinear finite element models, using a commercially available finite element package, ANSYS<sup>28</sup>. The masonry behavior is modeled using a solid element that can have its stiffness modified by the development of cracks and crushing. The fill is modeled as a Drucker–Prager material. Analysis enables good predictions of the actual behavior of a masonry arch bridge.

Depending on the accuracy required, the finite element model of a masonry arch can be two-dimensional or three-dimensional. More complex approaches are necessary for considering some types of defects but on the other hand often increasing the element dimension does not gives any additional information. It is therefore important to try to get a good balance between the element dimension and the calculation time.

In this thesis, only two-dimensional finite element modeling will be considered in order to have results comparable with the other methods treated (Thrust Line Analysis and Mechanism Methods). Three dimensional modeling in FEM is very important to model the whole structure, but requires a very high computational effort. Through two-dimensional modeling, it is possible to study the structure in the plane more quickly and to have a first idea of its behavior.

Two dimensional finite element model of a masonry arch bridge can be discretized in different ways, as just explained. *Figure 2.28* shows the different approaches that can be used: a) macro-modelling with an only homogeneous material; b) and c) simplified micro-modeling,

<sup>26</sup> [www.lusas.com](http://www.lusas.com)

<sup>27</sup> Fanning, P. J., and Boothby, T. E. (2001). “Three-dimensional modeling and full-scale testing of stone arch bridges.” *Comput. Struct.*, 79, 2645–2662.

<sup>28</sup> [www.ansys.com](http://www.ansys.com)

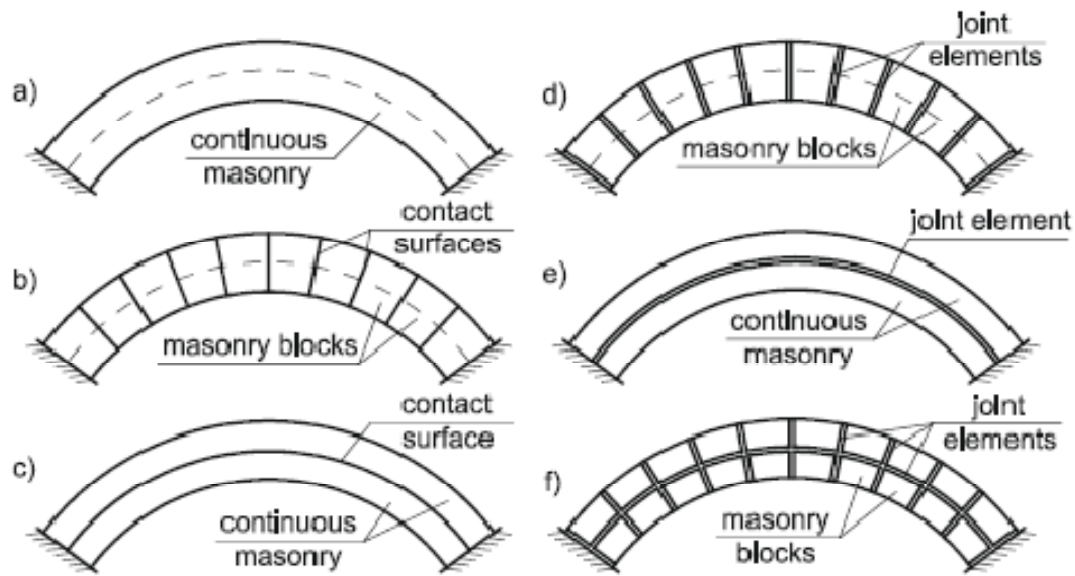


**Figure 2.28 Various Type of Discretization: a) macro-modelling; b) and c) simplified micro-modeling; d), e) and f) detailed micro-modeling**

that enable the detachment of adjacent parts simulating cracks; d), e) and f) detailed micro-modeling, where units, mortar and unit-mortar interface are modeled separately.

There are also different models that can be used to describe the masonry behavior: i) elastic; ii) elastic NRT; iii) elasto-plastic; iv) elasto plastic NRT; v) elasto-brittle NRT. Obviously linear elastic behavior is used mainly in the pre-failure behavior.

The next paragraph will deal with a particular elasto-plastic model developed by some Belgian researchers in the last years. It is very interesting to study the progressive opening of the different hinges.



## 2.6 Elasto-Plastic Model

The last paragraph of this chapter will deal with a particular closed form solution derived by some Belgian researchers<sup>29</sup> for the structural stability of arch bridges. Also this approach is based on the fundamental theorems of limit analysis and employs a simplified homogeneous material model<sup>30</sup> to determine the critical points with a relatively small modeling effort.

Firstly, a basic model is presented starting from the equilibrium equations. The geometry of the arch is described by the angle  $\theta$ , the radius of the centerline  $r(\theta)$ , the thickness of the arch barrel  $b(\theta)$ , the height of the backfill  $h$ , and the width of the arch  $B$ , as shown in *figure 2.29*. After solving the differential equilibrium equations, the analytical expressions for the internal forces are derived as a function of three constants of integration. To obtain an univocal solution, boundary conditions must be introduced. These equations are used to determine the three constants of integration, starting from the value of the abutment displacements. In this way it is possible to determine also the displacements in every point of the arch.

Then the material properties can be added to allow the occurrence of cracks and the subsequent formation of the hinges. The elasto-plastic model assumes a hinge to behave in a perfect plastic manner. The load factor is increased until a hinge has been formed and the boundary conditions are changed so the moment in the hinge stays constant. The process is repeated until the formation of the fourth hinge.

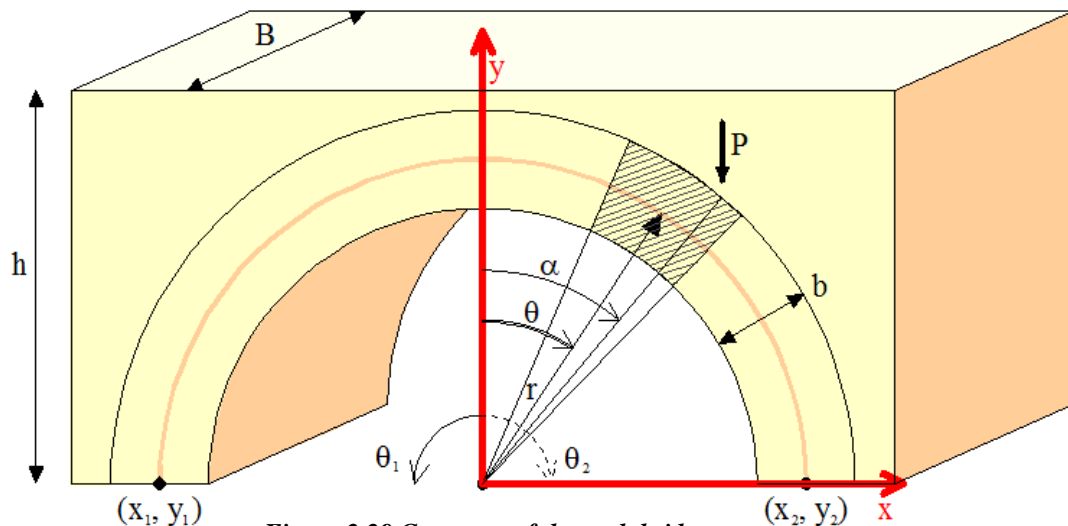


*Figure 2.29 Geometry of the arch bridge*

<sup>29</sup> Audenaert A., Peremans H. and De Wilde W.P. (2004), Static determination of the internal forces and displacement in arch bridges, *The masonry society Journal*, 22 (1), pp. 97-109

<sup>30</sup> Lourenco P. B., *Computational Strategies for Masonry Structures*, PhD thesis, Delft University, 1996

### a. Equilibrium equations

The first step is to derive the three equilibrium equations for an infinitesimal slice of the arch with an angular extent of  $d\theta$ , inclined from the vertical axis of the angle  $\theta$  (figure 2.30). The external forces that act on the infinitesimal piece are: in the radial direction  $F_r$ , and in the tangential direction  $F_\theta$ . To ensure the equilibrium of this infinitesimal element, the weight of this slice of arch  $W$  and the external forces applied on its extrados must be balanced by the internal forces and moments ( $N$ ,  $T$ ,  $M$ ). Thus, the equilibrium equations for normal force  $N$  (positive for tension stresses), shear force  $T$  (positive for clockwise rotation) and bending moment  $M$  (positive if the intrados fiber are compressed) were derived as follow:

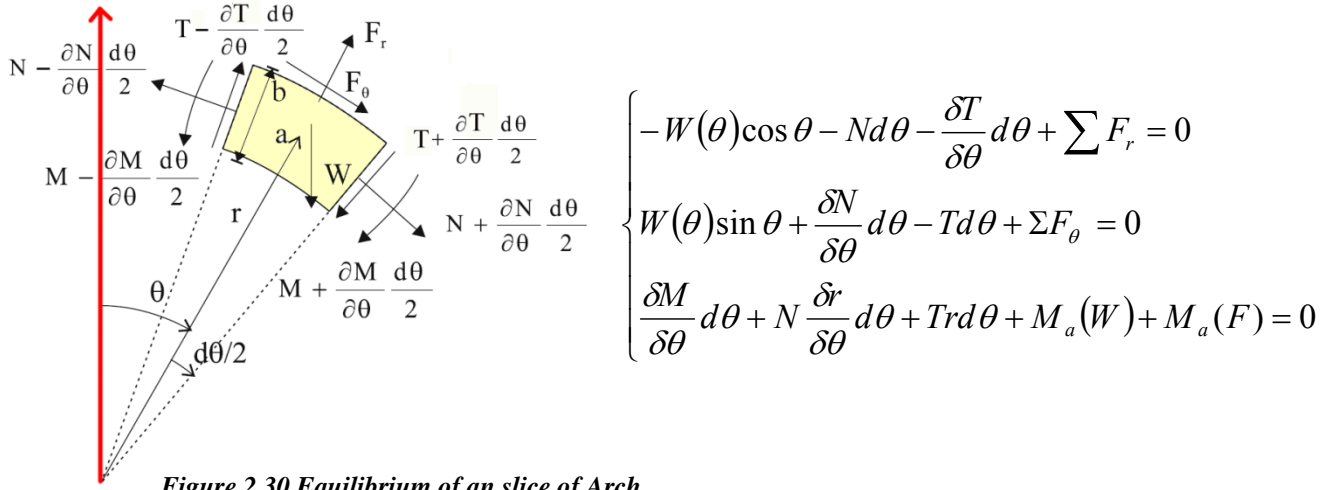


Figure 2.30 Equilibrium of an slice of Arch.

The terms  $M_a(W)$  and  $M_a(F)$  respectively indicate the moments of the resultant of the self weight and of the external forces, calculated in the pole  $a$ . The weight of the infinitesimal slice, of the filling and the external vertical point load can be expressed as a function of the angle  $\theta$  and of the position on the arch.

**Weight of an infinitesimal piece of Arch.** The self weight of this slice  $W(\theta)$  is expressed in function of: i) the radius  $r$ ; ii) the specific weight of the material  $\gamma$  [N/m<sup>3</sup>]; iii) the arch thickness  $b$ . It results from the subtraction of the triangular segment of arch with base =  $r - b/2$  to the bigger one with base =  $r + b/2$  (figure 2.31):

$$\begin{aligned} W &= \gamma \left[ \frac{1}{2} \left( r + \frac{b}{2} \right) \cdot \left( r + \frac{b}{2} \right) \cdot \sin d\theta \right] - \gamma \left[ \frac{1}{2} \left( r - \frac{b}{2} \right) \cdot \left( r - \frac{b}{2} \right) \cdot \sin d\theta \right] = \\ &= \frac{1}{2} \gamma \left[ \left( r + \frac{b}{2} \right)^2 d\theta - \left( r - \frac{b}{2} \right)^2 d\theta \right] = \frac{1}{2} \gamma [2rb] d\theta = \gamma b d\theta \end{aligned}$$

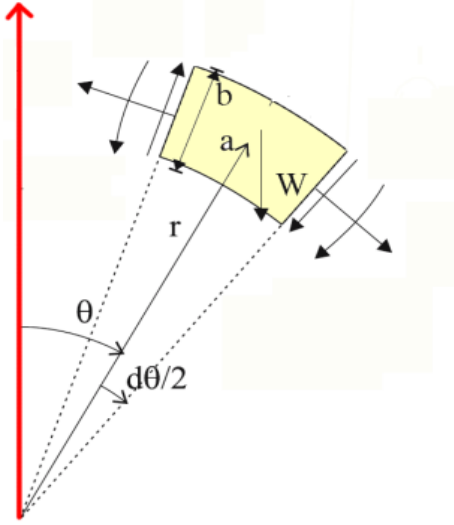


Figure 2.31 Weight of an slice of Arch.

Because the gravity center of the infinitesimal slice does not coincide usually with the pole, there will rise a moment ( $M_a(\theta)$ ) associated with the self weight  $W$ . The distance between the gravity center and the pole is called  $d$ .

$$d = r \frac{b^2}{12r^2}$$

$$M_a(\theta) = \gamma^3 \frac{\eta^3}{12} \sin \theta d \theta$$

Where  $\eta(\theta) = b(\theta) / r(\theta)$

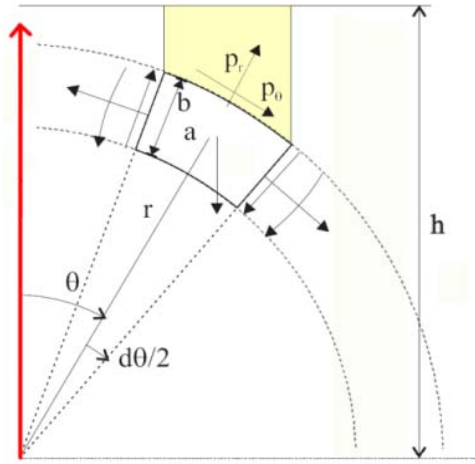


Figure 2.32 Distributed load resulting from backfill.

**Distributed load resulting from backfill.** The fill weight is a distributed load acting on the arch. The masonry arch bridges use a lot of filling above the arch to increase the dead load and prevent the formation of tensile stresses that occur when live loads move along the bridge. This load can be derived as a function of the height of the fill  $h$  and the specific weight of the fill  $\gamma_2$ . At first, the trapezoid area  $A_f$  (shown in figure 2.32) is determined.

$$A_f = \left[ \frac{(b_{\max} - b_{\min})}{2} \right] \cdot h$$

$$\text{Base } \frac{(b_{\max} - b_{\min})}{2} = h - \left[ r(\theta) + \frac{b(\theta)}{2} \right] \cos \theta$$

$$\begin{aligned} \text{Height } h &= \left( r + \frac{b}{2} \right) \left[ \sin \left( \theta + \frac{d\theta}{2} \right) \right] - \left( r + \frac{b}{2} \right) \left[ \sin \left( \theta - \frac{d\theta}{2} \right) \right] \\ &= d\theta \left( r + \frac{b}{2} \right) \end{aligned}$$

Then the trapezoid area is multiplied for the fill weight  $\gamma$  to obtain the total vertical load:

$$V(\theta) = \gamma_2 \left[ h - \left( r(\theta) + \frac{b(\theta)}{2} \right) \cos \theta \right] \left( r(\theta) + \frac{b(\theta)}{2} \right) d\theta \cos \theta$$

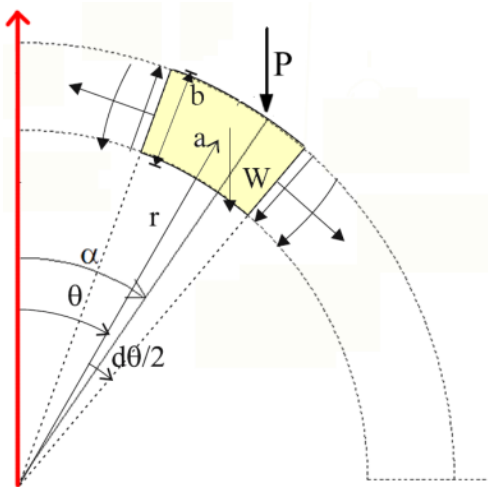


Figure 2.33 Concentrated load.

Finally, from the derivation of the vertical distributed load  $V(\theta)$  it is possible to define the contribution of the vertical load in the radial direction  $p_r d\theta$  and in tangential direction  $p_\theta d\theta$ :

$$p_r d\theta = -\gamma_2 \left[ h - \left( r(\theta) + \frac{b(\theta)}{2} \right) \cos \theta \right] \left( r(\theta) + \frac{b(\theta)}{2} \right) \cos^2 \theta \cdot d\theta$$

$$p_\theta d\theta = \gamma_2 \left[ h - \left( r(\theta) + \frac{b(\theta)}{2} \right) \cos \theta \right] \left( r(\theta) + \frac{b(\theta)}{2} \right) \cos \theta \sin \theta \cdot d\theta$$

**Concentrated load.** With regards to the concentrated load, it is assumed as mathematical model the following Dirac distribution:

$$\delta(\theta - \alpha) = 0, \quad \theta \neq \alpha$$

$$\int_{-\infty}^{+\infty} \delta(\theta - \alpha) d\theta = 1 \quad \theta = \alpha$$

It is clear that the distribution is zero in every point, with the only exception of the case  $(\theta = \alpha)$  where its value is defined implicitly by an integral expression. The concentrated load  $P$  applied at  $\theta = \alpha$  will be expressed as  $P\delta(\theta - \alpha)$ . The contribution of the concentrated load to the equilibrium equations is:

Component in radial direction:  $-P\delta(\theta - \alpha)\cos \theta d\theta$

Component in tangential direction:  $P\delta(\theta - \alpha)\sin \theta d\theta$

Moment respect to pole  $a$ :  $M_a(F) = P\delta(\theta - \alpha)[r(\alpha)\sin \alpha - r(\theta)\sin \theta]d\theta$

## b. Solving the equilibrium equations

Once the weight of the infinitesimal slice, of the filling and the external vertical point load are determined, it is possible to rewrite the equilibrium equations previously derived.

$$\begin{cases} -\gamma^2 \eta d\theta \cos \theta - Nd\theta - \frac{\delta T}{\delta \theta} d\theta - P\delta(\theta - \alpha)\cos \theta d\theta + p_r d\theta = 0 \\ \gamma^2 \eta d\theta \sin \theta + \frac{\delta N}{\delta \theta} d\theta - Td\theta + P\delta(\theta - \alpha)\sin \theta d\theta + p_\theta d\theta = 0 \\ \frac{\delta M}{\delta \theta} d\theta + N \frac{\delta r}{\delta \theta} d\theta + Trd\theta + \gamma^3 \frac{\eta^3}{12} \sin \theta d\theta + p_\theta d\theta \cdot \frac{b}{2} + P\delta(\theta - \alpha)[r(\alpha)\sin \alpha - r(\theta)\sin \theta]d\theta = 0 \end{cases}$$

Dividing all the above mentioned expressions for the term  $d\theta$ , makes possible to obtain the indefinite equilibrium equations for the slice of the arch as follows:

$$\begin{cases} -N - T' - \gamma r^2 \eta \cos \theta + p_r - P \delta(\theta - \alpha) \cos \theta = 0 \\ N' - T + \gamma r^2 \eta \sin \theta + p_\theta + P \delta(\theta - \alpha) \sin \theta = 0 \\ M' + Nr' + Vr + \gamma r^3 \frac{\eta^3}{12} \sin \theta + p_\theta \frac{b}{2} + P \delta(\theta - \alpha) [r(\alpha) \sin \alpha - r(\theta) \sin \theta] = 0 \end{cases}$$

In these equation, the derivative with respect to  $\theta$  is indicated by a prime while  $p_r$  is the radial component of the distributed force;  $p_\theta$  is the tangential component of the distributed force;  $\gamma$  is the specific weight of the arch masonry and  $\eta = b/r$ . In order to solve the three equations system, the equilibrium equation in the tangential direction has been derived:

$$N'' - T' + (\gamma r^2 \eta)' \sin \theta + \gamma r^2 \eta \cos \theta + p'_\theta + P \delta'(\theta - \alpha) \sin \theta + P \delta(\theta - \alpha) \cos \theta = 0$$

$$T' = N'' + (\gamma r^2 \eta)' \sin \theta + \gamma r^2 \eta \cos \theta + p'_\theta + P \delta'(\theta - \alpha) \sin \theta + P \delta(\theta - \alpha) \cos \theta$$

The last equation is substituted into the equilibrium equation in the radial direction, that becomes:

$$\begin{aligned} & -N - N'' - (\gamma r^2 \eta)' \sin \theta - \gamma r^2 \eta \cos \theta - p'_\theta - P \delta'(\theta - \alpha) \sin \theta - P \delta(\theta - \alpha) \cos \theta + \\ & - \gamma r^2 \eta \cos \theta + p_r - P \delta(\theta - \alpha) \cos \theta = 0 \end{aligned}$$

This quadratic equation can be rewritten as follow

$$N'' + N = q(\theta) - P \delta'(\theta - \alpha) \sin \theta - 2P \delta(\theta - \alpha) \cos \theta$$

where:  $q(\theta) = -(\gamma r^2 \eta)' \sin \theta - 2\gamma r^2 \eta \cos \theta - p'_\theta + p_r$

This function  $q(\theta)$  includes all the loads distributed in a continuous way that acts on the arch bridge, such as the self-weight and the weight of the filling. In order to determine the correct solution it is introduced the *unit step function*  $u_{step}(\theta - \alpha) = 0$

$$u_{step}(\theta - \alpha) = \begin{cases} 0, & \theta < \alpha \\ 1, & \theta \geq \alpha \end{cases}$$

Thus, the solution of this quadratic equation is in the form:

$$N(\theta) = [k_1 \sin \theta + k_2 \cos \theta] + N_p(\theta)$$

The term  $N_p(\theta)$  can be expressed as:

$$N_p(\theta) = u_1(\theta) \sin \theta + u_2(\theta) \cos \theta$$

$$\begin{aligned} \text{Where: } u_1(\theta) &= \int_0^\theta \cos \beta \cdot q(\beta) d\beta - P \left[ \int_0^\theta (\cos \beta \sin \beta \delta'(\beta - \alpha) + 2 \cos^2 \beta \delta(\beta - \alpha)) d\beta \right] \\ u_2(\theta) &= - \int_0^\theta \sin \beta \cdot q(\beta) d\beta - P \left[ \int_0^\theta (\sin^2 \beta \delta'(\beta - \alpha) + 2 \sin \beta \cos \beta \delta(\beta - \alpha)) d\beta \right] \end{aligned}$$

After simplification, these expressions became:

$$u_1(\theta) = \int_0^\theta \cos \beta \cdot q(\beta) d\beta - P u_{step}(\theta - \alpha); \quad u_2(\theta) = - \int_0^\theta \sin \beta \cdot q(\beta) d\beta$$

By inserting the values of  $u_1$ ,  $u_2$ , and  $N_p(\theta)$  in  $N(\theta)$  we obtain the analytical expressions of internal forces and moment, that are:

$$N(\theta) = k_1 \sin \theta + k_2 \cos \theta + \sin \theta \int_0^\theta \cos \beta q(\beta) d\beta - \cos \theta \int_0^\theta \sin \beta q(\beta) d\beta - P \sin \theta u_{step}(\theta - \alpha)$$

$$T(\theta) = k_1 \cos \theta - k_2 \sin \theta + \cos \theta \int_0^\theta \cos \beta q(\beta) d\beta + \sin \theta \int_0^\theta \sin \beta q(\beta) d\beta - P \cos \theta u_{step}(\theta - \alpha) + \gamma r^2 \eta \sin \theta + p_\theta$$

$$M(\theta) = k_3 - \int_0^\theta N(\beta) \cdot r' d\beta - \int_0^\theta T(\beta) \cdot r d\beta - \int_0^\theta \left[ \gamma r^3 \frac{\eta^3}{12} \sin \beta + p_\theta \frac{b}{2} \right] d\beta - P \int_0^\theta \delta(\beta - \alpha) [r(\alpha) \sin \alpha - r(\beta) \sin \beta] d\beta$$

So by resolving the differential equilibrium equations, the analytic equations of the internal forces and moment ( $N(\theta)$ ,  $V(\theta)$ , and  $M(\theta)$ ) are derived as a function of the constants  $k_1$ ,  $k_2$  and  $k_3$ . The constants are three because the fixed arch is three time hyperstatic. To find a univocal solution for the internal forces of the arch, it needs to introduce boundary conditions in the form of additional constraints.

### Boundary conditions

Bresse's equations<sup>31</sup> are introduced. These equations can be applied to calculate the vertical, horizontal and angular displacements of every point of the arch as a function of the displacement values of the boundary points. In particular, the displacements of the right abutment  $u_2$ ,  $v_2$  and  $\phi_2$  can be derived starting from the displacements of the left fixed abutment  $u_1$ ,  $v_1$  and  $\phi_1$  (figure 2.34):

$$\phi_2 = \phi_1 + \frac{1}{E} \int_{\theta_1}^{\theta_2} \frac{M}{I} \sqrt{r^2 + \left( \frac{\partial r}{\partial \theta} \right)^2} d\theta$$

$$u_2 = u_1 + (y_2 - y_1)\phi_1 + \frac{1}{E} \int_{\theta_1}^{\theta_2} \frac{N}{A} \frac{\partial x}{\partial \theta} d\theta + \frac{1}{E} \int_{\theta_1}^{\theta_2} (y_2 - y) \frac{M}{I} \sqrt{r^2 + \left( \frac{\partial r}{\partial \theta} \right)^2} d\theta$$

$$v_2 = v_1 - (x_2 - x_1)\phi_1 + \frac{1}{E} \int_{\theta_1}^{\theta_2} \frac{N}{A} \frac{\partial y}{\partial \theta} d\theta - \frac{1}{E} \int_{\theta_1}^{\theta_2} (x_2 - x) \frac{M}{I} \sqrt{r^2 + \left( \frac{\partial r}{\partial \theta} \right)^2} d\theta$$

where:  $u$  is the horizontal displacement;  $v$  is the vertical displacement;  $\phi$  is the rotation of the elastic line;  $A$  is the area of the cross-section;  $I$  is the rotational inertia of the cross section;  $E$  is the modulus of elasticity;  $x$  is the horizontal position coordinate; and  $y$  is the vertical position coordinate. The sign convention for the horizontal and vertical deflections are in accordance with the one used for the reference axis ( $x$ ;  $y$ ), while the angular deflection is assumed to be positive for clockwise rotations. The unique values of the three constants  $k_1$ ,  $k_2$  and  $k_3$  can be derived from the Bresse's equations only if the displacements and rotations in both the abutments are known.

Then  $N(\theta)$  and  $M(\theta)$  formulations can be inserted into the Bresse's equations, remembering that  $N(\theta)$ ,  $T(\theta)$ , and  $M(\theta)$  are linear functions of the constants  $k_1$ ,  $k_2$  e  $k_3$  and that all the operator applied to  $N(\theta)$  and  $M(\theta)$  in Bresse's equations are linear. The equations obtained can be written also in matrix notation, placing

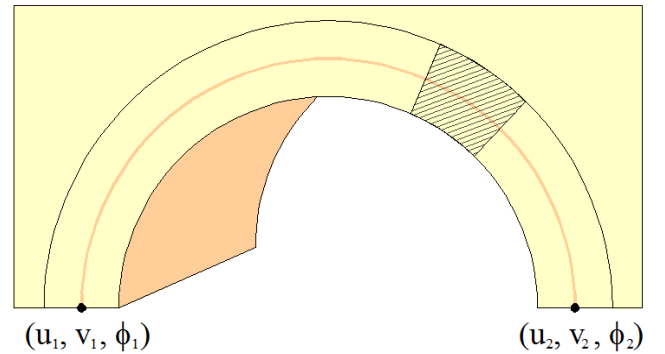


Figure 2.34 Deflections in the fixed supports

<sup>31</sup> Timoshenko S. P. (1953), *History of Strength of Materials*, New York, McGraw-Hill Book Co.

on the right side the terms containing the unknown constants  $k$ , and on the left side all known terms.

$$\bar{E} = A\bar{k}$$

$$\begin{bmatrix} E_{11} + E_{12}P \\ E_{21} + E_{22}P \\ E_{31} + E_{33}P \end{bmatrix} = \begin{bmatrix} a_{11} & a_{12} & a_{13} \\ a_{21} & a_{22} & a_{23} \\ a_{31} & a_{32} & a_{33} \end{bmatrix} \cdot \begin{bmatrix} k_1 \\ k_2 \\ k_3 \end{bmatrix}$$

If matrix  $A$  is non-singular matrix,  $k_1$ ,  $k_2$  e  $k_3$  can be determined uniquely. In Annex 2.1, Bresse's equations with the replacement of  $N(\theta)$  and  $M(\theta)$  formulations and the terms that composed matrix  $A$  and  $E$  are reported.

### Elastic-Plastic material properties

This analysis has not yet taken into account the mechanical characteristics of the material constituting the arch bridge. When considering a historic masonry structure, the influence of the crack rise and their development is a very important task that cannot be neglected for the success of the analysis. To simulate the behavior of the masonry, the following assumptions have been taken into account: i) on reaching a defined tensile strength  $\sigma_t$  a crack occurs; ii) on reaching a defined compressive strength  $\sigma_d$  the material behaves perfectly plastic; iii) for  $\sigma_d < \sigma < \sigma_t$  the material behaves linearly elastically.

Actually the tensile strength of masonry is much smaller than the compressive one, so it can be considered equal to zero, in accordance with Heyman's theory. Under this assumption, the possibilities of stress distributions are represented in *figure 2.35*, where  $x_f$  represents the height

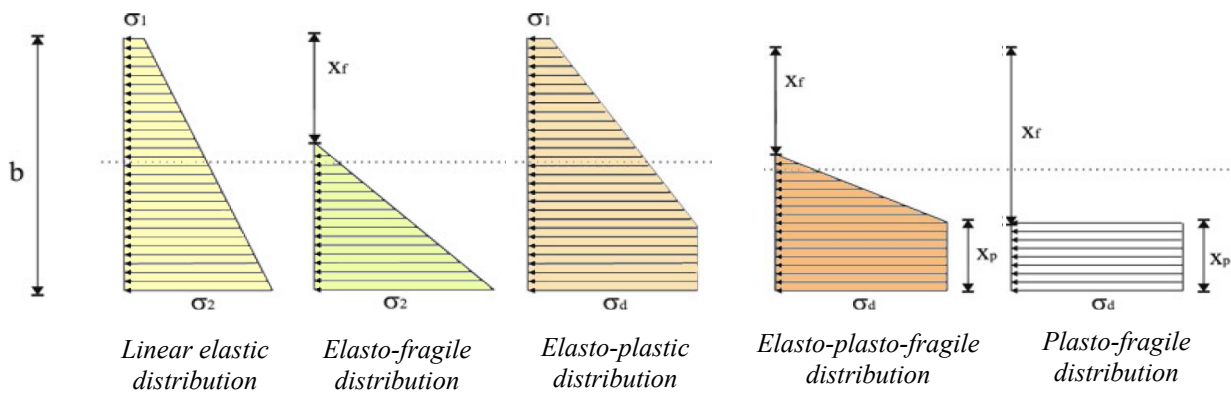


**Figure 2.35 Possible distribution of stress**



of the crack and  $x_p$  the height of the plastic section. Now the expressions of  $N(\theta)$  and  $M(\theta)$  can be normalized by introducing  $n_d(\theta)$  and  $m_d(\theta)$  respectively as:

$$n_d = \frac{N(\theta)}{-\sigma_d b}$$

$$m_d = \frac{M(\theta)}{-\sigma_d b^2}$$

where  $b$  represents height of the arch barrel. If we consider an  $(n_d ; m_d)$ -plane, each of the different stress distributions identifies a zone (Fig. 2.19.). The boundary surface of the diagram corresponds to the plasto-fragile distribution and to the formation of a plastic hinge.

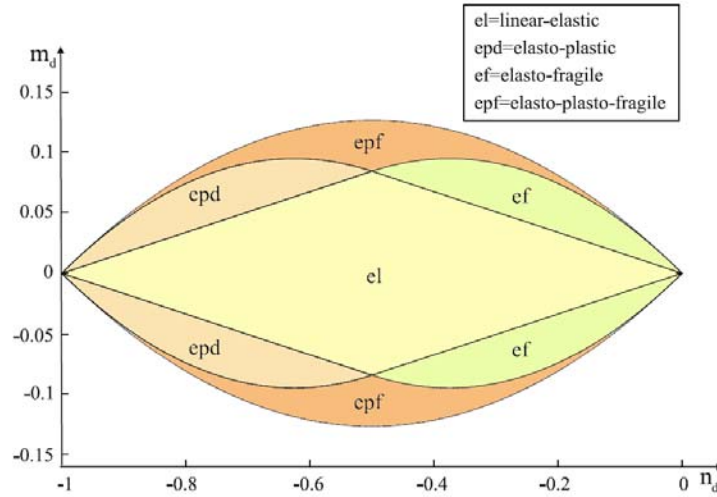


Figure 2.36 Envelope of the distribution of stress

**Definition of the boundary surface.** The boundary surface can be expressed by two expressions, one for the positive values of the moment (upper curve) and the other for the negative ones (lower curve), as following:

$$z_1 = m_d + 0.5n_d^2 + 0.5n_d$$

$$z_2 = -m_d + 0.5n_d^2 + 0.5n_d$$

The first condition, for which  $z_1$  or  $z_2$  is equal to zero, corresponds to the formation of the first plastic hinge.

**Construction of the Model**

The loading capacity of the arch is then studied as a function of the point load  $P$ . Assuming that both supports are fixed, the structure is statically indeterminate to the third degree of freedom and the collapse will happen as soon 4 hinges are formed. The first hinge appears for the smallest value of  $P$ , which gives rise to a normal force and a moment able to satisfy the relationship above. The corresponding angle  $\theta$  identifies the position of the first hinge. The process is repeated until the fourth hinge is formed. The equilibrium equations remain the same, only the boundary conditions change.

## **Annex 2.A**

---

### Bresse's equations with the replacement of $N(\theta)$ and $M(\theta)$ formulations

i) Bresse's First Equation.....	p. 51
ii) Bresse's Second Equation.....	p. 53
iii) Bresse's Third Equation.....	p. 55
iv) Matrix A.....	p. 57



## Bresse's First Equation

**The replacement of  $N(\theta)$  and  $M(\theta)$  formulations in Bresse's equations:**

$$\begin{aligned} \varphi_2 = \varphi_1 + \frac{1}{E} \int_{\theta_1}^{\theta_2} \{ & k_3 + \\ & - \int_0^\theta \left[ k_1 \sin \xi + k_2 \cos \xi + \sin \xi \int_0^\xi \cos \beta q(\beta) d\beta - \cos \xi \int_0^\xi \sin \beta q(\beta) d\beta - P \sin \xi u_{step}(\xi - \alpha) \right] \cdot r' d\xi \\ & - \int_0^\theta \left[ k_1 \cos \xi - k_2 \sin \xi + \cos \xi \int_0^\xi \cos \beta q(\beta) d\beta + \sin \xi \int_0^\xi \sin \beta q(\beta) d\beta - P \cos \xi u_{step}(\xi - \alpha) + \right. \\ & \left. + \gamma^2 \eta \sin \xi + p_\theta \right] \cdot r d\xi - \int_0^\theta \left[ \gamma^3 \frac{\eta^3}{12} \sin \xi + p_\theta \frac{b}{2} \right] d\xi + \\ & \left. - P \int_0^\theta \delta(\xi - \alpha) [r(\alpha) \sin \alpha - r(\xi) \sin \xi] d\xi \right\} \cdot \frac{1}{I} \sqrt{r^2 + \left( \frac{\partial r}{\partial \theta} \right)^2} d\theta \end{aligned}$$

**Matrix notation:**

$$\begin{bmatrix} E_{11} + E_{12}P \\ E_{21} + E_{22}P \\ E_{31} + E_{33}P \end{bmatrix} = \begin{bmatrix} a_{11}a_{12}a_{13} \\ a_{21}a_{22}a_{23} \\ a_{31}a_{32}a_{33} \end{bmatrix} \cdot \begin{bmatrix} k_3 \\ k_2 \\ k_1 \end{bmatrix}$$

**Bresse's First Equation Terms:**

$$\begin{aligned} E_{11} &= \varphi_2 - \varphi_1 + \frac{1}{E} \int_{\theta_1}^{\theta_2} \left( \int_0^\theta [f_{11}(\xi) + f_{21}(\xi) + f_{31}(\xi)] d\xi \right) \cdot \frac{1}{I} \sqrt{r^2 + \left( \frac{\partial r}{\partial \theta} \right)^2} d\theta \\ E_{12} &= \frac{1}{E} \int_{\theta_1}^{\theta_2} \left( \int_0^\theta [f_{12}(\xi) + f_{22}(\xi) + f_{32}(\xi)] d\xi \right) \cdot \frac{1}{I} \sqrt{r^2 + \left( \frac{\partial r}{\partial \theta} \right)^2} d\theta \end{aligned}$$

where:

$$f_{11}(\xi) = \left[ \cos \xi \int_0^\xi \cos \beta q(\beta) d\beta + \sin \xi \int_0^\xi \sin \beta q(\beta) d\beta + \gamma r^2 \eta \sin \xi + p_\theta \right] \cdot r$$

$$f_{21}(\xi) = \left[ \sin \xi \int_0^\xi \cos \beta q(\beta) d\beta - \cos \xi \int_0^\xi \sin \beta q(\beta) d\beta \right] \left( \frac{\partial r}{\partial \xi} \right)$$

$$f_{31}(\xi) = p_\theta \frac{b}{2} + \gamma r^3 \frac{\eta^3}{12} \sin \xi$$

$$f_{12}(\xi) = -\cos \xi u_{step}(\xi - \alpha) \cdot r$$

$$f_{22}(\xi) = -\sin \xi u_{step}(\xi - \alpha) \cdot \left( \frac{\partial r}{\partial \xi} \right)$$

$$f_{32}(\xi) = \delta(\xi - \alpha) |r(\alpha) \sin \alpha - r(\xi) \sin \xi|$$

## Bresse's Second Equation

**The replacement of  $N(\theta)$  and  $M(\theta)$  formulations in Bresse's equations:**

$$\begin{aligned}
 u_2 = u_1 + (y_2 - y_1)\varphi_1 + \frac{1}{E} \int_{\theta_1}^{\theta_2} & \left[ k_1 \sin \theta + k_2 \cos \theta + \sin \theta \int_0^\theta \cos \xi q(\xi) d\xi - \cos \theta \int_0^\theta \sin \xi q(\xi) d\xi + \right. \\
 & \left. - P \sin \theta u_{step}(\theta - \alpha) \right] \frac{\partial x}{A \partial \theta} d\theta + \frac{1}{E} \int_{\theta_1}^{\theta_2} \{ k_3 + \\
 & - \int_0^\theta \left[ k_1 \sin \xi + k_2 \cos \xi + \sin \xi \int_0^\xi \cos \beta q(\beta) d\beta - \cos \xi \int_0^\xi \sin \beta q(\beta) d\beta - P \sin \xi u_{step}(\xi - \alpha) \right] \cdot r' d\xi \\
 & - \int_0^\theta \left[ k_1 \cos \xi - k_2 \sin \xi + \cos \xi \int_0^\xi \cos \beta q(\beta) d\beta + \sin \xi \int_0^\xi \sin \beta q(\beta) d\beta - P \cos \xi u_{step}(\xi - \alpha) + \right. \\
 & \left. + \gamma^2 \eta \sin \xi + p_\theta \right] \cdot r d\xi - \int_0^\theta \left[ \gamma^3 \frac{\eta^3}{12} \sin \xi + p_\theta \frac{b}{2} \right] d\xi + \\
 & \left. - P \int_0^\theta \delta(\xi - \alpha) [r(\alpha) \sin \alpha - r(\xi) \sin \xi] d\xi \right\} \cdot \frac{(y_2 - y)}{I} \sqrt{r^2 + \left( \frac{\partial r}{\partial \theta} \right)^2} d\theta
 \end{aligned}$$

**Matrix notation:**

$$\begin{bmatrix} E_{11} + E_{12}P \\ E_{21} + E_{22}P \\ E_{31} + E_{33}P \end{bmatrix} = \begin{bmatrix} a_{11}a_{12}a_{13} \\ a_{21}a_{22}a_{23} \\ a_{31}a_{32}a_{33} \end{bmatrix} \cdot \begin{bmatrix} k_3 \\ k_2 \\ k_1 \end{bmatrix}$$

**Bresse's Second Equation Terms:**

$$\begin{aligned}
 E_{21} = u_2 - u_1 - (y_2 - y_1)\varphi_1 + \\
 - \frac{1}{E} \int_{\theta_1}^{\theta_2} & \left[ f_{41}(\theta) \frac{\partial x}{A \partial \theta} - \left( \int_0^\theta [f_{11}(\xi) + f_{21}(\xi) + f_{31}(\xi)] d\xi \right) \frac{y_2 - y}{I} \sqrt{r^2 + \left( \frac{\partial r}{\partial \theta} \right)^2} \right] d\theta \\
 E_{22} = - \frac{1}{E} \int_{\theta_1}^{\theta_2} & \left[ f_{42}(\theta) \frac{\partial x}{A \partial \theta} - \left( \int_0^\theta [f_{12}(\xi) + f_{22}(\xi) + f_{32}(\xi)] d\xi \right) \frac{y_2 - y}{I} \sqrt{r^2 + \left( \frac{\partial r}{\partial \theta} \right)^2} \right] d\theta
 \end{aligned}$$

where:

$$f_{11}(\xi) = \left[ \cos \xi \int_0^\xi \cos \beta q(\beta) d\beta + \sin \xi \int_0^\xi \sin \beta q(\beta) d\beta + \mathcal{r}^2 \eta \sin \xi + p_\theta \right] \cdot r$$

$$f_{21}(\xi) = \left[ \sin \xi \int_0^\xi \cos \beta q(\beta) d\beta - \cos \xi \int_0^\xi \sin \beta q(\beta) d\beta \right] \left( \frac{\delta r}{\delta \xi} \right)$$

$$f_{31}(\xi) = p_\theta \frac{b}{2} + \mathcal{r}^3 \frac{\eta^3}{12} \sin \xi$$

$$f_{41}(\theta) = \sin \theta \int_0^\theta \cos \xi q(\xi) d\xi - \cos \theta \int_0^\theta \sin \xi q(\xi) d\xi$$

$$f_{12}(\xi) = -\cos \xi u_{step}(\xi - \alpha) \cdot r$$

$$f_{22}(\xi) = -\sin \xi u_{step}(\xi - \alpha) \cdot \left( \frac{\partial r}{\partial \xi} \right)$$

$$f_{32}(\xi) = \delta(\xi - \alpha) |r(\alpha) \sin \alpha - r(\xi) \sin \xi|$$

$$f_{42}(\theta) = -\sin \theta u_{step}(\theta - \alpha)$$



## Bresse's Third Equation

**The replacement of  $N(\theta)$  and  $M(\theta)$  formulations in Bresse's equations:**

$$\begin{aligned}
 v_2 = v_1 - (x_2 - x_1)\varphi_1 + \frac{1}{E} \int_{\theta_1}^{\theta_2} & \left[ k_1 \sin \theta + k_2 \cos \theta + \sin \theta \int_0^{\theta} \cos \xi q(\xi) d\xi - \cos \theta \int_0^{\theta} \sin \xi q(\xi) d\xi + \right. \\
 & - P \sin \theta u_{step}(\theta - \alpha) \left. \right] \frac{\partial y}{A \partial \theta} d\theta - \frac{1}{E} \int_{\theta_1}^{\theta_2} \{ k_3 + \\
 & - \int_0^{\theta} \left[ k_1 \sin \xi + k_2 \cos \xi + \sin \xi \int_0^{\xi} \cos \beta q(\beta) d\beta - \cos \xi \int_0^{\xi} \sin \beta q(\beta) d\beta - P \sin \xi u_{step}(\xi - \alpha) \right] \cdot r' d\xi + \\
 & - \int_0^{\theta} \left[ k_1 \cos \xi - k_2 \sin \xi + \cos \xi \int_0^{\xi} \cos \beta q(\beta) d\beta + \sin \xi \int_0^{\xi} \sin \beta q(\beta) d\beta - P \cos \xi u_{step}(\xi - \alpha) + \right. \\
 & + \left. r^2 \eta \sin \xi + p_{\theta} \right] \cdot r d\xi - \int_0^{\theta} \left[ r^3 \frac{\eta^3}{12} \sin \xi + p_{\theta} \frac{b}{2} \right] d\xi + \\
 & \left. - P \int_0^{\theta} \delta(\xi - \alpha) [r(\alpha) \sin \alpha - r(\xi) \sin \xi] d\xi \right\} \cdot \frac{(x_2 - x_1)}{I} \sqrt{r^2 + \left( \frac{\partial r}{\partial \theta} \right)^2} d\theta
 \end{aligned}$$

**Matrix notation:**

$$\begin{bmatrix} E_{11} + E_{12}P \\ E_{21} + E_{22}P \\ E_{31} + E_{33}P \end{bmatrix} = \begin{bmatrix} a_{11}a_{12}a_{13} \\ a_{21}a_{22}a_{23} \\ a_{31}a_{32}a_{33} \end{bmatrix} \cdot \begin{bmatrix} k_3 \\ k_2 \\ k_1 \end{bmatrix}$$

**Bresse's Third Equation Terms:**

$$\begin{aligned}
 E_{31} = v_2 - v_1 + (x_2 - x_1)\varphi_1 + \\
 - \frac{1}{E} \int_{\theta_1}^{\theta_2} \left[ f_{41}(\theta) \frac{\partial y}{A \partial \theta} + \left( \int_0^{\theta} [f_{11}(\xi) + f_{21}(\xi) + f_{31}(\xi)] d\xi \right) \frac{x_2 - x_1}{I} \sqrt{r^2 + \left( \frac{\partial r}{\partial \theta} \right)^2} \right] d\theta \\
 E_{32} = - \frac{1}{E} \int_{\theta_1}^{\theta_2} \left[ f_{42}(\theta) \frac{\partial y}{A \partial \theta} - \left( \int_0^{\theta} [f_{12}(\xi) + f_{22}(\xi) + f_{32}(\xi)] d\xi \right) \frac{x_2 - x_1}{I} \sqrt{r^2 + \left( \frac{\partial r}{\partial \theta} \right)^2} \right] d\theta
 \end{aligned}$$

where:

$$f_{11}(\xi) = \left[ \cos \xi \int_0^\xi \cos \beta q(\beta) d\beta + \sin \xi \int_0^\xi \sin \beta q(\beta) d\beta + \mathcal{r}^2 \eta \sin \xi + p_\theta \right] \cdot r$$

$$f_{21}(\xi) = \left[ \sin \xi \int_0^\xi \cos \beta q(\beta) d\beta - \cos \xi \int_0^\xi \sin \beta q(\beta) d\beta \right] \left( \frac{\partial r}{\partial \xi} \right)$$

$$f_{31}(\xi) = p_\theta \frac{b}{2} + \mathcal{r}^3 \frac{\eta^3}{12} \sin \xi$$

$$f_{41}(\theta) = \sin \theta \int_0^\theta \cos \xi q(\xi) d\xi - \cos \theta \int_0^\theta \sin \xi q(\xi) d\xi$$

$$f_{12}(\xi) = -\cos \xi u_{step}(\xi - \alpha) \cdot r$$

$$f_{22}(\xi) = -\sin \xi u_{step}(\xi - \alpha) \cdot \left( \frac{\partial r}{\partial \xi} \right)$$

$$f_{32}(\xi) = \delta(\xi - \alpha) |r(\alpha) \sin \alpha - r(\xi) \sin \xi|$$

$$f_{42}(\theta) = -\sin \theta u_{step}(\theta - \alpha)$$

## Matrix A

The Matrix A can be defined as follow:

$$A = \begin{bmatrix} a_{11} & a_{12} & a_{13} \\ a_{21} & a_{22} & a_{23} \\ a_{31} & a_{32} & a_{33} \end{bmatrix}$$

Where:

$$a_{11} = -\frac{1}{E} \int_{\theta_1}^{\theta_2} \left[ \int_0^\theta \sin \xi \left( \frac{\partial r}{\partial \xi} \right) d\xi + \int_0^\theta \cos \xi \cdot r d\xi \right] \cdot \frac{\sqrt{r^2 + \left( \frac{\partial r}{\partial \theta} \right)^2}}{I} d\theta$$

$$a_{12} = -\frac{1}{E} \int_{\theta_1}^{\theta_2} \left[ \int_0^\theta \cos \xi \left( \frac{\partial r}{\partial \xi} \right) d\xi - \int_0^\theta \sin \xi \cdot r d\xi \right] \cdot \frac{\sqrt{r^2 + \left( \frac{\partial r}{\partial \theta} \right)^2}}{I} d\theta$$

$$a_{13} = \frac{1}{E} \int_{\theta_1}^{\theta_2} \frac{\sqrt{r^2 + \left( \frac{\partial r}{\partial \theta} \right)^2}}{I} d\theta$$

$$a_{21} = \frac{1}{E} \int_{\theta_1}^{\theta_2} \left\{ \sin \theta \left( \frac{\partial x}{A \partial \theta} \right) - \left[ \int_0^\theta \sin \xi \left( \frac{\partial r}{\partial \xi} \right) d\xi + \int_0^\theta \cos \xi \cdot r d\xi \right] \cdot \frac{(y_2 - y)}{I} \cdot \sqrt{r^2 + \left( \frac{\partial r}{\partial \theta} \right)^2} \right\} d\theta$$

$$a_{22} = \frac{1}{E} \int_{\theta_1}^{\theta_2} \left\{ \cos \theta \left( \frac{\partial x}{A \partial \theta} \right) - \left[ \int_0^\theta -\sin \xi r d\xi + \int_0^\theta \cos \xi \cdot \left( \frac{\partial r}{\partial \xi} \right) d\xi \right] \cdot \frac{(y_2 - y)}{I} \cdot \sqrt{r^2 + \left( \frac{\partial r}{\partial \theta} \right)^2} \right\} d\theta$$

$$a_{23} = \frac{1}{E} \int_{\theta_1}^{\theta_2} \frac{(y_2 - y)}{I} \cdot \sqrt{r^2 + \left( \frac{\partial r}{\partial \theta} \right)^2} d\theta$$

$$a_{31} = \frac{1}{E} \int_{\theta_1}^{\theta_2} \left\{ \sin \theta \left( \frac{\partial y}{A \partial \theta} \right) + \left[ \int_0^{\theta} \cos \xi \cdot r \cdot d\xi + \int_0^{\theta} \sin \xi \cdot \left( \frac{\partial r}{\partial \xi} \right) d\xi \right] \cdot \frac{(x_2 - x)}{I} \cdot \sqrt{r^2 + \left( \frac{\partial r}{\partial \theta} \right)^2} \right\} d\theta$$

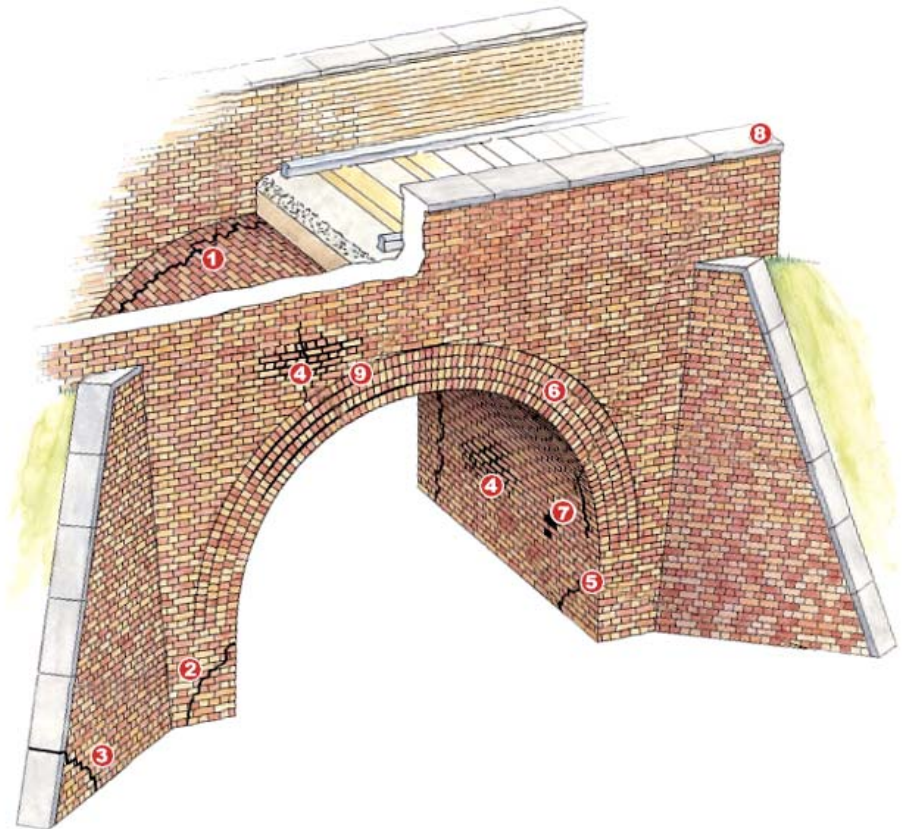
$$a_{32} = \frac{1}{E} \int_{\theta_1}^{\theta_2} \left\{ \cos \theta \left( \frac{\partial y}{A \partial \theta} \right) + \left[ \int_0^{\theta} -\sin \xi \cdot r \cdot d\xi + \int_0^{\theta} \cos \xi \cdot \left( \frac{\partial r}{\partial \xi} \right) d\xi \right] \cdot \frac{(x_2 - x)}{I} \cdot \sqrt{r^2 + \left( \frac{\partial r}{\partial \theta} \right)^2} \right\} d\theta$$

$$a_{33} = -\frac{1}{E} \int_{\theta_1}^{\theta_2} \frac{(x_2 - x)}{I} \cdot \sqrt{r^2 + \left( \frac{\partial r}{\partial \theta} \right)^2} d\theta$$

Chapter 3

## **Application to a Generic Masonry Arch Bridge**

---





### 3.1 SOMMARIO

*"Marco Polo descrive un ponte, pietra per pietra.*

*- Ma qual'è la pietra che sostiene il ponte? - chiede Kublai Kan.*

*- Il ponte non è sostenuto da questa o quella pietra, - risponde Marco, - ma dalla linea dell'arco che esse formano. Kublai Kan rimane silenzioso, riflettendo. Poi soggiunge: - Perché mi parli delle pietre? È solo dell'arco che m'importa. Polo risponde: - Senza pietre non c'è arco".*

Italo Calvino

Scopo di questa tesi è quello di confrontare fra di loro e valutare diversi metodi analitici e numerici per la verifica di ponti ad arco in muratura. La parte di valutazione è abbastanza difficile per via dei molti parametri materiali sconosciuti nei ponti esistenti. Prima di affrontare l'analisi di un ponte in muratura reale, in questo capitolo si analizzerà un ponte ad arco generico per dare una panoramica sull'utilizzo dei vari metodi. Per facilitare l'analisi, il ponte sarà caratterizzato da un arco a tutto sesto, incastrato alle estremità. Le proprietà materiali saranno ragionevolmente ipotizzate.

I metodi analizzati saranno quelli esposti nel capitolo 2: i) analisi limite attraverso la curva delle pressioni; ii) metodo dei meccanismi; iii) metodo agli elementi finiti. Per le suddette analisi, ci si avvarrà dei software descritti nel capitolo precedente. Per ultimo si applicherà anche il particolare approccio in forma chiusa, che sfrutta il modello materiale elasto-plastico: il vantaggio di questo approccio è quello di determinare i punti critici con uno sforzo computazionale relativamente basso e di evidenziare a quale carico corrisponda l'apertura di ogni cerniera. I vari metodi e modelli saranno confrontati fra di loro sulla base del carico limite ultimo e della posizione delle varie cerniere.

### 3.2 A Generic Arch Subjected to a Vertical Concentrated Load

The aim of this thesis is to compare and to evaluate different analytical and numerical methods to verify masonry arch bridges. The step of assessment is very difficult because many material parameters are unknown in existing structures. Before approaching the analysis of a real masonry bridge, this chapter will analyze a generic arch bridge to give a general overview on the use of various methods and different material models. To facilitate analysis, the bridge is characterized by a round arch. The material properties are reasonably hypothesized. The boundary conditions are assumed to be:

$$\varphi_1 = \varphi_2 = u_1 = u_2 = v_1 = v_2 = 0$$

where  $\varphi$ ,  $u$ ,  $v$  are the generalized displacements of the two supports<sup>1</sup>. The structure is statically determinate to the third degree and will collapse as soon the four hinges occur. A vertical concentrated point load  $P$ , applied at 0.75 (42.97°), and the weight of the backfill are imposed on the bridge.

The methods discussed are those described in chapter 2: i) Thrust Line Analysis Method, ii) Mechanism Method, iii) Finite Element Method. For the analyzes, the computer software described in the previous chapter will be used. Finally, the particular approach in closed form based on the elastic-plastic material model will be also be applied. The different methods and models will be compared with each other in terms of collapse load and the position of the four hinges.

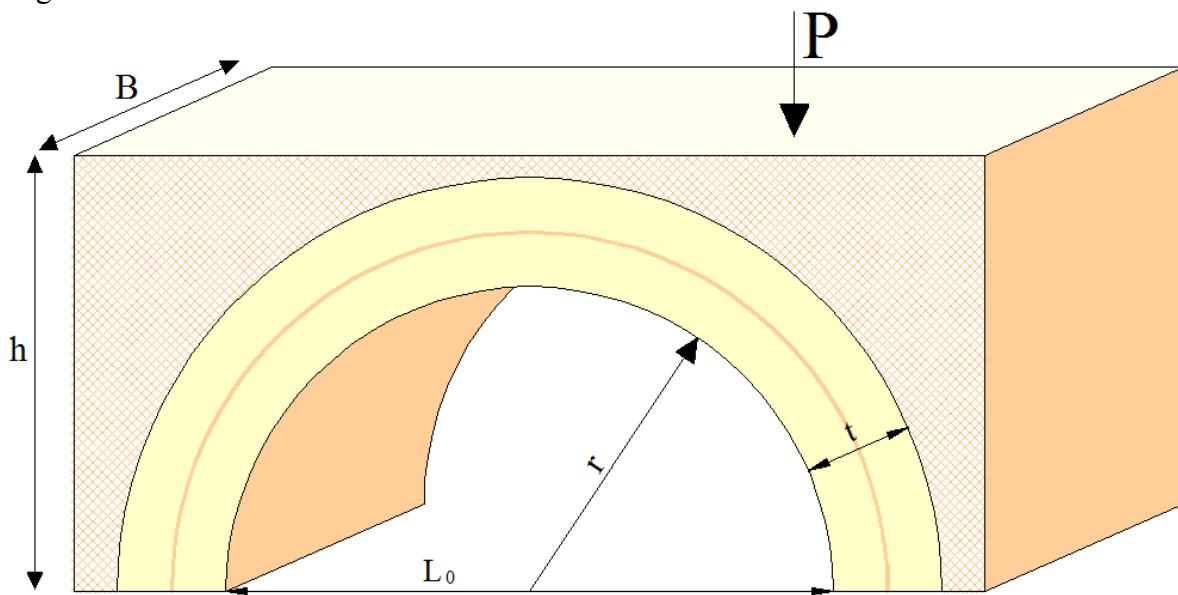


*Figure 3.1 Masonry arch under study*

<sup>1</sup> The subscript 1 stays for the left abutment; the subscript 2 stays for the right one.



The masonry arch bridge in exam has the following geometrical and material properties (as showed by *figure 3.1*):

**Basic Geometrical Parameters of the Arch:**

- Span  $L_0 = 2,80$  m;
- Radius  $r = 1,4$  m;
- Thickness of the Arch Barrel  $b = 0,5$  m;
- Height of the Backfill  $h = 2$  m;
- Width of the Arch  $B = 1$  m.

**Masonry data:**

The material is assumed to be homogeneous.

- Specific weight of the masonry arch  $\gamma = 21000$  N/m<sup>3</sup>;
- Young's Modulus = 5000 MPa;
- Poisson's ratio = 0,3;
- Compressive Strength of Masonry = 8 MPa.

**Backfill data:**

The material is assumed to be homogeneous.

- Specific weight of the backfill  $\gamma_2 = 21600$  N/m<sup>3</sup>;
- Young's Modulus = 15000 MPa;
- Poisson's ratio = 0.3;
- Angle of friction = 35°;
- Cohesion = 0.001;
- Angle of dilatency = 35°.

### 3.3 Archie-M and Ring

The software chosen to simulate the analysis of the generic masonry arch bridge through the Thrust Line Analysis Method and the Mechanism Method are Archie-M 2.4.1 and RING 3.0. Both the programs are based on the principles of the Limit Analysis: Archie-M uses the lower bound (static) theorem, while Ring uses the upper bound (kinematic) theorem.

Both the programs require as material input:

- For Masonry: unit weight ( $\text{KN/m}^3$ ) and compressive strength (MPa). In Archie-M, the upper limit for masonry compressive strength is 30 Mpa.
- For Backfill: unit weight ( $\text{KN/m}^3$ ) and angle of friction (degree). Ring requires also the value of the backfill cohesion, Archie-M not.

In both cases, the arch is divided into fourty blocks. The same type of load has been chosen for the analyzes with the two programs: it's a *1KN single Axle Load*.

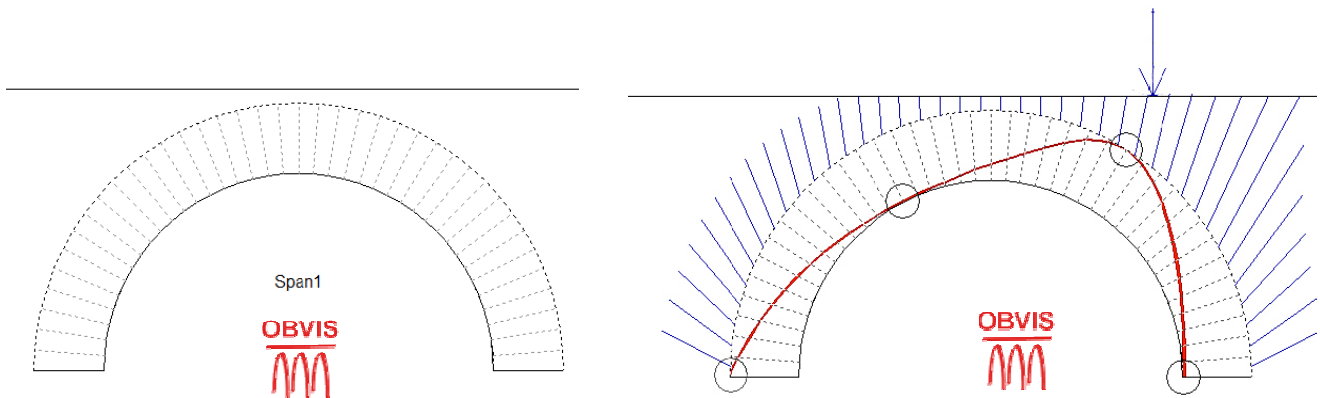


Figure 3.2 Analysis with the Thrust Analysis Method (Archie-M)

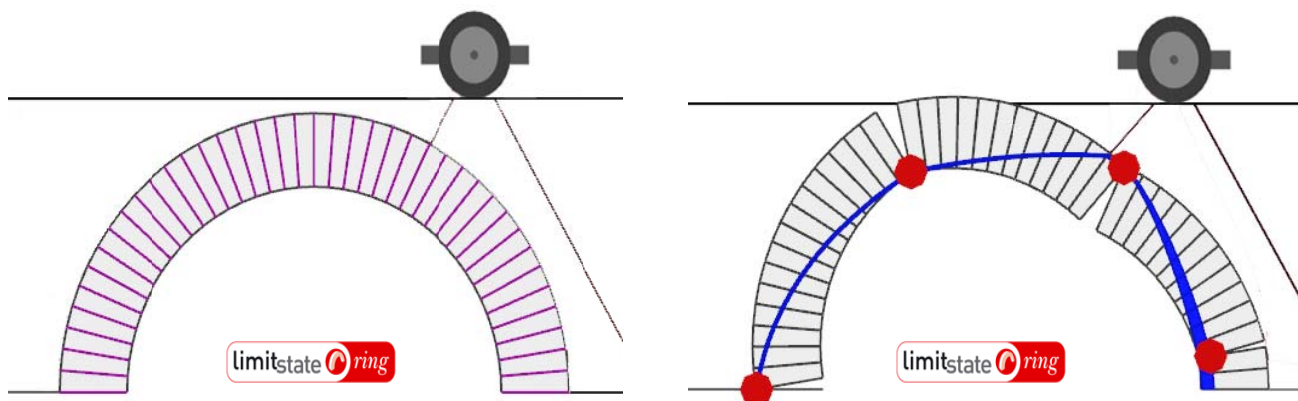


Figure 3.3 Analysis with the Mechanism Method (Ring)

**Considerations.** As *figures 3.2 and 3.3* illustrate, the positions of the hinges are almost the same for the two methods: i) one hinge is under the point where the concentrated load is imposed; ii) two hinges are in correspondence of the supports. The only difference is that in Archie-M the hinge near the right support corresponds with it, while in Ring the same hinge is positioned higher up on the line of the arch. In addition to hinge positions, Ring gives as graphic output also the failure mode. Concerning the collapse load, Archie-M estimates a load smaller than Ring: the first one is equal to 165.2 KN, the second one is equal to 558 KN.

**Sensitivity Analysis.** In this study, Ring is also used to perform a sensitivity analysis of the masonry arch bridge under study. A number of different parameters has been varied to identify their influence on the bridge behavior. The geometry parameters, such as span, rise and thickness of the arch, have not been not investigated in the analysis. The reason is that the geometric parameters are more easy to measure than the material parameters. The considered problems are:

- number of segments in the arch;
- angle of internal friction;
- unit weight of masonry;
- unit weight of backfill;
- height of the backfill.

The results are reported in a form of charts giving value of ultimate loads in relationship with the analyzed parameters (*figures from 3.4 to 3.8*).

**Figure 3.4: Parametric Study for number of segments in the Arch**

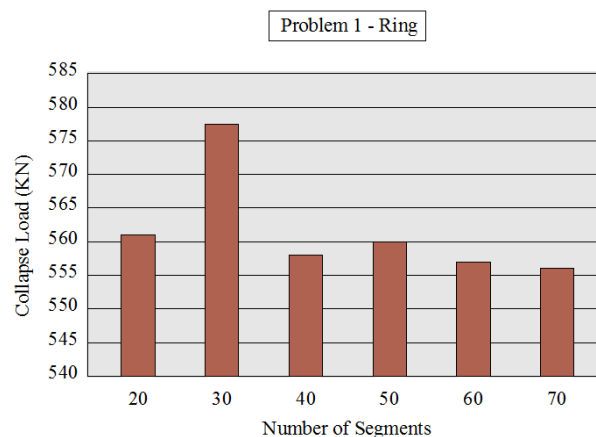


Figure 3.5: Parametric Study for angle of Internal friction

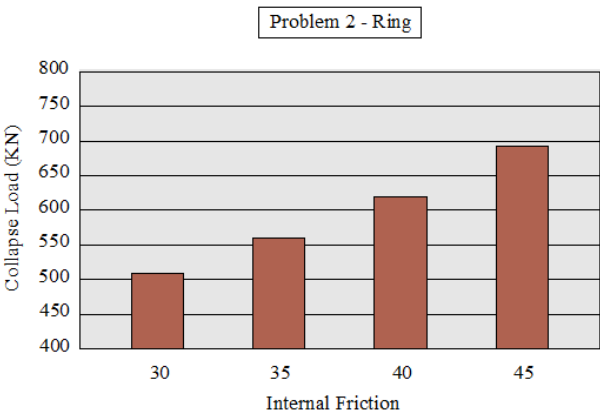


Figure 3.6: Parametric Study for the Unit Weight of Masonry

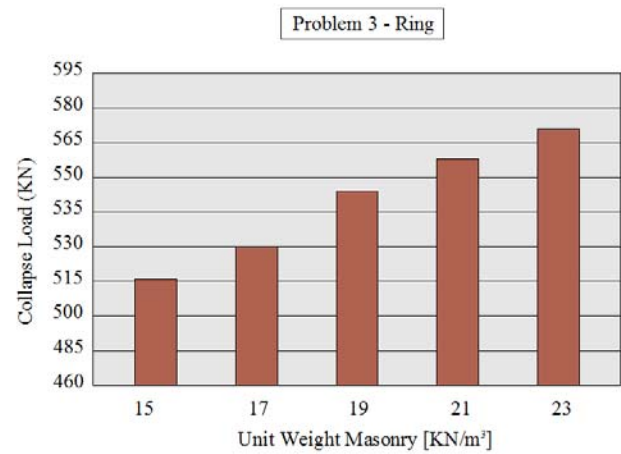
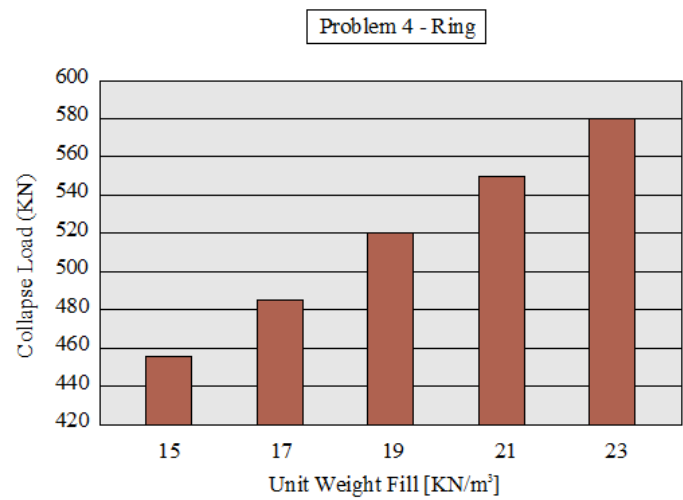
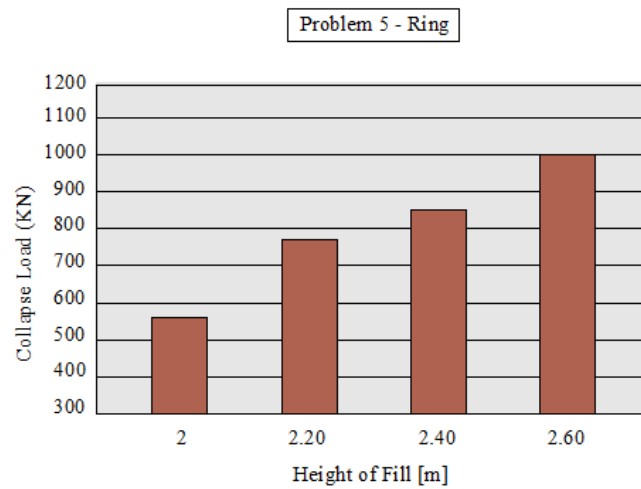


Figure 3.7: Parametric Study for the Unit Weight of Backfill



**Figure 3.8: Parametric Study for the height of Backfill**

Several deductions can be made from these parametric studies:

- the number of arch segments has a limited influence on the collapse load. A sufficient number of segments is equal to forty. This may lead to a very small overestimate of the load capacity, but allows to save computational effort;
- the increase of internal friction angle of the backfill gives higher values of the collapse load;
- both unit weights of masonry and of backfill have a stabilizing effect on the arch behavior. Their increase provides higher values of the collapse load;
- the presence of backfill over the arch has a crucial influence on the ultimate load.

### 3.4 Finite Element Method

The software chosen to simulate the analysis of the generic masonry arch bridge with the Finite Element Method is Abaqus<sup>2</sup>. Abaqus is able to solve a wide range of linear and non linear problems, that involve either static and dynamic response. The software is divided into modules that respect the logic of the organizational process. The modules are:

- Part: where the elements of the model can be created;
- Property : where materials and sections of each part can be defined;
- Assembly: where it's possible to create instances of the parts and to position the instances in a global coordinate system, thus creating the assembly.
- Step: where it is possible to create analysis steps and specify output requests;
- Load: where the load, boundary condition, and field managers can be defined;
- Mesh: where the mesh can be generated;
- Job: where jobs are created and their progression is monitored;
- Visualization: where the output database is analyzed.

**Masonry Properties.** Defining the material property is the most delicate step. Between the various types of discretizations described in chapter 2, the macro-modeling is chosen, trying to

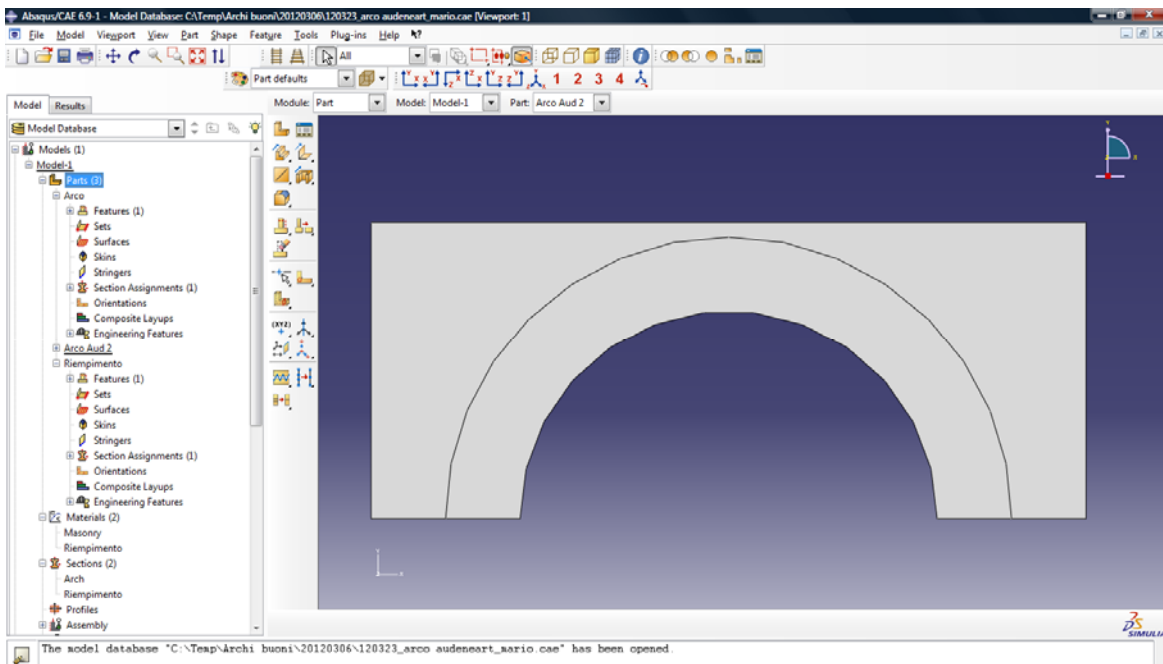


Figure 3.9 Abaqus's screen

<sup>2</sup> ABAQUS: [www.simulia.com](http://www.simulia.com).

take advantage of constitutive laws already implemented in the software and using equivalent materials to model masonry. The general description of a 2D nonlinear constitutive model of a concrete-like masonry consists of three elements: i) pre-failure behavior; ii) limit domain; iii) post-failure behavior. The pre-failure behavior is considered as linear elastic for both compression and tension. The data requested are the Young's Modulus and the Poisson's Ratio.

There are various limit domains for concrete-like material. All of them have similar shape based on Von Mises domain in compression and assume a considerably limited tensile strength. The material model used to defined the properties of masonry outside the elastic range is the concrete smeared cracking model. This material model is based on the William-Warke Criterion, just explained in chapter 2. The data needed to characterize the material behavior are: i) Comp Stress, that is the absolute value of compressive stress; ii) Plastic Strain. Table 3.1 reports the values used, that come from simple static tests performed by University of Pavia. The compressive strength is 8 MPa.

Comp stress (MPa)	Plastic strain
1.05	0
1.5	0.000261
2.13	0.000696
2.6	0.001172
2.94	0.001981
3.25	0.002524
3.31	0.003379
3.39	0.004254
3.38	0.004555
3.34	0.004864

*Table 3.1 Data requested for Smeared Crack Model*

When the stresses pass the limit boundary, the material starts to behave in accordance with assumed post-failure conditions. Abaqus offers several options. The “Tension stiffening” option allows to define the strain-softening behavior for cracked concrete, by means of a post-failure stress-strain relation or by applying a fracture energy cracking criterion. In this case, the post-failure behavior is defined as a function of the displacement at which a linear loss of strength after cracking gives zero stress.

The Failure Ratios are used to define the shape of the failure surface. Four failure ratios can be specified: i) the ratio of the ultimate bi-axial compressive stress to the ultimate uni-axial compressive stress; ii) the absolute value of the ratio of the uniaxial tensile stress at failure to the ultimate uniaxial compressive stress; iii) the ratio of the magnitude of a principal component of plastic strain at ultimate stress in biaxial compression to the plastic strain at ultimate stress in uniaxial compression; iv) the ratio of the tensile principal stress at cracking, in plane stress, when the other principal stress is at the ultimate compressive value, to the tensile cracking stress under uniaxial tension.

Ratio 1	Ratio 2	Ratio 3	Ratio 4
2	0.041	1.28	1.45

*Table 3.2 Failure Ratios*

**Backfill Properties.** A backfill can be modelled by means of 2D elements, that provide to transfer live loads and passive reaction on the arch barrel. The material of the soil is usually nonlinear defined by Mohr-Coloumb or Drucker-Prager limit criteria but also a crude approach involving linear elastic material is allowed. In this case a Drucker-Prager domain is used. The data requested are: i) angle of friction; ii) Flowstress Ratio; iii) Dilatation Angle.

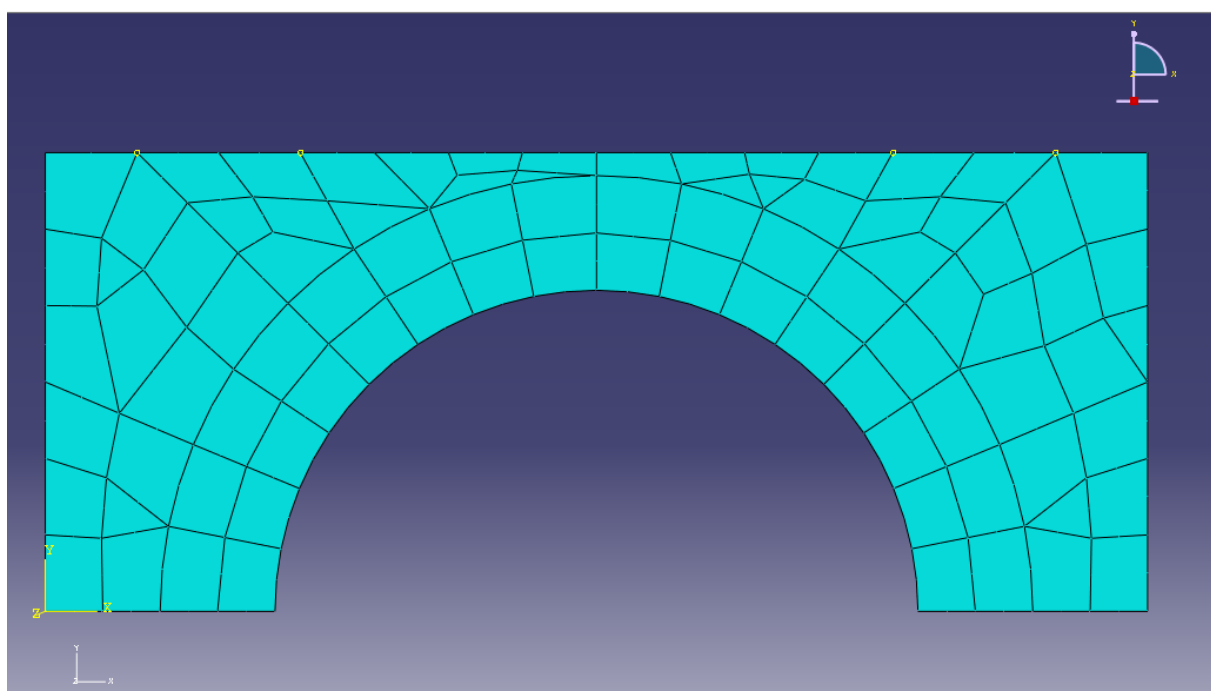


*Figure 3.10 Mesh used*



**Collapse load.** The analysis is non linear and requires an iterative solver. A Lower Bound Approach is used as criterion to determinate the maximum sustainable vertical load sustainable. Then as maximum load, this study considers the load required to form three hinges and initiate a fourth. The collapse load calculated is about 279 KN. In *figure 3.11*, there are reported the principal stresses in the plane: the tension stresses are highlighted in grey. Under the point of application of the vertical load, a hinge occurs as expected. Two hinges opens near the two fixed supports, but not in correspondence. The location of these hinges is in good agreement with the experimental study on the arch, except for the one that opens near the left support. In fact this hinge occurs at intrados, while it has to open at extrados. However the results indicate that the a priori assumption regarding the occurrence of two hinges in the two support points which is frequently made is only approximately true.

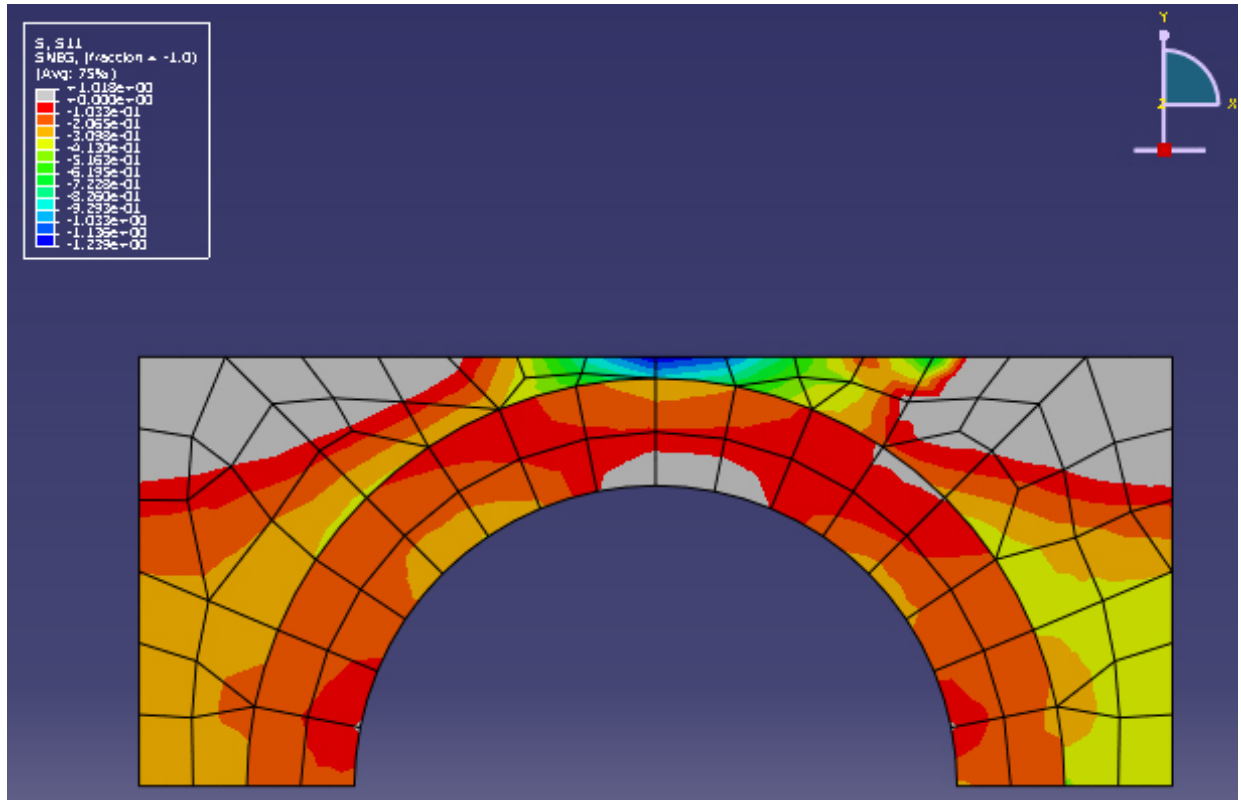


*Figure 3.11 Principal Stresses in the Plane*

### 3.5 Elasto-Plastic Model

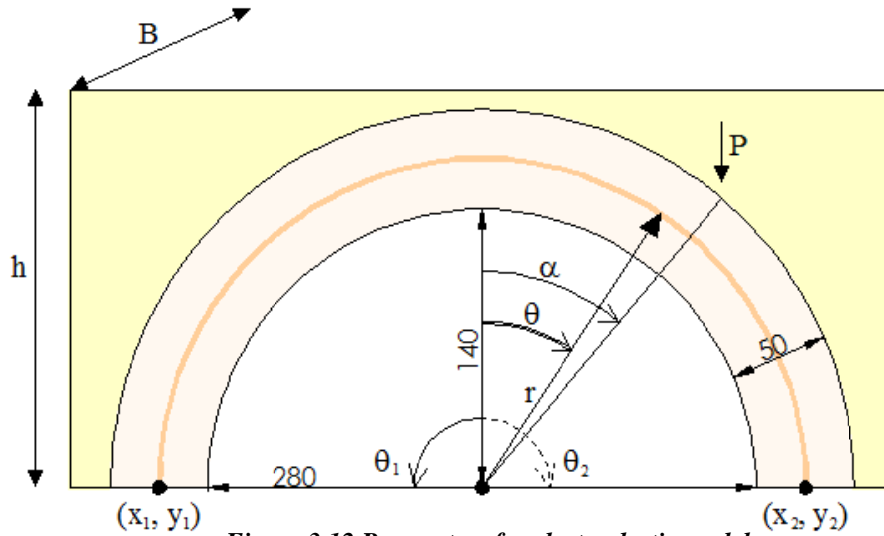


Figure 3.12 Parameters for elasto-plastic model

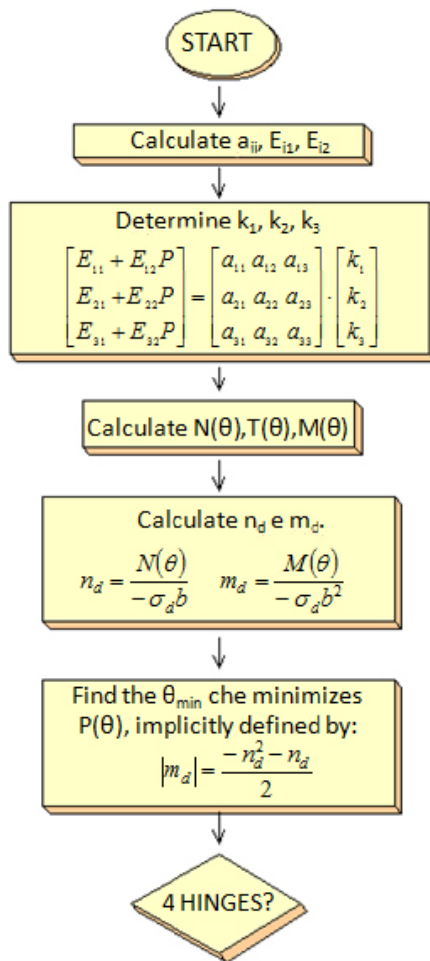


Figure 3.13 Flowchart of the Algorithm

The elasto-plastic model presented in the previous chapter is now used to determine the maximum vertical load of the masonry arch bridge under study. Besides the geometric characteristics explicated in the first paragraph, the model requires other parameters that can be deduced: i) the values of  $\theta_1$  and  $\theta_2$  (figure 3.12); ii) the cartesian coordinates of the two support points  $(x_1, y_1, x_2, y_2)$ . The masonry arch bridge is statically determinate to the third degree and will collapse as soon the four hinges occur. The different steps are reported in a schematic way in the following: the first one is to determine the first hinge. Figure 3.13 shows the flowchart of the numerical algorithm.

#### First hinge.

A. Calculate  $E_{i1}$ ,  $E_{i2}$  and  $a_{ij}$ :

$$E = \begin{bmatrix} -0.001023071455 - 0.9001357490 \cdot 10^{-8} P \\ 0.0007044915938 + 0.4547496860 \cdot 10^{-8} P \\ 0.001688067904 - 0.1399526619 \cdot 10^{-8} P \end{bmatrix}$$

$$ia := \begin{bmatrix} -0.1208649326 \cdot 10^8 & -0. & -0.7325147430 \cdot 10^7 \\ 0.3934072695 \cdot 10^8 & 0.3745228447 \cdot 10^8 & -0. \\ -0.1354014926 \cdot 10^8 & -0.2245554244 \cdot 10^8 & 0. \end{bmatrix}$$

B. Determine the value of the constants of integration  $k_1, k_2, k_3$ :

$$k_1 := -0.00002 + 0.1190465854 P$$

$$k_2 := -13863.55518 - 0.1838058012 P$$

$$k_3 := -1967.20068 + 0.0197632153 P$$

C. Inserting  $k_1, k_2, k_3$  in the differential equilibrium equations, it is possible to express the internal forces in terms of the load  $P$  unknown:

$$\begin{aligned} N &:= k_1 \sin(\theta) + k_2 \cos(\theta) + \sin(\theta) \cdot \int (\cos(\theta) \cdot q, \theta=0 \dots \theta) - \cos(\theta) \cdot \int (\sin(\theta) \cdot q, \theta=0 \dots \theta) - P \sin(\theta) \cdot \text{ustep}(\alpha, \theta); \\ V &:= k_1 \cos(\theta) - k_2 \sin(\theta) + \cos(\theta) \cdot \int (\cos(\theta) \cdot q, \theta=0 \dots \theta) + \sin(\theta) \cdot \int (\sin(\theta) \cdot q, \theta=0 \dots \theta) - \\ &P \cos(\theta) \cdot \text{ustep}(\alpha, \theta) + \Gamma \cdot r^2 \cdot \eta \cdot \sin(\theta) + p \cdot \theta; \\ M &:= k_3 - \int (V \cdot r, \theta=0 \dots \theta) - \\ &\int (\Gamma \cdot r^3 \cdot \eta^3 / 12 \cdot \sin(\theta) + p \cdot \theta \cdot b / 2, \theta=0 \dots \theta); \end{aligned}$$

D. Then the normalized version of  $N(\theta)$  and  $M(\theta)$ , i.e.  $n_d$  and  $m_d$ , can be calculated:

$$\begin{aligned} n_d &:= 0.2500000000 \cdot 10^{-6} (-0.00002 + 0.1190465854 P) \sin(\theta) \\ &+ 0.2500000000 \cdot 10^{-6} (-13863.55518 - 0.1838058012 P) \cos(\theta) + 0.2500000000 \cdot 10^{-6} \sin(\theta) \\ &(21663. \sin(\theta) \cos(\theta) + 21663. \theta + 77976. \sin(\theta) \cos(\theta)^3 + 27360. \sin(\theta)^3 - 54720. \sin(\theta) \cos(\theta)^2 - 109440. \sin(\theta)) - \\ &0.2500000000 \cdot 10^{-6} \cos(\theta) \\ &(21663. + 17325. \cos(\theta)^2 - 38988. \sin(\theta)^4 - 27360. \sin(\theta)^2 \cos(\theta) - 54720. \cos(\theta) + 54720. \cos(\theta)^3 - 38988. \cos(\theta)^4); \\ &- 0.2500000000 \cdot 10^{-6} P \sin(\theta) \begin{cases} 0 & \theta < 0.75 \\ 1 & 0.75 \leq \theta \end{cases} \\ m_d &:= 0.02659686664 - 0.1417581784 \cdot 10^{-6} P + 0.1650000000 \cdot 10^{-10} \sin(\theta) - 0.9821343295 \cdot 10^{-7} \sin(\theta) P \\ &+ 0.008685213025 \cos(\theta) + 0.1516397860 \cdot 10^{-6} P \cos(\theta) - 0.01397070000 \cos(\theta)^3 - 0.01787197500 \sin(\theta) \theta \\ &+ 0.006433020000 \cos(\theta)^5 - 0.02872800000 \cos(\theta)^2 - 0.006433020000 \cos(\theta) \sin(\theta)^4 - 0.008577360000 \sin(\theta)^2 \cos(\theta) \\ &+ 0.8250000000 \cdot 10^{-6} P \begin{cases} 0. & \theta < 0.7500000000 \\ 1. & \text{otherwise} \end{cases} \sin(\theta) - 0.5623519770 \cdot 10^{-6} P \begin{cases} 0. & \theta < 0.7500000000 \\ 1. & \text{otherwise} \end{cases} \end{aligned}$$

E. Calculate  $\theta_{min}$  that minimizes  $P(\theta)$ :

$$z_1 = m_d + 0.5n_d^2 + 0.5n_d$$

$$z_2 = -m_d + 0.5n_d^2 + 0.5n_d$$

The two functions  $z_1$  and  $z_2$  can't be simultaneously zero. If  $z_1$  and  $z_2$  are plotted as a function of the angle  $\theta$ , at increasing of point load the function  $z_2$  approaches zero (3.14). This condition corresponds to the formation of the first plastic hinge. The first value of load, for which  $z_2$  is equal to zero, corresponds to the value of load  $P_{max1} = 37200$  N and  $\theta_{max1} = 0.7163$ .

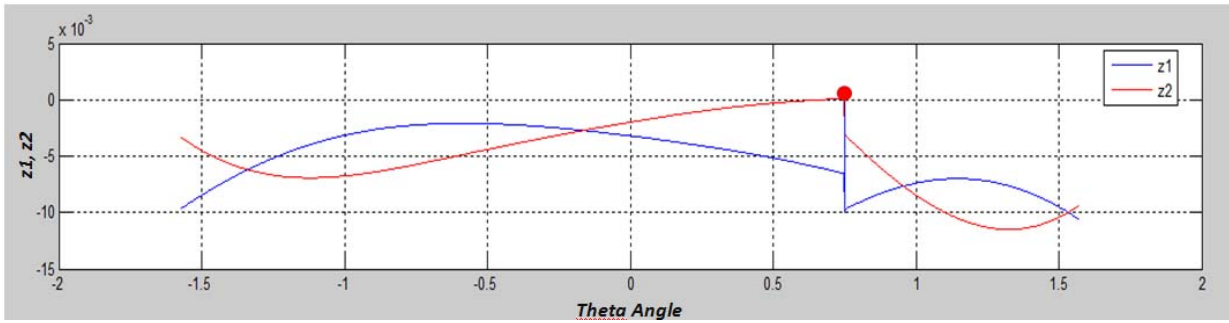


Figure 3.14 Formation of the first hinge

### Second hinge.

In the presence of a hinge, the structure becomes statically indeterminate to the second degree. The new value for  $P$  is now given by  $P = P_{max1} + \Delta P$ , where  $P_{max1}$  is just determined and  $\Delta P$  is the unknown value.

A. Equilibrium equations must be rewritten as a function of the new increment  $\Delta P$  unknown:

$$N(\theta) = k_1 \sin \theta + k_2 \cos \theta + \sin \theta \int_0^\theta \cos \beta q(\beta) d\beta - \cos \theta \int_0^\theta \sin \beta q(\beta) d\beta - P_{max1} \sin \theta_{step}(\theta - \alpha) - \Delta P \sin \theta_{step}(\theta - \alpha)$$

$$T(\theta) = k_1 \cos \theta - k_2 \sin \theta + \cos \theta \int_0^\theta \cos \beta q(\beta) d\beta + \sin \theta \int_0^\theta \sin \beta q(\beta) d\beta - P_{max1} \cos \theta_{step}(\theta - \alpha) - \Delta P \cos \theta_{step}(\theta - \alpha)$$

$$+ \gamma r^2 \eta \sin \theta + p_\theta$$

$$M(\theta) = k_3 - \int_0^\theta V(\beta) r d\beta - \int_0^\theta \left[ \gamma r^3 \frac{\eta^3}{12} \sin \beta + p_\theta \frac{b}{2} \right] d\beta$$

B. The new boundary conditions can be expressed as:

$$M_{\max 1} = M(\theta_{\max 1})$$

$$u_2 = u_1 + (y_3 - y_1)\varphi_1 + (y_2 - y_3)\varphi_2 + \frac{1}{E} \int_{\theta_1}^{\theta_2} \frac{N}{A} \frac{\partial x}{\partial \theta} d\theta + \frac{1}{E} \int_{\theta_1}^{\theta_2} (y_3 - y) \frac{M}{I} r d\theta$$

$$v_2 = v_1 + (x_3 - x_1)\varphi_1 - (x_2 - x_1)\varphi_2 + \frac{1}{E} \int_{\theta_1}^{\theta_2} \frac{N}{A} \frac{\partial y}{\partial \theta} d\theta - \frac{1}{E} \int_{\theta_1}^{\theta_2} (x_3 - x) \frac{M}{I} r d\theta$$

C. The expressions of  $N(\theta)$ ,  $M(\theta)$  and  $T(\theta)$  are replaced in boundary conditions, redefining the matrices:

$$\begin{bmatrix} E_{11} + E_{12}P \\ E_{21} + E_{22}P \\ E_{31} + E_{32}P \end{bmatrix} = \begin{bmatrix} a_{11} & a_{12} & a_{13} \\ a_{21} & a_{22} & a_{23} \\ a_{31} & a_{32} & a_{33} \end{bmatrix} \cdot \begin{bmatrix} k_1 \\ k_2 \\ k_3 \end{bmatrix}$$

D. The three constants of integration  $k_1$ ,  $k_2$ ,  $k_3$  can be calculated as:

$$k1 = 4298.991217 + 0.03253555874 P$$

$$k2 = -21392.80399 - 0.2370884169 P$$

$$k3 = -1158.802301 + 0.1403638416 P$$

E. Calculate the increase  $\Delta P_{\max 1}$  regards to  $P_{\max 1}$  and the position of the second hinge:

$$\Delta P_{\max 1} = 28760 \text{ N e } \theta_{\max 2} = -1.57$$

Also in this case, the function  $z_2$  reaches the zero first.

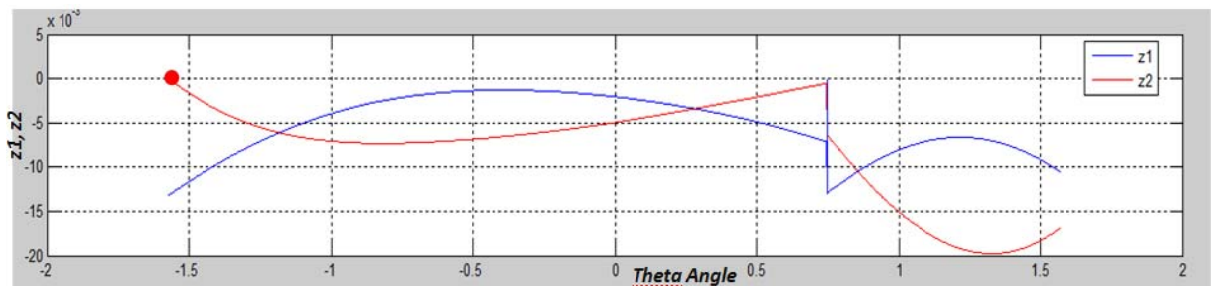


Figure 3.15 Formation of the second hinge

**Third Hinge.**

The structure is now one degree statically indeterminate.

- A. The equilibrium equations and boundary conditions are rewritten as function of the new conditions.
- B. The three constants of integration  $k_1$ ,  $k_2$ ,  $k_3$  are calculated as:

$$k_1 := 5236.166396 + 0.05652328061 P$$

$$k_2 := -28214.13658 - 0.1292173379 P$$

$$k_3 := 2880.858807 + 0.1199459778 P$$

- C. Calculate the increase  $\Delta P_{max2}$  regards to  $P_{max2}$  and the position of the third hinge:

$$\Delta P_{max2} = 24800 \text{ N e } \theta_{max3} = -0.4021$$

In this case the function  $z_1$  reaches the zero first.

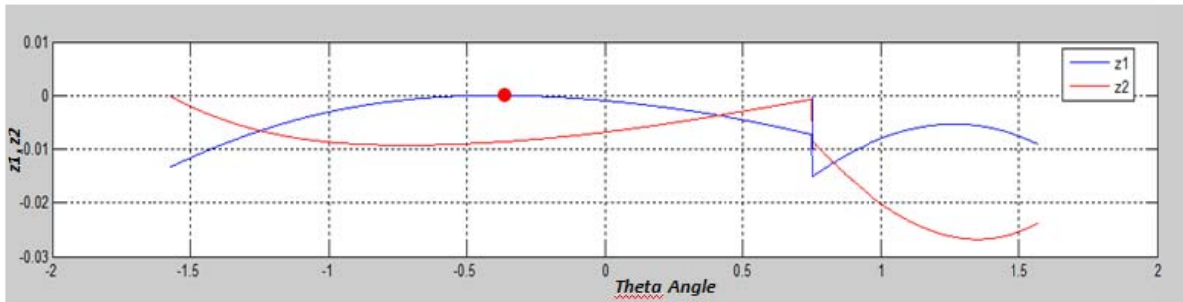


**Figure 3.16 Formation of the third hinge**

**Fourth Hinge.**

- A. The equilibrium equations and boundary conditions are rewritten as function of the new conditions.
- B. The three constants of integration  $k_1$ ,  $k_2$ ,  $k_3$  are calculated as:

$$k_1 := 6637.227869$$

$$k_2 := -31417.08998$$

$$k_3 := 5853.999908$$

C. Calculate the increase  $\Delta P$  regards to  $P_{max3}$  and the position of the fourth hinge:

$$\Delta P_{max3} = 43.400 \text{ N} \text{ e } \theta_{max4} = 1.33$$

Also in this case the function  $z_1$  reaches the zero first.



Figure 3.17 Formation of the fourth hinge

**Considerations.** The collapse load is obtained by summing the  $P_{max1}$  and the increments  $\Delta P_{max1}$ ,  $\Delta P_{max2}$ ,  $\Delta P_{max3}$  calculated for the different hinges. Its value is 134160 N. As figure 3.18 shows, the first hinge opens under the point where the load is imposed. The second hinge occurs at the springing, in the left abutment. The fourth hinge occurs close to the right support, but not exactly in. The location of these hinges is in good agreement with the experimental study on the arch and with Heyman's theory.

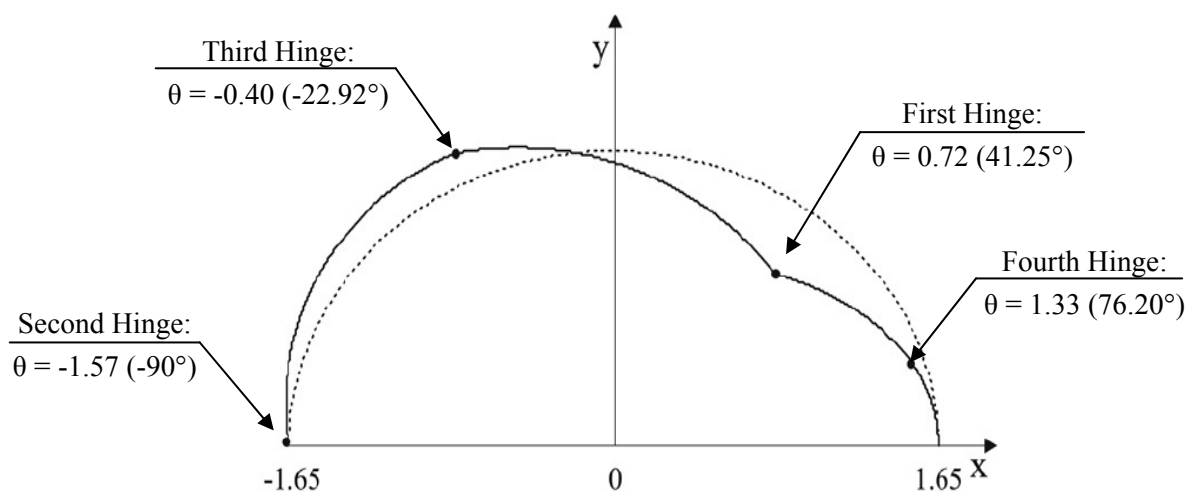
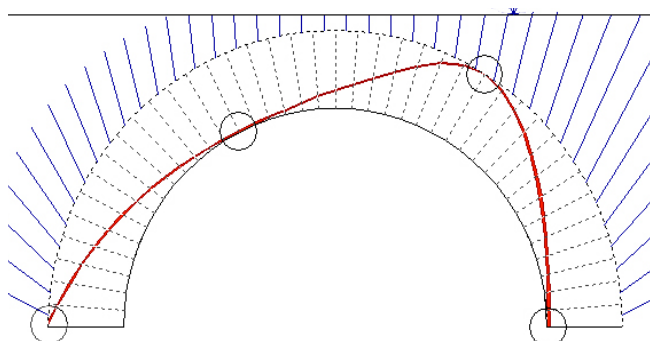
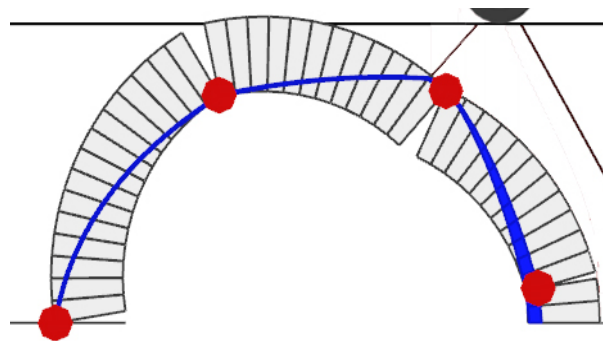


Figure 3.18 Position of the Four Hinges

### 3.6 Comparison between results



*Figure 3.19 Thrust Line Analysis (Archie-M)*



*Figure 3.20 Mechanism Method (Ring)*

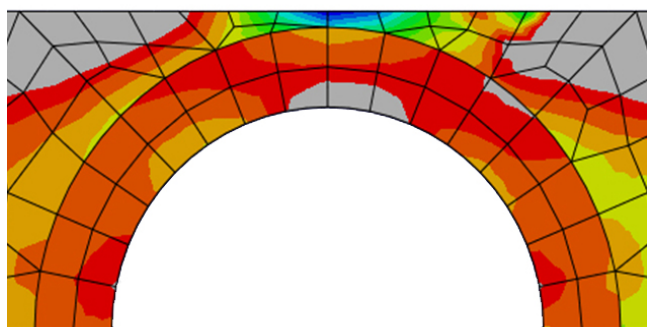


*Figure 3.21 Finite Element Method*

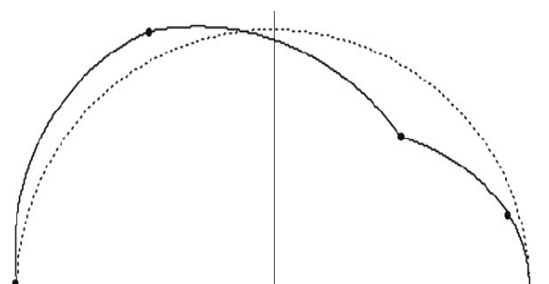


*Figure 3.22 Elasto-Plastic Model*

Different analytical and numerical methods for the assessment of masonry arch bridges have been applied to a generic arch bridge. Concerning the hinge positions, Ring, Archie-M and the elasto-plastic model have shown similar results. Small differences are found near the point of application of concentrated load, probably due to the different distribution of live load in the various models. There are little differences also concerning the position of fourth hinge near the right support. In particular, in Archie-M the hinge corresponds with the support, while in Ring and in the elasto-plastic model the same hinge is positioned higher up on the line of the arch. Concerning the hinge positions in the finite element model, there is a good correspondence with the other models for the first hinge - that occur under the point of load application - and for the fourth hinge - that opens near the right support. The positions of the other hinges are different from those of other models. In fact the third hinge moves to the arch center, while the second hinge occurs at intrados and not at extrados. The differences between the first three models and the finite element model can be explained, thinking to the different conceptual bases: Archie-M, Ring and the Elasto-Plastic model derive from the principles of limit state



analysis, while the Finite Element Model comes from a completely different approach. However the results indicate that the a priori assumption regarding the occurrence of two hinges in the two support points which is frequently made is only approximately true.

	FIRST HINGE (rad)	SECOND HINGE (rad)	THIRD HINGE (rad)	FOURTH HINGE (rad)	Collapse Load (KN)
ARCHIE-M	0.60	-1.57	-0.47	1.57	165
LIMITSTATE RING	0.60	-1.57	-0.40	1.41	558
FINITE ELEMENT	0.67	-1.37	0	1.37	279
ELASTO- PLASTIC	0.72	-1.57	-0.40	1.33	138

*Table 3.3 Hinge position and Failure Load for Different Methods*

Concerning the collapse load, elasto-plastic model and Archie-M have shown a comparable behavior. The Ring collapse load is significantly higher than the others, probably for two reasons. The first one is that the other three models use a lower bound approach to determinate the maximum vertical load sustainable, while Ring uses an upper bound approach. The second one is that the rigid-plastic model neglects the elasticity of the masonry. This factor is very important when the thickness of the arch is big as in the bridge in exam. This example demonstrates that the elasticity of the material has a great influence on the determination of the collapse load. The differences in the collapse load can be summarized as follows: Elasto-Plastic collapse load  $\leq$  Archie-M collapse load  $\leq$  Finite Element collapse load  $\leq$  Ring collapse load.

**Worst load position.** In this example, the position of the load has been determined a priori to compare between them the various methods. Actually, for practical reasons it's very interesting to study the worst load position that gives rise to the smallest collapse load. So the last analysis made on the generic arch bridge is of this type. The most critical position is founded at 2025 mm from the left abutment, about at a quarter of the span, as expected. The maximum load that can be applied at this point has been calculated with Ring and is equal to 250 KN.



## Chapter 4

# Case Study of Clemente Bridge

---





## 4.1 SOMMARIO

*“Ti piaceva di fermarti sul ponte, che valica il Savio col grande arco quasi romano; appoggiato al pacifico parapetto guardavi l’acqua poca e lenta passare laggiù tanto in basso.. Di sul ponte è più facile orientarsi: c’è la rocca dietro, a ridosso, con gli avanzi della vecchia murata, che coronano l’ultimo colle strapiombante sul fiume; tutto l’alto bacino del Savio a monte, e il piano aperto a valle fino al mare si dispongono intorno a questo centro naturale come in un quadro perfetto, dove ogni particolare ha il suo posto certo. ”*

Renato Serra

Il caso studio oggetto della presente ricerca è il Ponte Clemente, situato sul fiume Savio a Cesena. Si tratta di un ponte stradale simmetrico, con struttura ad arco in muratura. Le tre campate sono caratterizzate da archi a sesto ribassato, sostenuti da massicci pilastri. Per quanto riguarda la storia, nel 1729 Papa Benedetto XIII autorizza l’inizio dei lavori in seguito al crollo dell’esistente ponte in legno, ma è solo nel 1733 che i lavori iniziano con la successione di Papa Clemente XII, che dà il suo nome al ponte. Nel 1771 il ponte si può dire completato. Diversi sono gli architetti chiamati a dare pareri o a partecipare attivamente all’opera in questo periodo: tra i più noti ricordiamo Ferdinando Fuga e Luigi Vanvitelli. Il ponte non soffre nel tempo particolari danni fino alla seconda guerra mondiale, quando le truppe tedesche in ritirata fanno saltare l’arcata centrale, da subito ricostruita dagli Alleati.

Attualmente il Ponte presenta cricche verticali vicino ai piloni di nord-est e di sud-est. Non si tratta di fenomeni recenti, infatti vengono già citati in una relazione del 1776. Queste lesioni oggi appaiono stabili e i bordi consolidati.

Le caratteristiche meccaniche dei materiali costituenti la struttura portante del ponte sono state stimate attraverso prove di compressione monoassiale sui mattoni e di punzonamento sulla malta. Per quanto riguarda la geometria della sezione dell’arco, in assenza di dati certi, sono state formulate diverse ipotesi in accordo con le evidenze rilevate sul ponte dall’ultima campagna di lavori nel 2010.

Nelle analisi svolte, Ring e Archie-M riproducono quasi le stesse modalità di collasso: la posizione critica del live load è identificata sulla prima campata e in maniera simmetrica sulla terza. Il carico di collasso di Archie-M è di poco inferiore a quello di Ring. Tra i due modelli, si possono riscontrare piccole differenze nella collocazione delle cerniere poiché la posizione critica del live load si trova vicino ai sostegni. Poiché lo spessore dell’arco è molto grande, con Ring si è anche valutata l’ipotesi che ogni arco fosse formato da due archi sovrapposti. Per quanto riguarda il metodo agli elementi finiti e il modello elasto-plastico, i risultati si stanno ancora valutando.





## 4.2 A Bridge, a Symbol: a brief description

The case study object of this research is the Clemente Bridge, located in Cesena<sup>1</sup>. Clemente Bridge, also known as *Old Bridge*, is the most ancient bridge in Cesena and also one of symbols of the city. In fact Cesena is known as the city “*de’ font, de’ pont, de’ Mont*”<sup>2</sup>.



**Figure 4.1** City of “*fountain, bridge, Montain*”: a) *Masini Fountain*; b) *Clemente Bridge*; c) *Mount Abbey*

As the other two symbols of the city – Masini Fountain and Mount Abbey – the bridge has a glorious history and offers a magnificent example of the past techniques. So it is a monument preserved by the Authority, but at the same time continues to perform its function of connection between the city center and the *Oltresavio* neighborhood, despite the change of means of transport and the increase of the traffic.

Clemente bridge is a road bridge and has a humpback pavement. It is collocated on the ancient layout of the *via Aemilia* and spans the Savio River at one of the narrowest points in the city. Clemente Bridge represents even now one of the most important accesses to the city, though in 1919 the Risorgimento Bridge was built down south and the Via Emilia was deviated. The structure of the bridge is symmetrical and is formed by three masonry arches that show a segmental shape. The arches are supported by massive piers, endowed with triangular cutwaters both at upstream and at downstream. The bridge reaches a total length of about 111 m and has an average width of 8.30 m, including the parapets. Its height is about 15 m in the maximum point. The most important geometric data regarding the three arches – as width or rise – and regarding the four supports – as height or thickness – are provided in *Table 4.1* and in *Table 4.2*.

<sup>1</sup> Cesena is an Italian town of 97.500 inhabitants of the province of Forlì-Cesena in Emilia-Romagna. It is placed about 90 km south-east of Bologna

<sup>2</sup> “*de’ font, de’ pont, de’ Mont*” is a dialectal form that can be traducted as “*city of fountain, of bridge, of Montain*”

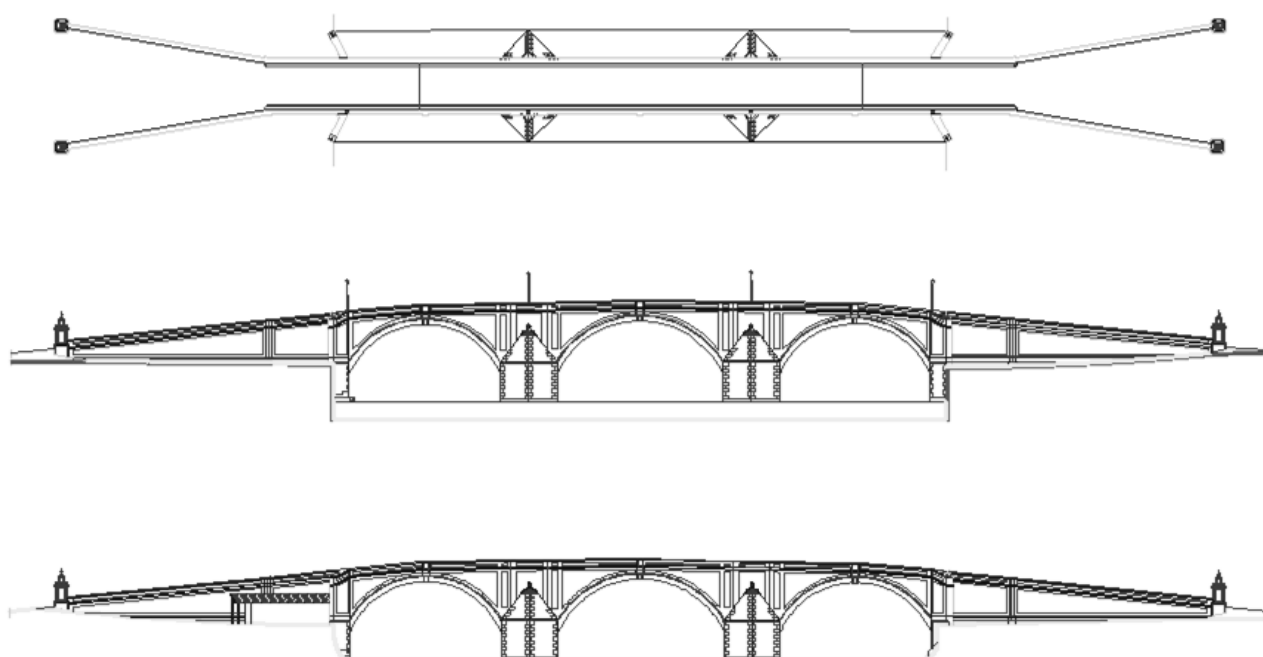


**Figure 4.2 Recent Survey: Plan, North Front and South Front of Clemente Bridge**

	<b>Span</b>	<b>Rise</b>
Arch 1	22730 mm	7380 mm
Arch 2	24900 mm	7900 mm
Arch 3	22740 mm	7620 mm

**Table 4.1 Geometric Arch Data Table**

	<b>Height</b>	<b>Thickness</b>
Left Abutment	4185 mm	3180 mm
Pier 1	4250 mm	8490 mm
Pier 2	4150 mm	8520 mm
Right Abutment	4150 mm	3190 mm

**Table 4.2 Geometric Pier Data Table**

Data come from the latest survey carried out in 2006. Three are the principal surveys on the Clemente Bridge remembered by source materials:

- In 1812, Papal Civil Engineers<sup>3</sup> took a census of existing bridges in the Rubicone Department: on this occasion draw up a table containing the data of the bridges surveyed, including the Clemente Bridge, called here as *the New Bridge in Cesena*;
- In 1993, Simona D'Altri Dardereri effected dimensional controls in order to check the previous measuring during the writing of her degree thesis with the supervision of Salvatore Di Pasquale<sup>4</sup>;
- In 2006 Cantori Architectural Firm redid the survey, when the Public Administration commissioned it to replace the ornamental elements in white limestone from Istria.

<sup>3</sup> Archivio di Stato di Forlì, *Genio Civile*, b. 3, II-6, 1812

<sup>4</sup> Salvatore Di Pasquale, Architect, Full Professor of Mechanics of Structures, Academic Dean at Firenze and Catania



### 4.3 Historical Notes

The city of Cesena had to wait many centuries before to have a stable and durable masonry bridge, that would allow the *via Aemilia* to cross the Savio River. In fact the Savio River has been subject to continuous flooding and frequent movements of the riverbed: so it had always caused the collapse of the structures built before Clemente Bridge. Various attempts were made during the time: in Roman Age in the area of actual Risorgimento Bridge, in Medieval Age in the place where nowadays rises Clemente Bridge. Other provisional bridges were built in wood. During the lordship of Malatesta, a stone bridge with five arched spans was built: the central ones were higher than the two lateral to allow the river in flood to pass more easily. In spite of all, in 1684 it was ruined by the water violence.

In 1729 after the collapse of the last wooden bridge, Pope Benedetto XIII authorized the beginning of works of the new masonry bridge based on a draft by Antonio Felice Facci. The architect assumed to recover the two remaining arches of the Malatesta bridge and to build three new arches to the East (*see figure 4.3, in legend AB*): so the project consisted in five arched bridge provided with deep foundations. Unfortunately Pope Benedetto XIII didn't see the start of works because he died the next year.

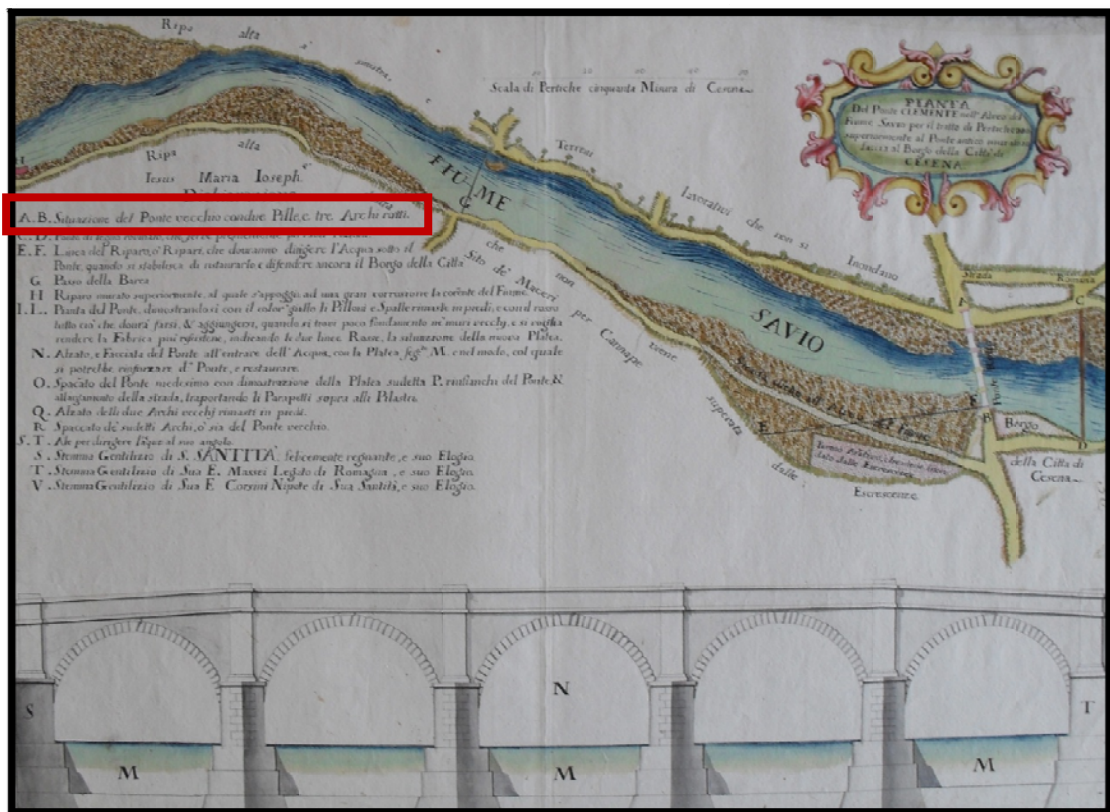


**Figure 4.3 Facci's Project.**  
Plan and Front in a copy of Mauro Guidi conserved at Malatestiana Library at Cesena



**Figure 4.4** *Wooden Model commissioned to Domenico Cipriani in 1734*

The bridge construction began only in 1733 with the succession of Pope Clemente XII, who made possible the starting with the bequest of five thousand crowns. In his honour the bridge was called Clemente Bridge. At once the deep foundations were started to built. Regarding the bridge geometry, the Pope liked Facci's project, but preferred to have the advice of other experts. In fact before to realize important public works in His communities, the Pope often submitted the projects to influential architects, that evaluated the technical and financial feasibility: in this case he commissioned Ferdinando Fuga, who in the same years had built Corsini Palace for Him. In 1733 Fuga went to Cesena and met the work supervisor Domenico Cipriani. In his relation to Pope, he proposed to reduce the number of the spans: not five, but three exactly as in a bridge designed by him on Milicia River, near Palermo in Sicily. The new solution is well illustrated by Cipriani's wooden model realized in 1734 (*figure 4.4*) and by Mauro Guidi's original drawing (*figure 4.5*): nowadays both are conserved at Malatestiana Library at Cesena. The three masonry arches show a segmental shape.



**Figure 4.5** *Fuga's Project. Plan and Front in a drawing of Mauro Guidi*



Figure 4.6 P. C. Borboni: a) Dome of Mount Abbey; b) Church of St. Augustine; c) Church of St. James

In the thirty years following the work authorization, only the deep foundation were realized. It happened for financial reasons: in fact Cesena was often invaded by enemy troops and was forced to suspend works at the site of the bridge. In the meantime, a wooden bridge was built further down: it was demolished by the river in flood in 1764. In the same year Cesena community decided to restart the bridge construction on the foundation just realised. The task was given to Pietro Carlo Borboni, one of the municipal architects: he can be considered the bridge's real architect. Beyond the bridge, he built in Cesena the Chapel of Our Lady in the Cathedral, the church of the Servants, the church of St. Zenone, the dome of the Mount Abbey, the church of St. Augustine and in Cesenatico the Church of St. James. Once obtained the bridge supervision, Borboni elaborated a new project, that was submitted to the opinion of Ferdinando Fuga and Luigi Vanvitelli. The last one approved it, making some changes: he defined a bigger diameter for the arches, increased the pier size and changed the wing direction. Works resumed in April of 1766 after thirty years of interruption.

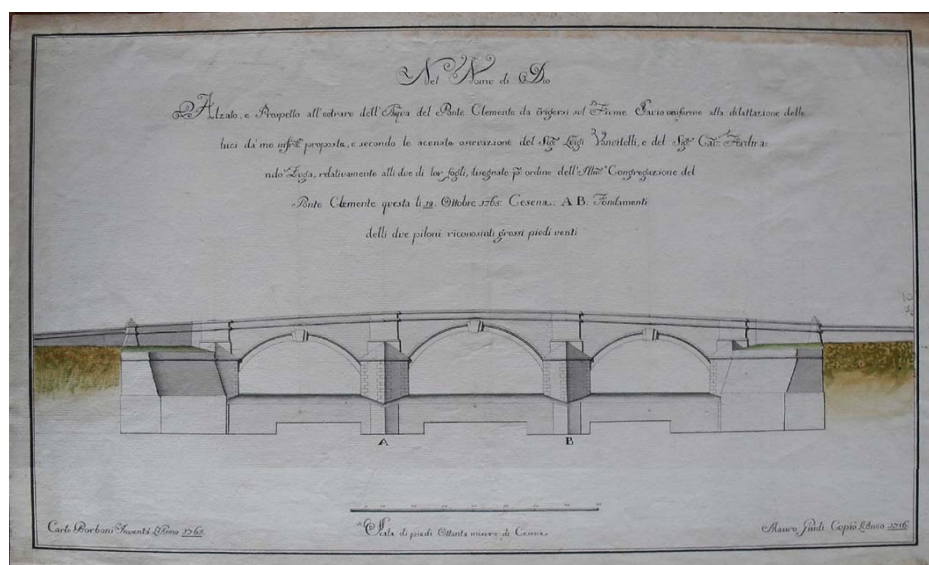


Figure 4.7 Borboni's Project modified following Fuga and Vanvitelli's directions (Guidi's copy)





*Figure 4.8 Frontal View of the Clemente Bridge*

Additional ten years were needed to finish the construction. In 1771 the bridge was open to transit, accessible even if incomplete. Bridge Congregation's verbal of 14 april 1773 reported: *"In the last years the bridge is practicable, and a toll is requested, now the marble has to be put down on the banks of that Bridge."*<sup>5</sup> The bridge was completed by Borboni's nephew: in fact in 1773 Borboni died and the work direction passed to Agostino Azzolini, that had long collaborated with him. Azzolini changed foundation shape in the central span, giving it a semicircular form in order to allow better water flowing: besides he posed ornamental elements in white limestone from Istria.

Old graphic documentations of Clemente Bridge come almost uniquely from the drawings of Mauro Guidi, who did his apprenticeship in Azzolini's workshop between 1780 and 1787. In these years he could see, copy and elaborate Borboni's projects, completing them with on-site survey. Some of his drawing are reported in the previous pages and are still preserved in the Malatesta Library at Cesena.

Clemente Bridge was built when the Mechanics of Structures was experiencing an important theoretical development. In France, Philippe de la Hire (1640-1718) was writing treatises on a static theory of the arches and the vaults: his models based on funicular polygon gave a first scientific contribution to the study of the arch stability. Even if in France significant progresses were made, in Italy the architects remained anchored to practice learned on the construction site and to the Proportion rules, contained in the ancient treatises until Vitruvio. So Clemente Bridge was realized following the constructive principles endorsed by the experience: the dimensions of the arches were determined, trying to ensure the greatest free surface for the water passage. *Prudentia Massima*<sup>6</sup> was recommended by Luigi Vanvitelli and not the respect

<sup>5</sup> *"Da qualche anno si passa, e si esige il Padaggio, ora resta tuttavia da mettere una porzione di Marmi sulle sponde del detto Ponte."*

<sup>6</sup> That is *"Utmost caution"*. Vanvitelli wrote it in a letter to Pope Nuncio in 1765.

of mathematics theories. Also Proportion rules were disregarded because could not guarantee alone the stability of structure, as already argued by Galileo in his treatises.

In the next centuries, bridge's transformation were often thought about. In fact three arch bridge had some advantages, but also some drawbacks. For example, in winter it was very difficult to go up the two long side ramps with carts, especially with ice. So in 1836 was proposed the demolition of segmental arches and consequently their reconstruction into elliptical shapes, as in France. But it all came to nothing. In 1919 Risorgimento Bridge was built down south and the Via Aemilia was deviated, but Clemente Bridge remained one of the most important accesses to the City Centre.

The bridge withstood the river attacks and didn't suffer important damages until the Second World War. Throughout the summer of 1944 the Allies tried to bomb the bridge, but they failed to damage it. Conversely the Germans succeeded in purpose. In the night of 20 October 1944 – the same day of liberation – German troops in retreat mined the structure and blew the central arch<sup>7</sup>. At once Canadian engineers provided to restore the passage with a Bailey bridge (*figure 4.9*). At the same time they provided to rebuild the masonry central arch together with the local administration: the reconstruction was made so well that today it is identifiable only by the brick's different shade (*figure 4.10*). In March 1945 the bridge was practicable, but was not yet finished in all its parts.



**Figure 4.9 Bailey Bridge on the central arched span destroyed by the German troops. 1944.**

<sup>7</sup> “... allora sistemammo alcune granate da mortaio nell’arcata centrale assieme ai restanti 3 chilogrammi di esplosivo e al detonatore. Appiccammo fuoco alla miccia. [...] Corremmo al ponte e constatammo che uno degli archi si era disintegrato.” (Cronaca Truppe Tedesche)



*Figure 4.10 Historic photo from the archive of the Superintendence of Monuments*

The rehabilitation of the stacks and parapets continued under the direction of the honorary inspector Monuments Professor Giannetto Malmerendi<sup>8</sup>: in 1952 all the works were finished.

Unfortunately the post-war restorations are not documented. The candidate is gone to State Archive of Forlì, to Historic Archive of Cesena and to Technical Office of Cesena; she has contacted the Technical Service Basin of Emilia Romagna and the Savio Building Firm, that had realized the work. Nothing is present, apart from three documents: i) a letter of Superintendent of Monuments, that gave recommendations on the curtain restoration in 1946 ii) a good survey of the damage to curtains, perhaps attached to some economic evaluation for the restoration of the monument, without date, heading or signatures; iii) an estimate of the works required for bridge completion made by Corps of Engineers of Forlì (*Annex 4.A*).

So it's difficult to define the mode of reconstruction of the central vault: for this reason, the candidate made some assumptions, that will be discussed in *Paragraph 4.4*.

<sup>8</sup> Giannetto Malmerendi was also the author of one of the two existing paintings representing the reconstruction of 1945.

**Actual state.** Currently the bridge is in quite good conditions. It presents vertical cracks over the piers both on the south front and particularly on the north one. This is not a recent phenomenon: a report of Giuseppe Brunelli in 1776 mentioned it, attributing to "*compression that happens at first in all the new constructions, especially when they are heavy and high.*"<sup>9</sup> These cracks were already present to a small extent on the parapets too. In 1993 also the road surface next to the east pier presented an evident crack between the opposite platforms (*figure 4.12*). Today these cracks have stable and consolidated edges, so probably there are not static involvements. Moreover the structure presents minor cracks on the walls of the lateral ramps and on the central arch between the old structure and the reconstructed one: any static influence can be dismissed.

Besides, in some structural elements such as piers and the vaults, there are serious damages to masonry surfaces due to the direct hits of Second World War's bombs. For example, the south-east arch has severe damages in the profile for the lack or failure of many bricks. In these cases, a complete reconstruction of masonry surface should be made with the use of the *cuci scuci* technique: damaged bricks should be removed and replaced with other elements, similar in shape, dimensions, shade and manufacturing techniques. In particular, special mortars for restoration should be used: these mortars should have mechanical strength equal to ancient ones in order to avoid different mechanical performances.

Nowadays the bridge is considered a reduced loading bridge. Few years ago, Public Administration proposed to reduce traffic on the bridge to one-way: the proposal was appropriate, given the current situation, but even now the situation has not changed.

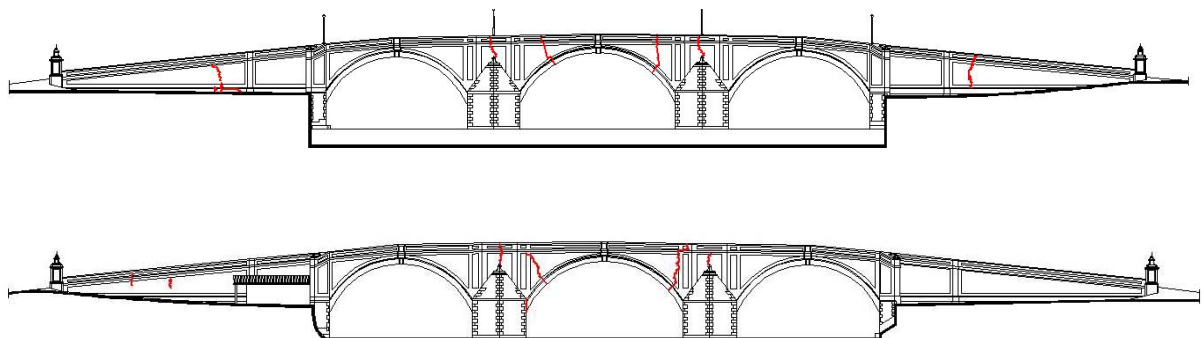


**Figure 4.11 Crack Distribution: i) North front, ii) South Front**

<sup>9</sup> From the letter of Giuseppe Brunelli, papal hydrostatic expert (23 luglio 1776): "*Finalmente le piccole crette accadute fin da principio alla sommità della fabbrica, cioè nei parapetti e nei poggiuoli, siccome non sonosi in seguito più accresciute, non ponno secondo l'arte attribuirsi a difetto di fondamenti, ma piuttosto a quel callo ossia compressione che accade da principio in tutte le nuove fabbriche, massime quando sono pesanti, ed elevate.*"



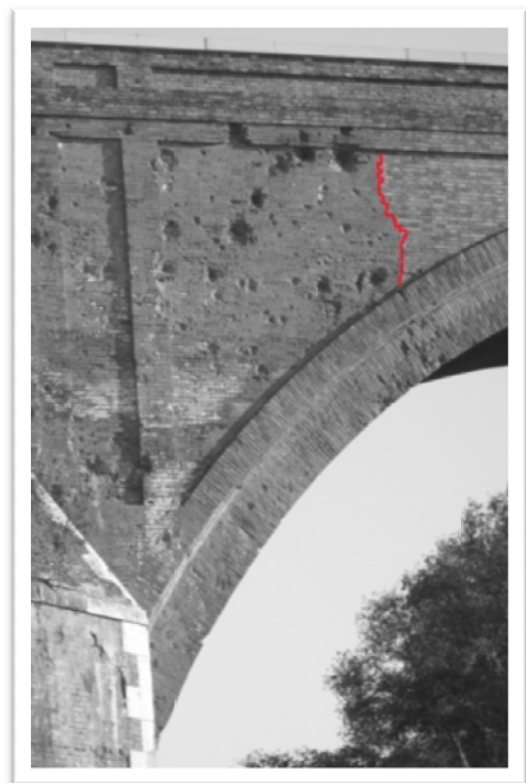
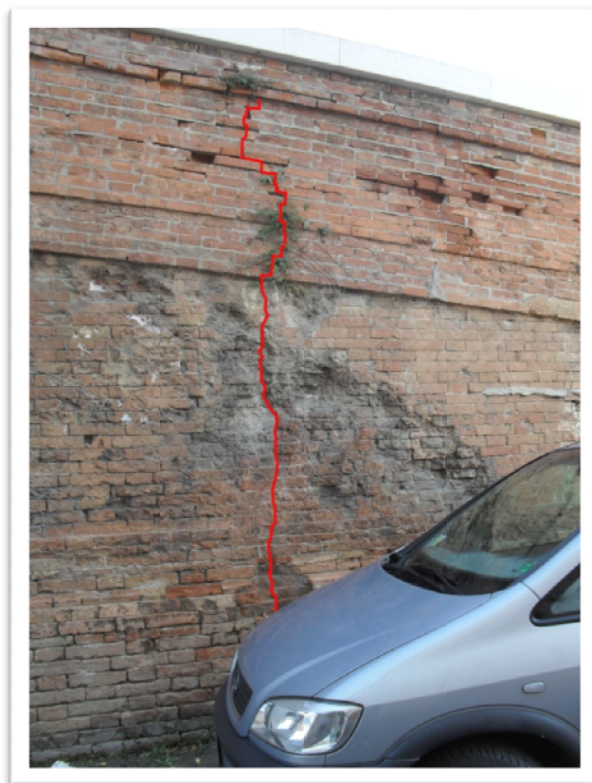
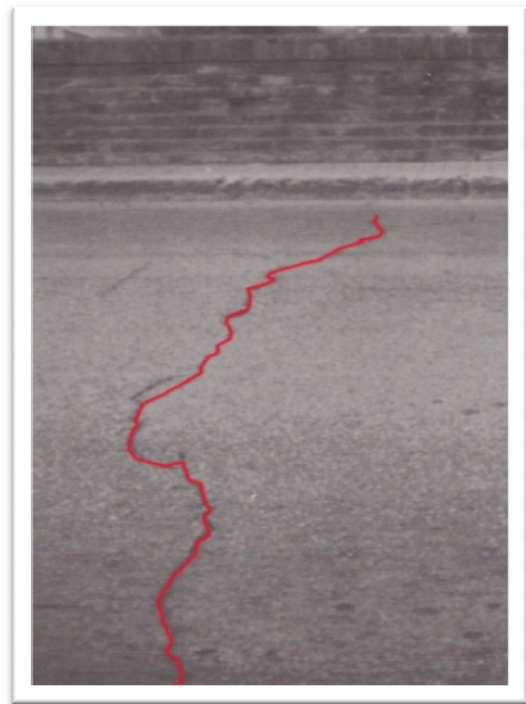


**Figure 4.12 Present State: i) vertical cracks over the piers; ii) crack on road surface in 1993; iii) cracks on lateral ramps; iv) on the central arch between the old structure and the reconstructed one.**



## 4.4 Analysis of Constructive Techniques

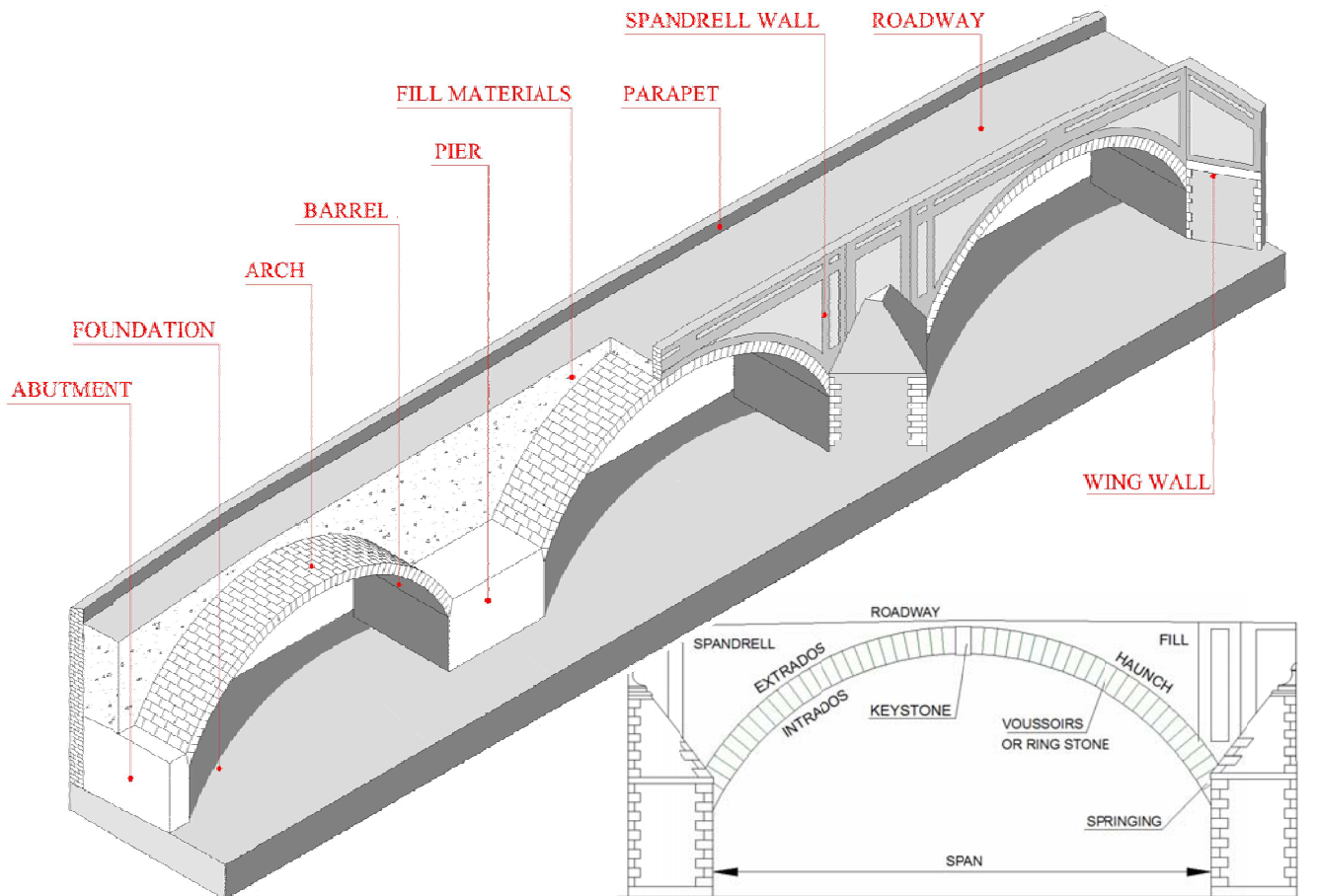


*Figure 4.13 Constitutive Elements of Clemente Bridge: Isometric Cross Section and Front View*

As just mentioned, Clemente Bridge was realized using traditional techniques endorsed by thousand-years experience, exactly as it happened in the ancient constructions. In particular, the constructive conception of this masonry arch bridge is essentially rooted in the roman construction model of substructure. The substructure can be so schematized: (i) the intrados of the vault stands on the provisional rib under construction; (ii) the spandrel walls are made of bricks and are connected with the arch below, making the structure very solid with a low stress states; iii) the piers are very wide.

However Clemente Bridge differs from Roman bridges due to the arch shape. Roman Bridges had semicircular arches with a rise-span ratio 1:2, while the arches of Clemente Bridge have a segmental shape, with a lower rise-span ratio. The reason is to maintain the road level as low as possible and not to obstruct the flow of the river, especially when Savio is in flood.

The constitutive elements that characterize Clemente Bridge, as illustrated in *fig. 4.13*, are:

- Arches: main supporting elements. They are characterized by:
  - Crown: the highest part of the arch;
  - Haunch: part of the arch between the springing and the crown;
  - Keystone: voussoir at the crown of the arch;
  - Span: space between two piers;
  - Spandrel: area above the extrados arch and below deck level;
  - Springing: point where the end of an arch meets the abutment or the pier;
  - Voussoir: unit that composes the arch.
- Abutment: end support of a bridge that resists to the horizontal thrust of the arch;
- Fill Material: rubble or earth used to fill the space between the arch and the deck level;
- Foundations: superficial structure on which piers and abutment stay;
- Pier: support between two arched spans;
- Spandrel Wall: lateral wall that contains the fill materials over the arch;
- Wing Wall: lateral wall of an abutment, forming a support and a protection to it.

In the following, the principal constitutive elements of Clemente Bridge are examined in relation to the constructive technique, that characterize them.

## Foundations

For a masonry arch bridge, the foundations are critical. The large thrusts of the arches need to be transferred down to keep the structure in a correct position. In 1684 the lack of a foundation was one of the causes of the collapse of the previous stone bridge. In fact the river in flood dug the ground under the piers: once the piers fell, also the arches followed them. When in 1729 a new bridge was proposed to build, the foundations were the first thing to think about. As in Roman bridges, timber piles were used: oak piles were required, at least seven feet

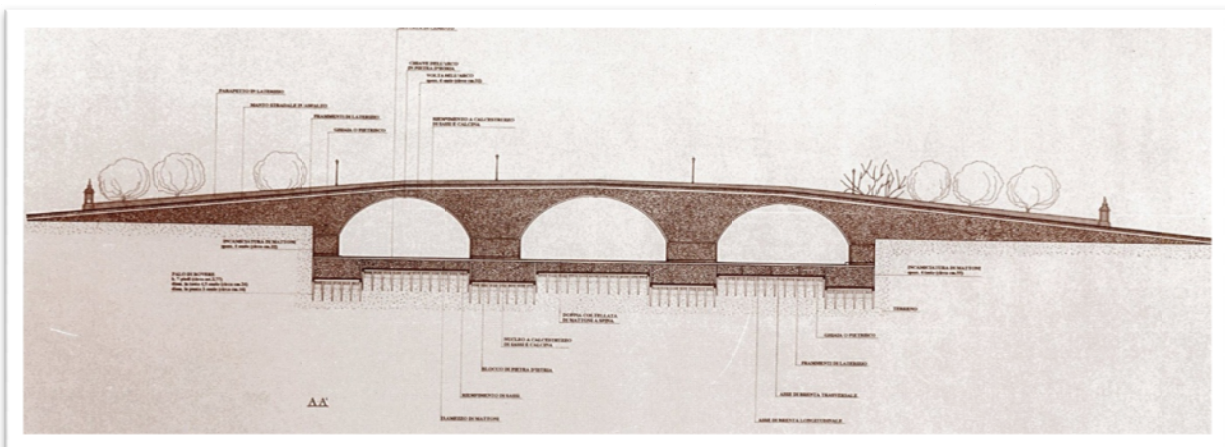


**Figure 4.14 Reconstructive Hypothesis of Simona D’Altri Darderi**



*Figure 4.15 Photo of the actual condition of the foundations: bottom right the oak piles*

long (3.77 m) and four ounces and half wide at the top (0.24 m)<sup>10</sup>. The piles were disposed into regular meshes and connected together in order to distribute the vertical load. The interspaces between the piles are filled with little stones. Over the top of the piles, bricks were collocated also in order to avoid that moisture corroded the pile heads. Then, the inside of the compartment created by piles was cleared by water and filled with inert materials. All the operations were conducted during the summer period when the river level was low, using a lot of workforce. As just remembered, the foundations were realized over thirty years, mainly for economic reasons. Once realized, the foundations had the form of a large raft, ninety-five meters long: nowadays they are still visible and give rise to a small waterfall down-river. In correspondence with the north side of foundations when Savio is dry, the top of some piles can be seen, as in *figure 4.15*.

### **Vertical Elements: Abutments and Piers**

The vertical bearing elements of the bridge are divided into abutments and piers. The abutments are the final vertical supports realized according to the bank. They withstand the

<sup>10</sup> It is reported in the Proceedings of Bridge Congregation, conserved at the Historic Archive of Cesena.

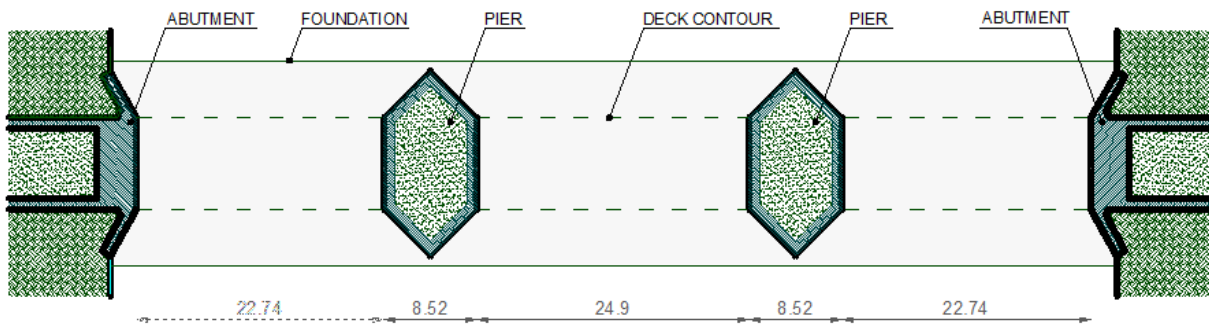


Figure 4.16 Plan of the Clemente Bridge

relevant horizontal thrust of the last span. Their section is hidden and is conditioned by the outline of the ground: so it is very difficult to know how they are actually composed. The lateral wing walls are all one with the abutment.

The piers are the vertical supports between two spans: they withstand essentially vertical actions. The pier sizing depends on two types of requirements: i) the pier must ensure the structure stability; ii) at the same time the pier must be more slender as possible in order to allow the river in flood to pass easily. The equilibrium between these two factors is not easy. Until the eighteenth century, stability was usually preferred to the slenderness. So the piers of Clemente Bridge seem too large to support only the arch thrust. The choice depended on three different reasons: i) the spans were not equal so the resultant of thrusts of the two adjacent arches was inclined and the pier was also subject to shear; ii) the centerings were not enough to allow the disarmament of all arches at the same time so initially the piers were subjected to an asymmetric thrust; iii) besides, in case of one arch's collapse, the piers should have been able to support the remaining vault thrust, without turn over until the arch reconstruction. As mentioned, during the Second World War a span collapsed. If Clemente Bridge had been designed according to the mathematics theories of De la Hire, it would have supported hardly this asymmetric thrust and probably the bridge would be totally collapsed.

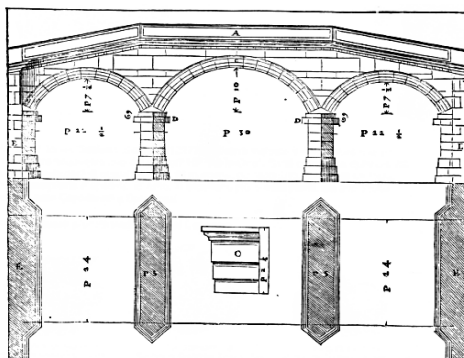


Figure 4.17 Palladio,  
"A bridge of my invention", 1570

In order to allow the river in flood to pass easily, the architects of the Clemente bridge used mainly two strategies: i) they reduced the number of the piers in the river bed from four to two; ii) they endowed the piers with cutwater both at upstream and at downstream. In particular the upstream cutwaters were used to protect the piers by the impact of tree trunks swept by the flood.



The presence of the cutwaters is important also from the static point of view, because they increase the resistant section both respect to live load and respect to overturning. As in Roman bridges, the cutwaters have a triangular profile characterized by an angle of ninety degrees: this shape facilitated the cutwater construction, as Palladio suggested in his treatises.

### Arches

The arches of Clemente Bridge have a segmental shape and have spans that vary from 23 to 25 meters. The candidate has carried out various researches to reconstruct the geometry of the section of the arches, both the ancient ones built in the eighteenth century and the central one rebuilt after the war. As remembered before, she visited State Archive of Forlì, Historic Archive and Technical Office of Cesena. Unfortunately the researches did not lead to any significant results. So she contacted Simona D'Altri Darderi, that wrote her degree thesis on this bridge, and the Cantori Architectural Firm, that realized various work on the bridge between 2009 and 2010, in particularly restoring the docks in limestone and remaking the sidewalks. D'Altri Darderi has hypothesized that the vault thickness is 80 cm, equivalent to the lower arch, while the upper arch would seem an architectural connection with the above brick curtain. On the contrary, Cantori Architectural Firm has hypothesized that the arch would have an average thickness around 120 cm. In fact during the excavations around the sidewalks on the central arch, they found bricks arranged to coast to sixty cm deep, that were assumed as part of



Figure 4.18 Bridge Front with wooden centerings used to construct time. Copy of Mauro Guidi

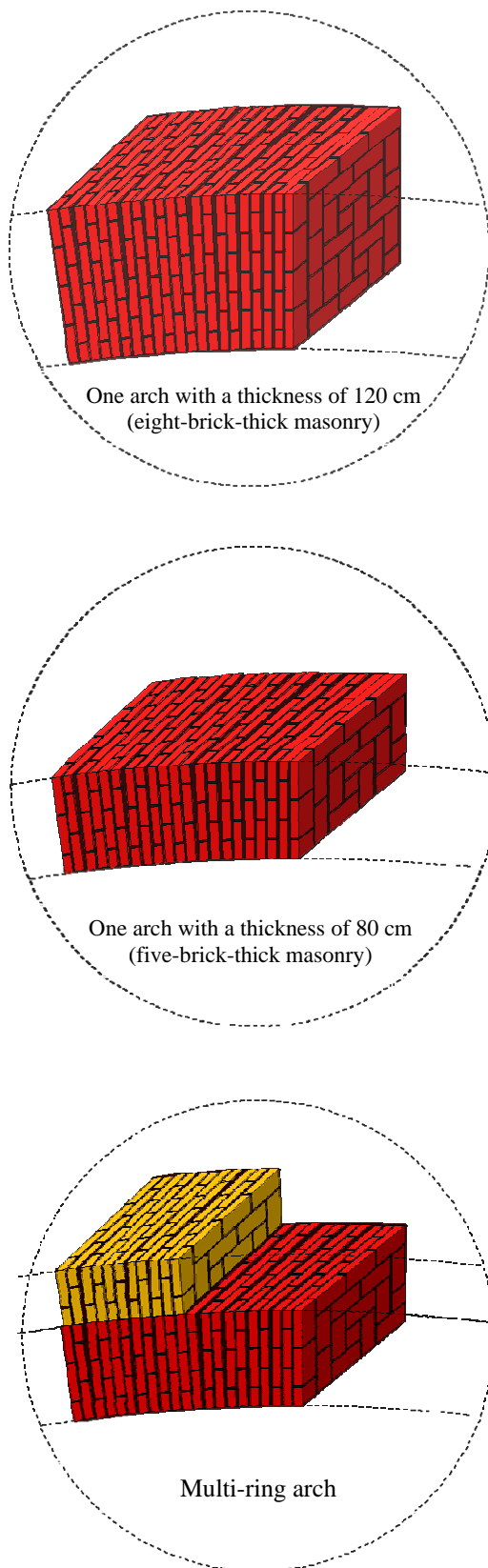


**Figure 4.19** Reconstructive hypotheses of the section of vault

the extrados of the vault. Unfortunately, excavations have focused only on the portions relating to the sidewalks, so it is not possible to prove that the arch was made with a constant rectangular cross section. However they had no photo of detail that would witness their hypotheses: the only photo, that they had, reports a panoramic of the excavations (see Annex 4.B), but anything useful is not visible. In the absence of reliable data, the candidate formulated three hypotheses in accordance with the data exposed, that are developed with the two-dimensional models in the next paragraphs. The three hypotheses as illustrated in *figure 4.19* are :

- the vault is one with a thickness of 120 cm (eight-brick-thick masonry);
- the vault is one with a thickness of 80 cm (five-brick-thick masonry);
- the vaults are two and are superimposed. The thickness of the lower one is 80 cm, while the thickness of the upper one is 40 cm.

The hypothesis of two separated vaults is supported by some constructions of the same period built near the bridge, as the buttresses of the external wall of the fortress park in *figure 4.20*.

Concerning the vault construction, is very interesting the design of Mauro Guidi (*figure 4.18*), that describes the temporary wooden structures used to sustain the arches at the beginning.

As reported by sources, the centerings were made by oaks wood and should have been fifteen, five for every vault. Actually the number was lower because the finances lacked. Probably the centerings used were four: this hypothesis was supported by the number of longitudinal cracks present on the vault nowadays (*figure 4.21, annex 4.2*). The centerings were sustained only at the vault springing by two vertical wooden pillars, that were collocated next to the pier or the abutment and set on the foundation. The design of the centerings is classical, similar to those reported in the nineteenth-century manuals. Struts and chains composed a complex polygonal structure, that was inscribed in the diameter of the vault.

In general in this bridge, all the structural elements are classical and were realized using traditional techniques. The big arches almost Romans, the foundations on wooden piles, the oversizing of the piers in order to ensure the structure stability, the triangular profile of the cutwaters, the polygonal geometry of the centerings: all remember that, in building this bridge, the aim was not to experience something new, not to invent, but to guarantee a stable and durable bridge after centuries of failed attempts.



*Figure 4.20 External wall of the fortress park*

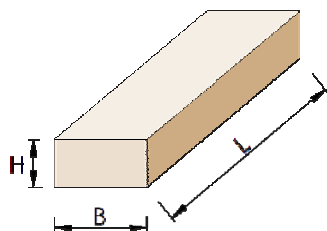


*Figure 4.21 Longitudinal cracks on the vault*

## 4.5 Analysis of Materials

The assessment of the actual conditions of the existing masonry constructions plays a main role in the design of the intervention to be performed. Information about different aspects have to be acquired, including dimensional data of the constituent elements (i.e. brick and mortar layers), local defects and the mechanical characteristics of materials. The quantity and quality of the data collected affects the degree of precision of the analysis methods used in the building assessment. The acquisition of these data may be occur through historical researches, visual surveys or tests to perform directly on on-site materials and construction elements.

Firstly, in the case study of Clemente Bridge, the candidate has identified the different types of masonry that constitute the whole work. The oldest ones, still intact, are handmade and almost certainly come from different furnaces. The post-war recoveries are made with new drawn bricks, even if the superintendent had prescribed that were handmade as the ancient ones (annex 4.1). The main dimensions are shown in *Table 4.3*.



Lenght L (cm)	Base B (cm)	Height H (cm)
31	14,5	6,0
30	14,0	7,0
30	14,0	5,0
29	14,0	6,5
29	14,0	6,0
27	13,0	6,5
27	13,0	6,0

**Table 4.3** *The main dimensions of the Clemente Bridge bricks: i) in pink the ancient ones; ii) in orange the post-war restorations*

One of the main purposes of the evaluation of masonry mechanical characteristics is to provide strength values, elastic properties and other parameters to be used as input data for the implementation of finite element models. There are two different approaches that may be employed for the evaluation of the masonry mechanical properties, even if everyone has limitations in the applicability and in the reliability of obtained results.

The first way is to obtain from the existing structure masonry wallets similar to those



required by the technical standards<sup>11</sup> to test in compression or diagonal compression. In historical constructions of particular architectural value, this way is difficult to follow because it is not possible to obtain samples large enough to be tested in laboratory.

So it is possible to estimate the masonry mechanical properties from the data obtained by laboratory tests on individual components (brick and mortar). In fact it is well known that the masonry mechanical characteristics are strictly dependent on those of the constituent materials even if, actually, an established theory that allows to deduce the masonry strength by the resistance of the individual components does not exist. European standards<sup>12</sup> provide tables and correlations able to resolve partially this problem.

Taking into account the historical importance of the investigated bridge, the candidate has taken a series of samples of mortar and brick from the south-east wing wall, that are subsequently tested in the laboratory.



**Figure 4.22 South East Wing Wall**



**Figure 4.23 Sampling Point**



**Figure 4.24 The three brick sample**

<sup>11</sup> See Italian technical standards (NTC 2008), Chapter 11.10.3: “The experimental characteristic compression strength is determined on  $n$  wallets ( $n \geq 6$ ), following both for the preparation for the test that the methods indicated below. The samples (wallets) should have the same characteristics of the studied masonry, and each of them must consist of at least three layers of resistant brick and must respect the following limitations: Length ( $b$ ) at least two block lengths; Height/width ratio ( $l/t$ ) ranging between 2.4 and 5”.

<sup>12</sup> UNI EN 1996-1-1: Eurocode 6. Design of masonry structures. General rules for reinforced and unreinforced masonry structures



*Fig 4.25 Bricks samples rectified before load application*

### ***Brick compressive strength***

So three bricks (namely *M1*, *M2* and *M3*) were taken from the bridge walls to estimate their mechanical characteristics. Samples were obtained cutting these brick specimens as shown in *Table 4.4*. The loaded faces were subsequently rectified.

After the preparation phases, the samples were subjected to compression tests, carried out by loading the brick along actual wall loading direction. The ultimate compression strength values obtained from laboratory tests are reported in *Table 4.4*.

	Resistant section (mm)	High (mm)	Strength (N/mm <sup>2</sup> )
M1	55,0 x 57,0	56,3	19,3
M2	57,0 x 59,5	59,1	21,4
M3	48,5 x 48,8	50,2	34,0

*Table 4.4 Brick compression strength*

### ***Mortar compressive strength***

The mechanical characterization of the mortar is a difficult task because of two factors: at first the reduced thickness of the joints, on average 10-15mm but not constant, secondly the difficulty to take samples due to adhesion between the mortar and the brick.

However, if it is possible to extract from the masonry small portions of the mortar joints without damaging them, it is possible to employ a test that is commonly called punching test. This test consists in subjecting to compression a portion of the extract. So two samples (*Ma1* and *Ma2*) were taken from the bridge walls of the Clemente. The layer of mortar extracted has a thickness of 10-15 mm. In order to make reliable the test, the part of

the sample subjected to cape must have a diameter of at least 50 mm, even if the compression will affect a diameter of only 20/30 mm. Unfortunately in this case, it has not been possible to obtain a sample of 50x50 mm section because the specimen broke in an irregular manner at the time of cutting. So cylinder of 20 mm were realized. The test on the specimen was then performed by determining the punching resistance as the ratio between the breaking load and the resisting section of mmq 314, that is the section of the punch. The flatness of the bearing surfaces was provided with a plaster cape<sup>13</sup>. The test was performed under displacement control with a rate of about 0.0075 mm·s<sup>-1</sup> while the processes of loading under force control with a rate of 0.05 MPa·s<sup>-1</sup>. Therefore, it was a rather slow test. The compressive strength is defined as:

$$f_m^c = 1,96 \frac{F_{ult}}{\pi \phi^2}$$

Where:  $f_m^c$  mortar compression strength;  
 $F_{ult}$  sample collapse load.

This equation includes the effects of friction at the interface punch/sample and provides the uniaxial compressive strength of mortar but unfortunately no information can be obtained on the elastic modulus of the mortar. The mortar compression strength values obtained from laboratory tests are reported in *Table 4.5*.

	Thickness (mm)	Strength (N/mm <sup>2</sup> )
Ma1	9,9	10,2
Ma2	14,9	6,3

*Table 4.5: Mortar Compression strenght*

<sup>13</sup> Soaked mortar to saturation prior to execution of the cape.



*Fig 4.26 Bricks failure Mechanism*





**Figure 4.27** The two mortar sample



**Figure 4.28** Compression test on mortar sample: i) before load application; ii) failure mechanism

### Mechanical characteristic of masonry

In accordance with Eurocode 6, the characteristic compressive strength of masonry should be determined from the results of the tests used as parameters for the equation:

$$f_k = K \cdot f_b^{0,7} \cdot f_m^{0,3} \quad (2)$$

where:

$f_k$  is the characteristic compressive strength of the masonry, in  $\text{N/mm}^2$

$K$  is a constant (for Clemente Bridge is 0,55) and, where relevant, modified according to table 1.4

$f_b$  is the normalized mean compressive strength of the units, in the direction of the applied action effect, in  $\text{N/mm}^2$

$f_m$  is the compressive strength of the mortar, in  $\text{N/mm}^2$

In the absence of a value determined by experimental tests, the short term secant modulus of elasticity of masonry ( $E$ ) for structural use may be taken to be  $K_E \cdot f_k$  (the recommended value of  $K_E$  is 1000), while the shear modulus may be taken as 40% of the elastic modulus.

So after all the experimental analysis, the mechanical characteristics of the Clemente Bridge's masonry were determined and reported in *Table 4.6*. The certificates of laboratory tests are show in *Annex 4.C*.

$f_b$	$f_m$	$K$	$f_k$	$E$	$G$
(MPa)	(MPa)		(MPa)	(MPa)	(MPa)
24,9	8,25	0,55	9,83	9830	3932

**Table 4.6:** Clemente Bridge masonry mechanical characteristics

As regards the evaluation of the mechanical properties of masonry, there are the limits previously indicated. It

must be noted, however, that often the crisis of a masonry structure is not due so much to the achievement of high stress, but to the formation of failure mechanisms due to motions of rigid body portions or structural elements, such as those that will be discussed below.

Masonry Unit		General purpose mortar	Thin layer mortar (bed joint $\geq 0.5$ mm and $\leq 3$ mm )	Lightweight mortar of density	
				$600 \leq \rho_d \leq 800 \text{ kg/m}^3$	$800 < \rho_d \leq 1300 \text{ kg/m}^3$
Clay	Group 1	0.55	0.75	0.30	0.40
	Group 2	0.45	0.70	0.25	0.30
	Group 3	0.35	0.50	0.20	0.25
	Group 4	0.35	0.35	0.20	0.25
Calcium Silicate	Group 1	0.55	0.80	‡	‡
	Group 2	0.45	0.65	‡	‡
Aggregate Concrete	Group 1	0.55	0.80	0.45	0.45
	Group 2	0.45	0.65	0.45	0.45
	Group 3	0.40	0.50	‡	‡
	Group 4	0.35	‡	‡	‡
Autoclaved Aerated Concrete	Group 1	0.55	0.80	0.45	0.45
Manufactured Stone	Group 1	0.45	0.75	‡	‡
Dimensioned Natural Stone	Group 1	0.45	‡	‡	‡

‡ Combination of mortar/unit not normally used, so no value given.

*Table 4.7 Values of K given by the Normative*

## 4.6 Comparison between the different Methods

The structural analysis of the Clemente Bridge is performed through the Thrust Line Analysis Method and the Mechanism Method. The computational modeling tools used for this masonry arch bridge are the same used for the generic masonry arch bridge, that is Archie-M 2.4.1 and RING 3.0. As just remembered in chapter 2, both the software are based on Heyman's Theory and on the principles of Limit analysis: Archie-M uses the lower bound theorem, while Ring uses the upper bound theorem. Archie-M gives as graphic output the position of a potential thrust-line and the hinge position for any given loading regime. In Archie-M, the collapse load can be estimate by varying the load value until a sufficient number of hinges is formed. On the contrary, Ring allows to identify the ultimate limit state, determining the percentage of live load, that will lead to the collapse. As a result of the Ring's analysis, the minimum adequacy factor for the live load is obtained, together with a graphic representation of the thrust line and the failure mode.

In the case of Clemente Bridge, Ring e Archie-M reproduce almost the same mode of collapse. The bridge is modeled as in-plane structure. The software require as input: i) geometry; ii) material properties; iii) loading.

The principal geometric data of the Clemente Bridge are provided in the first paragraph of this chapter and derived by a site survey. As remembered in the paragraph 4.4, the only geometric unknown quantity is the arch thickness. Three are the hypotheses contemplated: i) the vault is one with a thickness of 120 cm (eight-brick-thick masonry); ii) the vault is one with

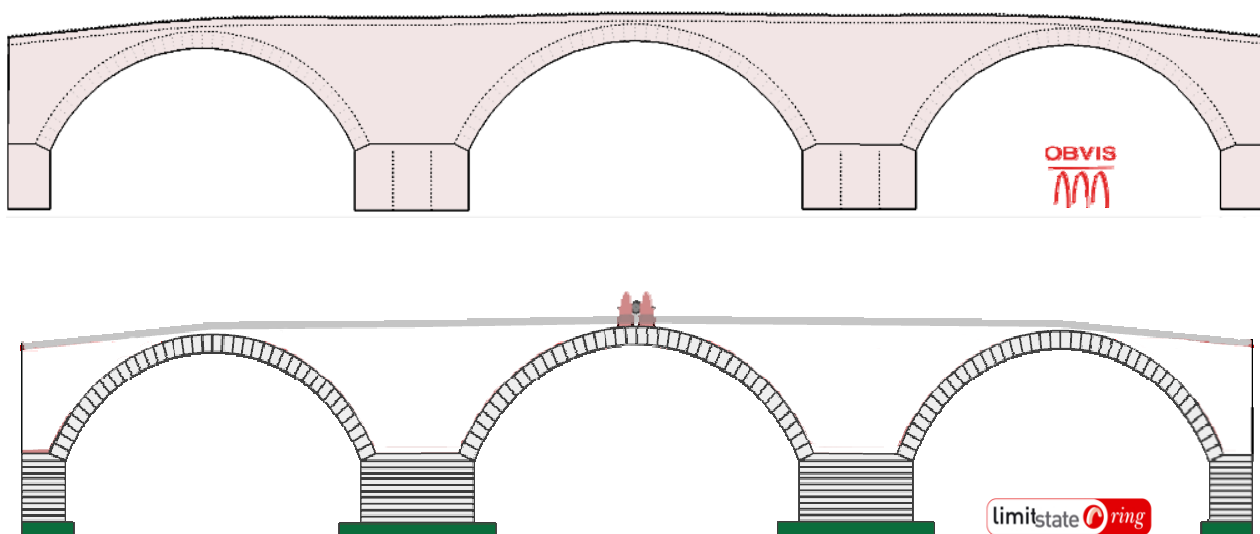


*Figure 4.29 Geometric Model of the Bridge: i) Archie-M; ii) Ring*

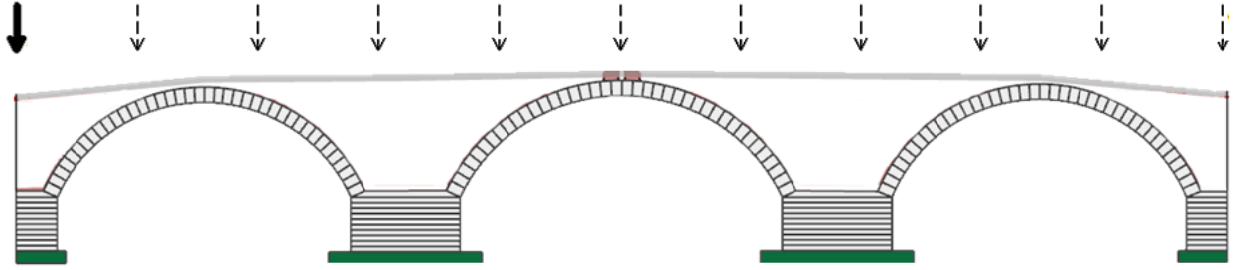


Figure 4.30 Eleven load cases considered

a thickness of 80 cm (five-brick-thick masonry); the vaults are two and are superimposed (the thickness of the lower one is 80 cm, while the thickness of the upper one is 40 cm). The first two hypotheses are analyzed both with Archie-M and Ring, while only Ring is able to study the third hypothesis, that is to analyze multi-ring arches enabling separations between the various rings. In order to save computational effort, in the software every arch is divided in 40 blocks and every pier in 20 blocks. As demonstrated in chapter 3, this leads to a very small overestimate of the predicted carrying capacity of the real structure.

Regarding the material properties, both the programs require as material input: i) for masonry arch, the unit weight ( $\text{KN/m}^3$ ) and the compressive strength (MPa); ii) for backfill, the unit weight ( $\text{KN/m}^3$ ) and the angle of friction (degree). The masonry properties are derived by the tests on the material components, reported in the previous paragraph. The unit weight is  $15,53 \text{ KN/m}^3$ , the compressive strength is 9,83 Mpa in accordance with the Eurocode 6. Unfortunately it has not been possible to test the backfill material due to the historical value of

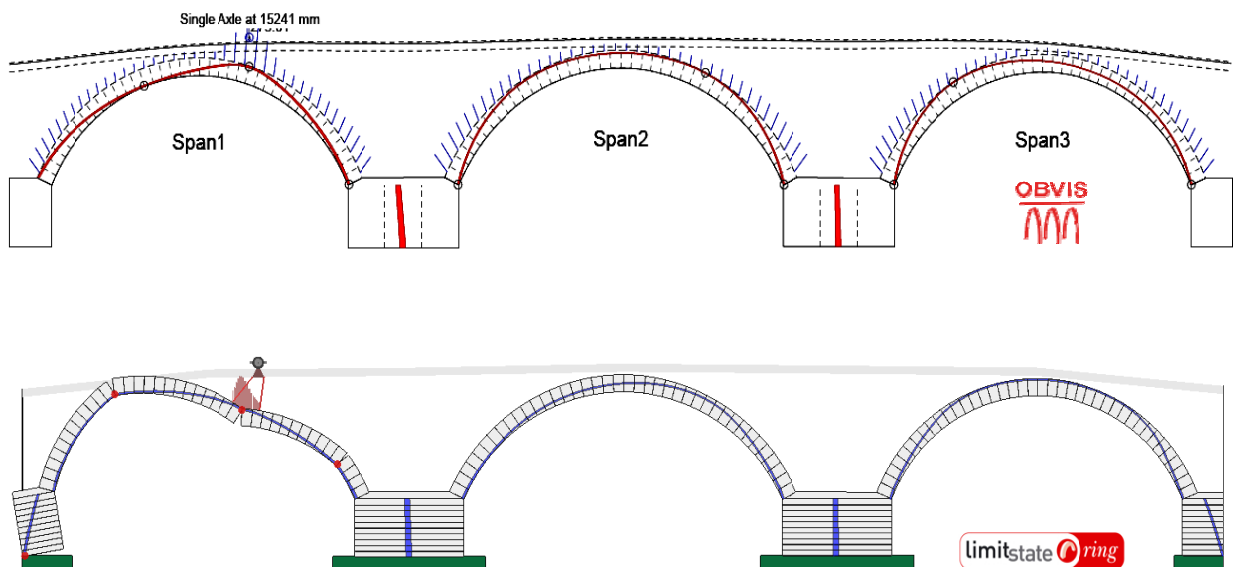


Figure 4.31: Collapse Modes: i) Archie-M; ii) Ring

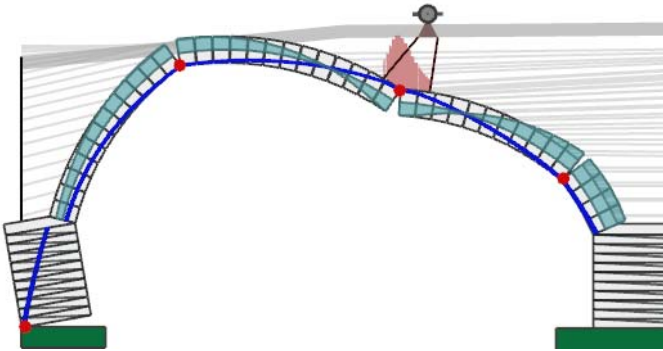


Figure 4.32: First span: failure mode and bending moment

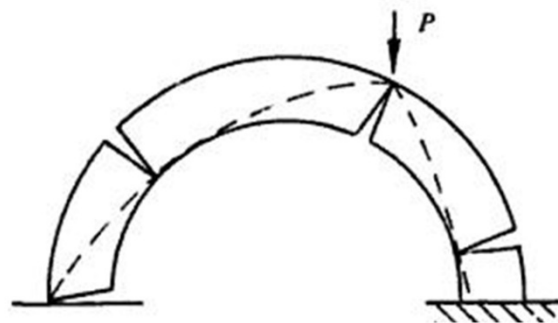


Figure 4.33: Heyman's Point Load

the bridge. So in absence of comprehensive test results on backfill, typical values found in similar surveyed bridges have been considered to assume. The unit weight is considered  $18 \text{ KN/m}^3$ , the angle of friction is considered 30 degree.

Regarding the load condition, it's used a EU single axle load<sup>14</sup>. To simulate the loading vehicle movement across the bridge and to identify the critical position, a series of load cases are taken into account. Firstly the whole bridge is divided into ten parts: eleven load case are considered (*figure 4.30*). Once individuated the worst load position, the sequel step is to thicken the load cases around this zone to determine the exact condition that results in the lowest adequacy factor (*figure 4.34*).

Ring e Archie-M reproduce almost the same mode of collapse. In both cases, the critical position of the load is the third one from the left springing, on the first span (*figure 4.30*). Obviously as the structure is symmetrical, there is a mirror-like collapse condition also on the third span. As illustrated in *figure 4.31*, at limit state the collapse is connected with the formation of a number of hinges enough to transform the stable arch in a unstable mechanism. In particular, on the first span the hinges open in alternating way in the intrados and in the extrados, following a pattern comparable to that described by Jacques Heyman for the point load case. Concerning the hinge location, there are small differences between Ring and Archie-M because the critical position of the live load is close to the supports (*table 4.8*). As just remembered, two different arch thicknesses are analyzed with Archie-M and Ring: the results reported in *table 4.8* and *4.9* highlights that there are small differences in hinge positions between the two hypotheses. In *figure 4.32* it can be observed also that the bending moment is equal to zero whenever the trust line pass the axle line, while it is maximum close to the hinges.

<sup>14</sup> The load is about 112.82 KN.



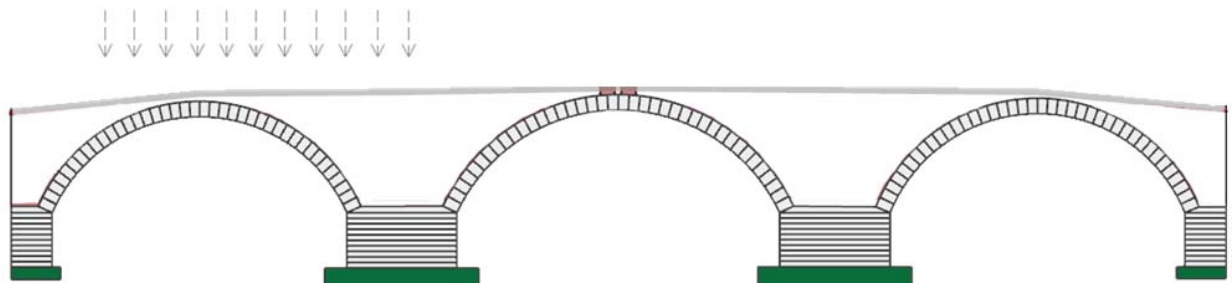


Figure 4.34: Eleven Load Case thickened around the worst load position

Load Case	Ring 3.0				Archie-M 2.4.3.1			
LC1	4	13	23	38	1	13	24	39
LC2	0	6	16	26	4	16	26	40
LC3	0	8	18	29	8	18	28	40
LC4	0	9	20	33	0	11	20	31
LC5	0	11	23	35	0	12	23	36
LC6	0	12	25	36	0	14	25	40
LC7	0	13	27	38	0	16	28	40
LC8	0	14	29	40	0	17	30	40
LC9	0	14	31	40	0	18	31	40
LC10	0	15	32	40	0	18	32	40
LC11	0	15	34	40	0	18	32	40

Table 4.8 Hinge Positions for different load positions, arch thickness 1,2 m

Load Case	Ring 3.0				Archie-M 2.4.3.1			
LC1	5	13	22	35	3	13	22	31
LC2	0	7	15	25	4	15	25	40
LC3	0	9	18	28	9	18	27	40
LC4	0	10	20	32	0	11	20	31
LC5	0	12	23	34	0	13	23	40
LC6	0	14	25	36	0	15	26	40
LC7	0	15	27	37	0	17	28	40
LC8	0	15	29	39	0	18	30	40
LC9	0	16	31	40	0	18	32	40
LC10	0	16	33	40	0	18	32	40
LC11	0	17	34	40	0	18	32	40

Table 4.9 Hinge Positions for different load positions, arch thickness 0,8 m

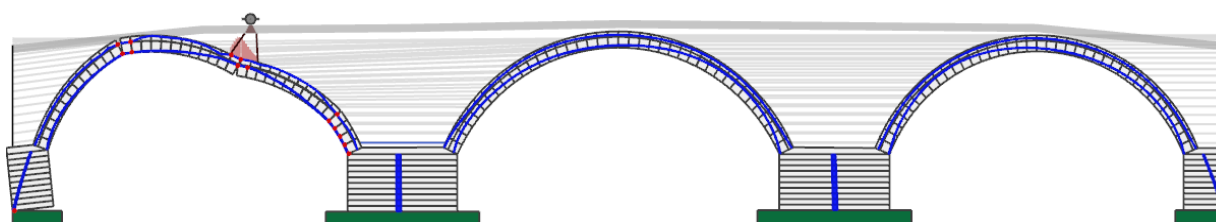


*Figure 4.35: Multi-ring arch: failure mode*

Concerning the collapse load value, Archie-M collapse load is smaller than Ring's one both for arch thickness equal to 1.2 and for arch thickness equal to 0.8 m (*table 4.10 and table 4.11*). Obviously, the collapse load calculated for the arch thickness of 0.8 m is smaller than the other one. About the collapse load, other considerations can be made analyzing the graphs contained in *table 4.10 and 4.11*. The first diagram shows the ratio between the collapse load of Archie-M and Ring in relation to the different load positions and arch thickness. The red line divides the graphic into two areas: over the red line there are Archie-M collapse loads higher than Ring's ones (case 3,4 and 5). The analysis reliability becomes lower in load case 10 and 11<sup>15</sup>. In the second diagram, the difference % between the collapse load of Archie-M and Ring is reported in relation to different load cases and arch thickness. Analyzing the graph trend, it's clear how the end positions<sup>16</sup> are the most critical ones for the analysis due to the variances in the results, where in the intermediate positions the differences are more attenuate. In particular analyzing the arch of thickness equal to 1,2 m, the difference % between the results obtained in the intermediate load cases is lower than 20%. These results underlines the reliability of the analysis under precise load conditions.

As there are no certainties on the constructive modes and the arch thickness is very high, it is also supposed that every arch may be made by two debonded rings, separated in the model by frictional contacts. As remembered in paragraph 4.4, the hypothesis of two separated vaults is supported by some constructions of the same period built near the bridge. Obviously in this analysis, the value of the minimum adequacy factor decreases compared to the one-ring arch analyzed before (*table 4.12*). This factor highlights the loss of bearing capacity for the bridge. Also in this case the critical load position is on the first span, but obviously there are two thrust line for every span and an higher number of hinges. (*figure 4.35*)

<sup>15</sup> Load Cases 10 and 11 where the ratio is respectively 0,42 and 0,19 for  $b = 1,2\text{m}$ ; or 0,28 and 0,14 for  $b = 0,8\text{m}$ .

<sup>16</sup> Load Cases 1,2,8,9,10,11.

Load Case	Position x [mm]	Minimum Adequacy Factor	
		Ring 3.0	Archie-M 2.4.3.1
LC1	6027	72,9	39,8
LC2	7868	53,2	40,4
LC3	9710	37	37,13
LC4	11551	30,2	36,8
LC5	13393	26,8	30
LC6	15234	25,6	23,74
LC7	17075	29	25
LC8	18917	46,2	35
LC9	20758	79,8	50
LC10	22600	191	79,8
LC11	24441	761	145,6

*Table 4.10 Load Case positions and Minimum Adequacy Factor, arch thickness 1,2 m*

Load Case	Position x [mm]	Minimum Adequacy Factor	
		Ring 3.0	Archie-M 2.4.3.1
LC1	6027	45,2	32,7
LC2	7868	36,2	21,7
LC3	9710	26,1	25,2
LC4	11551	21,4	21,9
LC5	13393	18,6	17,6
LC6	15234	17,8	13,4
LC7	17075	20,3	14,8
LC8	18917	32,1	15
LC9	20758	53,8	20,6
LC10	22600	120	33,5
LC11	24441	413	59,3

*Table 4.11 Load Case positions and Minimum Adequacy Factor, arch thickness 0,8 m*

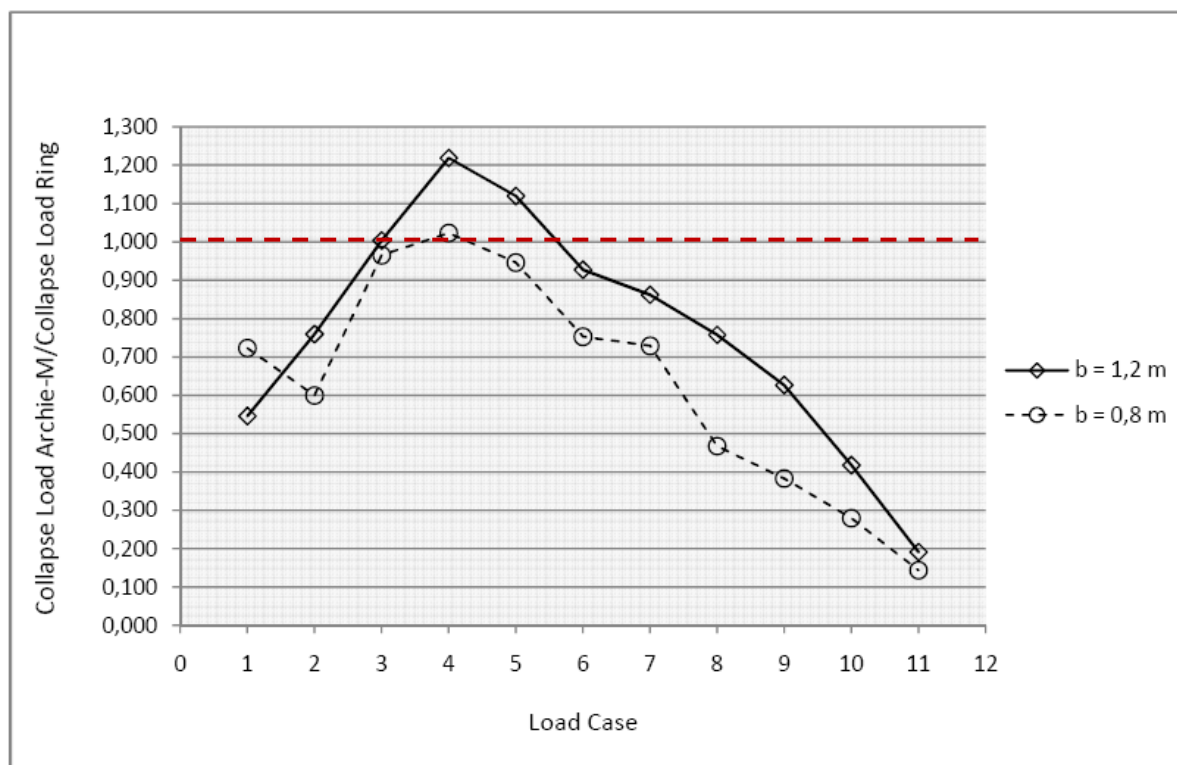


Figure 4.36 Collapse Load ratio for different positions and thickness

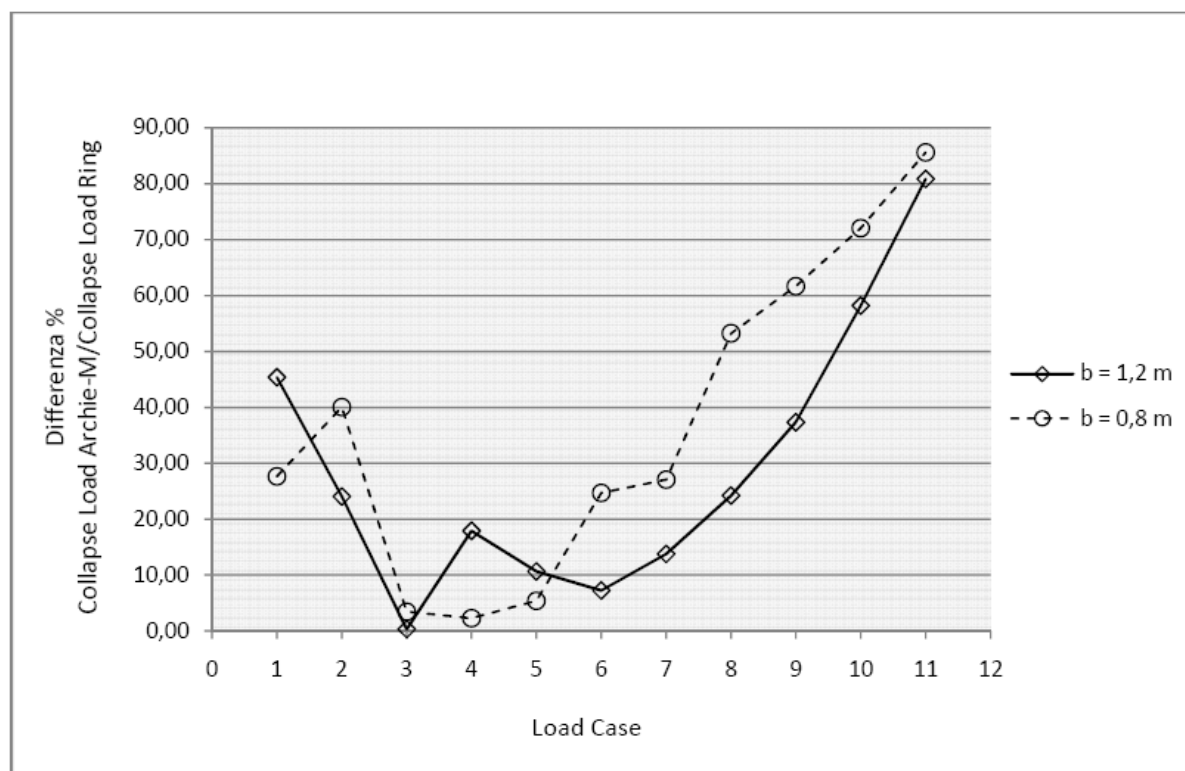


Figure 4.37 Difference % collapse load ratio for different position and thickness

Load Case	Position x [mm]	Collapse Load Ring 3.0 [kN]	
		One-ring	Multi-ring
LC1	6027	8224,58	5437,92
LC2	7868	6002,02	3971,26
LC3	9710	4174,34	3113,83
LC4	11551	3407,16	2549,73
LC5	13393	3023,58	2154,86
LC6	15234	2888,19	1963,07
LC7	17075	3271,78	2075,89
LC8	18917	5212,28	3091,27
LC9	20758	9003,04	5031,77
LC10	22600	21548,62	11090,21
LC11	24441	85856,02	35651,12

Table 4.12 Minimum Adequacy Factor for One-ring arch and multi-ring arch

**Italian Technical Standards.** The last analysis concerns the study of Clemente Bridge in accordance to the Italian “*Technical Standards for the Construction*” of 2008. These standards impose different load conditions according to the bridge category. Clemente Bridge belongs to the second category, because only reduced live loads can cross it. In this case, the Standards suppose to divide the bridge into two lanes, loading them with different point and distributed loads. Nevertheless, the Standards emphasize that the load disposition has to be chosen so to obtain the most unfavourable project conditions. Thus, referring to the Italian Standards but at the same time simulating a static test condition, the bridge is loaded symmetrically on the middle axle, overestimating the loads prescribed by the Standards. In this way, a combination of two types of loads is considered, ensuring higher safety standards: i) double axle tandem point load  $Q_{ik}$  of 440 kN, characterized by a loaded length of 400 mm and a width between the axles of 2000 mm; ii) a distributed load  $q_{ik}$  of 7.20 kN/m<sup>2</sup> over all bridge length (figure 4.38).

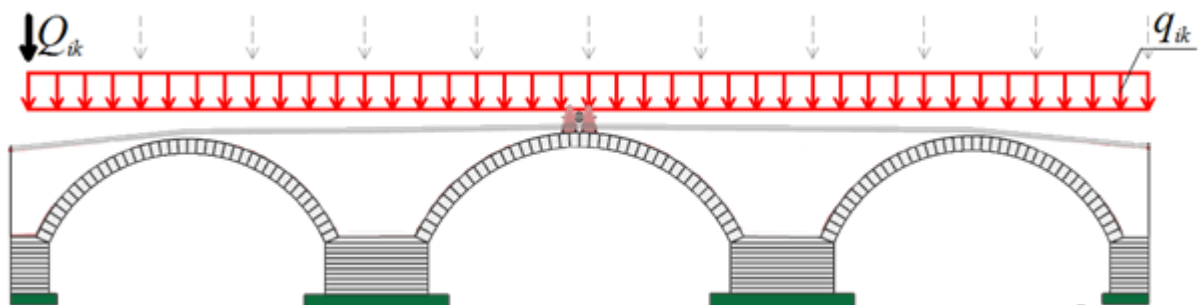


Figure 4.38 Clemente Bridge's analysis in accordance to Italian Technical Standards

The analysis is performed though Ring. The critical position is always on the first span, with the double axle load spaced between 17,61 m and 19,21 m from the left springing. In this case the minimum adequacy factor is equal to 3.98, so the bridge can be considered safe concerning the Italian Technical Standards.

## **Annex 4.A**

---

### **Post war Documentation**

- i) Letter of Superintendent of Monuments, that gave recommendations on the curtain restoration in 1946.....p. 119
- ii) A survey of the damage to curtains, perhaps attached to some economic evaluation for the restoration of the monument.....p. 120
- iii) Estimate of the works required for bridge completion made by Corps of Engineers of Forlì.....p. 126





a

BOLOGNA, 16 Agosto 1945  
VIA BELLE ARTI 42 - TEL. 191

**SOPRINTENDENZA AI MONUMENTI  
DELLA ROMAGNA**  
Province di FERRARA - FORLÌ - RAVENNA

Al Sindaco del Comune di CESENA

Prot. N. 832 Class. \_\_\_\_\_  
Risp. a lett. N. \_\_\_\_\_ del \_\_\_\_\_  
Allegati \_\_\_\_\_

OGGETTO: Cesena - Ponte Vecchio sul Savio

64/12  
Att. Esaminato  
4 GIU. 1955

Riferendomi al sopralluogo compiuto al Ponte in oggetto, in corso di restauro, raccomando vivamente di fare tutto il possibile perchè il rivestimento esterno in laterizio venga eseguito con mattoni a mano delle dimensioni di quelli antichi; gli elementi sagomati anch'essi lavorati a mano dai mattoni cotti, e la stuccatura, dove sarà escluso il cemento, sia fatta con malta di calce colorita in pasta per evitare che, se la sabbia ha un tono grigio, asciugando resti di colore freddo. Basterà in tal caso mescolare del colore giallo, evitando in ogni caso la polvere di mattone.

I rifacimenti dovranno essere limitati alla cortina caduta, procurando di consolidare le parti rimaste per testimonianza del tipo costruttivo originale.

Il restauro già eseguito durante l'amministrazione degli Alleati, mal riuscito, dovrà essere almeno patinato secondo i suggerimenti che saranno dati al momento opportuno, e cioè quando il ponte sarà restaurato completamente.

Confido nella passione dell'Autorità Comunale e nella valentia del Sig. Ing. Capo Dott. Tellarini, perchè il Ponte Vecchio sul Savio, uno dei più mirabili esempi medioevali della Romagna, riprenda il tipico aspetto artistico che aveva prima di aver subito le offese belliche.

**MUNICIPIO DI CESENA**  
P. G. N.º 18178 10 AGOSTO 1945  
CAT. 40. CLASSE \_\_\_\_\_ FASC. 944

IL SOPRINTENDENTE AI MONUMENTI  
(Arch. Capezzuoli Corrado)  
*Corrado Capezzuoli*

all. 6

FIGURE ED ANNOTAZIONI

②

LAVORI DI RIPARAZIONE E -  
RESTAURO DEL PONTE VECCHIO  
SUL SAVIO IN CESENA -

IMPRESA: COOP. VALLE DEL SAVIO

LIBRETTO DELLE MISURE -

3

DATA della misura 1	ARTICOLO dell' Elenco 2	INDICAZIONE DEI LAVORI E DELLE PROVVISTE 3	Fattori (1) 4	Prodotti 5
30-6-1946	7	Più area sinistro a valle Volta con molta di cemento.		
		4.10 x 0.45 x 0.80	1.476	
		4.50 x 0.60 x 0.80	2.160	
		2.50 x 0.70 x 0.80	1.400	
		3.30 x 0.60 x 0.58	1.148	
		2.50 x 0.90 x 0.58	1.305	
		3.60 x 1.20 x 0.58	2.508	
		1.20 x 1.00 x 0.58	0.696	
		1.00 x 0.50 x 0.30	0.150	
		0.50 x 0.70 x 0.30	0.105	
		0.30 x 0.80 x 0.30	0.072	
		1.40 x 0.58 x 0.45	0.365	
		1.30 x 0.45 x 0.30	0.1575	
		1.50 x 0.35 x 0.45	0.236	
		1.45 x 0.80 x 0.30	0.348	
		6.20 x 0.80 x 0.30	1.488	
		9.20 x 0.58 x 0.45	2.448	
			<u>Summano me</u>	<u>16.030</u>
		da dedursi		
		0.80 x 0.45 x 0.30	0.108	
		0.90 x 0.45 x 0.30	0.081	
		1.10 x 0.20 x 0.45	0.099	
			<u>Totale deduzioni me</u>	<u>0.288</u>
			<u>Restano me</u>	<u>15.742</u>

(1) - I fattori si scrivono in colonna, separando con una lineetta trasversale quelli appartenenti a prodotti diversi.

Soc. Coop. MURALE VALLE DEL SAVO  
CESENA  
Fecini

15

DATA della misura	ARTICOLO dell' Elenco	INDICAZIONE DEI LAVORI E DELLE PROVVISTE	Fattori (1)	Prodotti
1	2	3	4	5
5-12-1946	6	Ricostruzione murature sotto il fianco imposta dell' arco -  $(4.35 \times 0.80 \times 0.35) - (1.50 \times 0.35 \times 0.35)$ $4.35 \times 1.10 \times 0.65$ $4.35 \times 0.95 \times 0.80$ $4.35 \times 1.65 \times 1.10$	1035 3110 3305 7890	15344
5-12-1946	5	Conglomerato cementizio per fon- dazione - $2.80 \times 1.30 \times 2.20$	8008	8008
7-12-1946	7	Ricostruzione dell' imposta dell' arco di mezzo a valle (lato sinistro) a valle  $3.80 \times 0.80 \times 0.30$ $3.20 \times 0.58 \times 0.30$ $3.50 \times 2.60 \times 0.26$	0902 0556 1113	2651
11-12-1946	7	Ricostruzione dell' imposta dell' arco di mezzo a monte (lato sinistro) a monte  $(4.00 \times 0.80 \times 0.30) - (0.80 \times 0.30 + 0.50 \times 0.30 \times 0.30)$ $3.00 \times 0.58 \times 0.30$ $2.60 \times 3.50 \times 0.24$	0847 0522 1099	2468

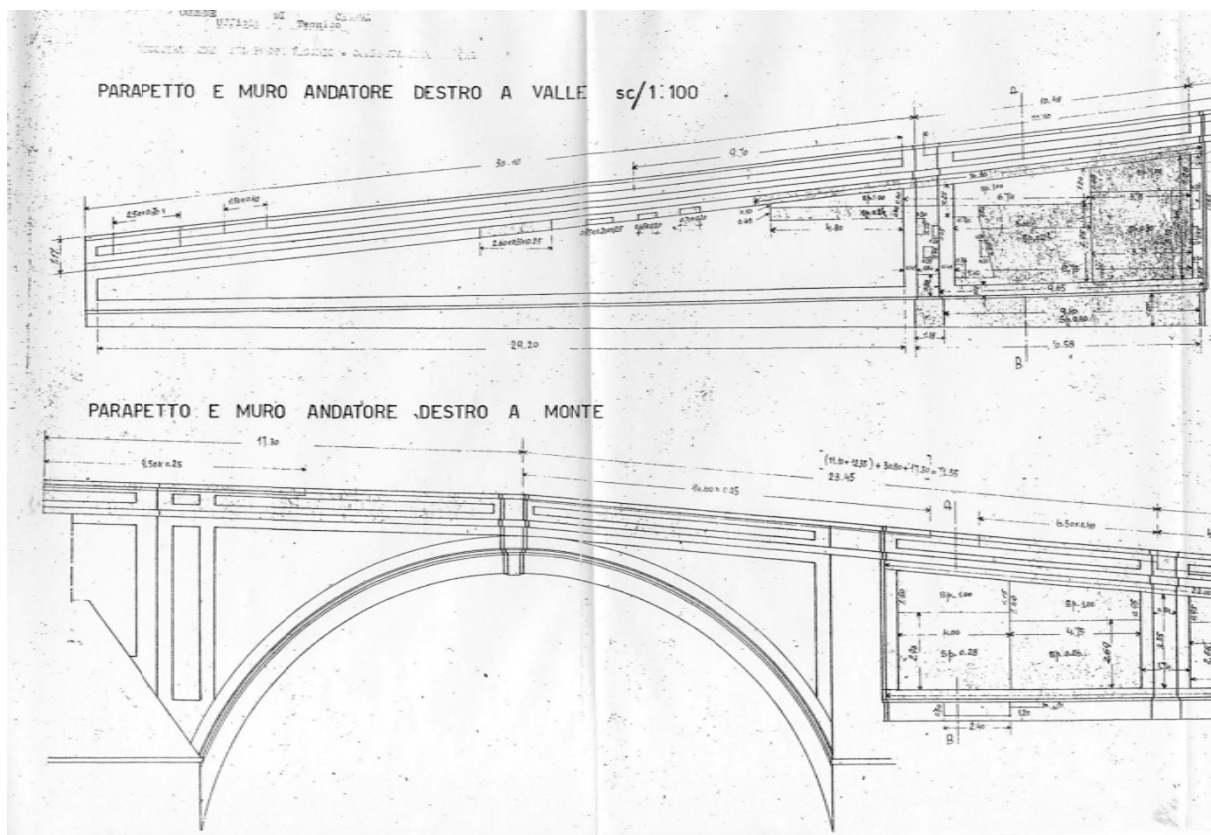
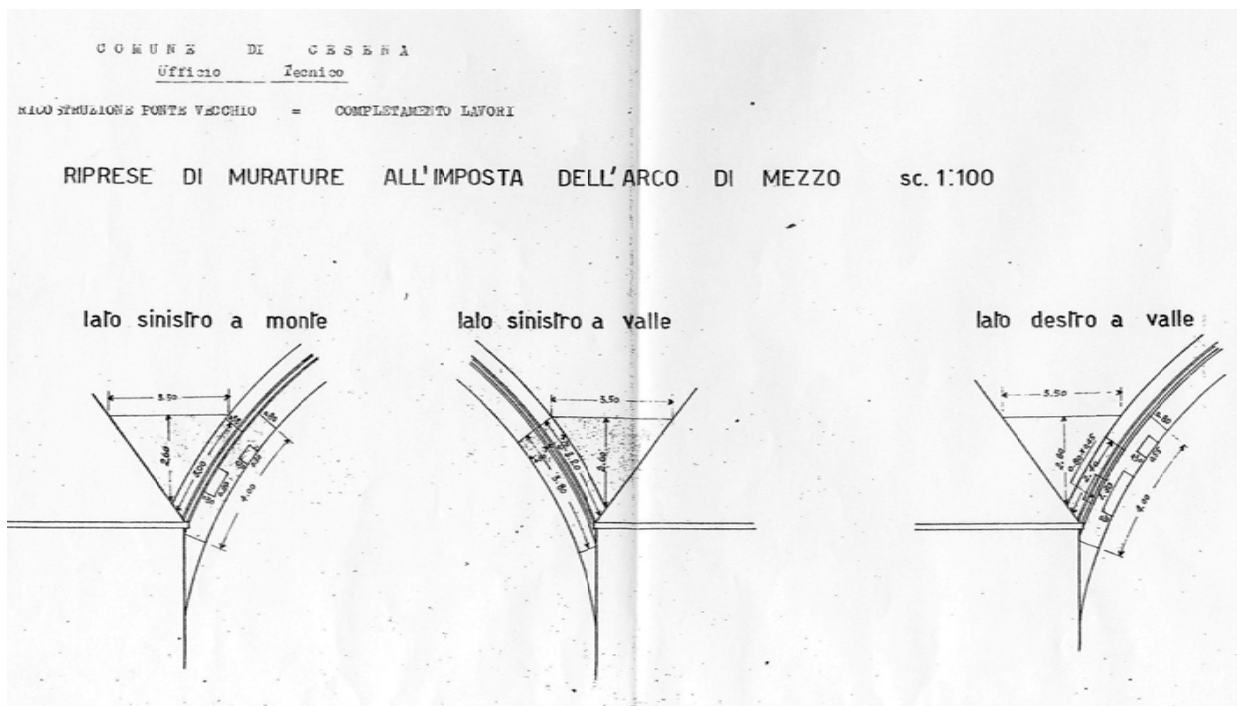
(1) - I fattori si scrivono in colonna, separando con una lineetta trasversale quelli appartenenti a prodotti diversi.

Sed. Com. MURATORI VALLE del SAVO  
CEENA

17

DATA della misura	ARTICOLO dell' Elenco	INDICAZIONE DEI LAVORI E DELLE PROVVISTE	Fattori (1)	Prodotti
1	2	3	4	5
14-12-1946	7	Ricostruzione dell' imposta dell' arco di mezzo a valle (lato destro) <i>a valle</i> $[(4,00 \times 0,80 \times 0,30) - [(1,30 \times 0,30 + 0,55 \times 0,30) \times 0,30]]$ $(2,40 \times 0,58 \times 0,30) - (0,80 \times 0,45 \times 0,30)$ $3,50 \times \frac{2,60}{2} \times 0,25$	0,79 0,309 1,113	2,212
14-12-1946	7	Ricostruzione dell' imposta dell' arco di mezzo a monte (lato destro) <i>a monte.</i> $3,90 \times 0,80 \times 0,30$ $2,70 \times 0,58 \times 0,30$ $3,50 \times \frac{2,60}{2} \times 0,25$	0,936 0,469 1,092	2,497
16-12-1946	8	Ricostruzione muratura alla piamida sovrastante il rostro (Pilone destro a valle) $3,40 \times 1,30 \times 0,30$ $1,05 \times 0,30 \times 0,35$ $\frac{1,40 + 1,20}{2} \times 1,60 \times 0,30$	1,325 0,110 0,576	2,011
17-12-1946	6	Ricostruzione di murature alla piamida sovrastante il rostro. Pilone destro a valle. $2,35 \times \frac{1,70}{2} \times \frac{2,35}{3}$ $3,20 \times \frac{1,80}{2} \times \frac{2,40}{3}$	1,564 2,304	3,868

(1) - I fattori si scrivono in colonna, separando con una lineetta trasversale quelli appartenenti a prodotti diversi.









# MINISTERO DEI LAVORI PUBBLICI

Provveditorato Regionale alle Opere Pubbliche per l'Emilia

UFFICIO DEL GENIO CIVILE DI FORLÌ

## DANNI BELlici

PERIZIA dei lavori occorrenti per il completamento del ponte  
Vecchio sul Savio in Comune di Cesena -

Importo £. 5.720.000 -

## RELAZIONE

Il Ponte Vecchio sul Savio di proprietà del Comune di  
Cesena, fu gravemente danneggiato dagli eventi bellici.

L'Amministrazione Comunale in un primo tempo al fine di  
consentire il transito sul ponte, provvide, a sue spese, alla rico-  
struzione delle arcate e dei parapetti distrutti ed allè sistemazio-  
ne provvisoria del piano stradale con detriti e terra.

Trastrandosi ora di completare i lavori al fine della defi-  
nitiva sistemazione dell'opera, questo Ufficio ha compilato una perizia  
che prevede tutte le opere necessarie per il suo completamento, rima-  
nendo escluse ogni possibilità di lavori complementari eccetto che per  
casi eccezionali e del tutto imprevedibili.

Detti lavori sono:

- la demolizione dei marciapiedi e di murature deteriorate e sconnesse,  
la scarifica del piano stradale, la ricostruzione della muratura dei  
pilastri di testata, delle fognature, del muretto di recinzione, del  
sottofondo stradale, della massicciata, la pavimentazione con emulsio-  
ne bituminosa ed infine la sistemazione delle cornici ed elementi deco-  
rativi in massello di pietra di Trani.

L'importo della perizia è di £. 5.720.000 - di cui lire  
981.000- a disposizione dell'Amministrazione per lavori in economia.

I prezzi applicati sono stati desunti in parte da regolari



analisi ed in parte ragguagliati a quelli correnti sul mercato.

Si dà atto che il Comune di Cesena ha provveduto, ai sensi della legge 29/3/1953 n.230, alla denuncia del danno come risulta da dichiarazione allegata.

I lavori di cui si tratta la presente relazione sono inclusi fra quelli da finanziarsi coi fondi per l'Esercizio finanziario in corso.

18307  
N° \_\_\_\_\_ FORLÌ \_\_\_\_\_

L' INGEGNERE DIRIGENTE

(V. de Luca)



ir.



## **Annex 4.B**

---

On site photos

















## **Annex 4.C**

---

### **Results of laboratory tests on samples taken on site:**

- i) Results of Compression Test on Brick Samples..... p. 137
- ii) Results of Compression Test on Mortar Sample.....p. 138





IMPOSTA DI BOLLO IN CASO D'USO - art.46 - parte II  
D.P.R. 26/10/72 n.642 e successive modificazioni

**PROVINCIA DI BOLOGNA**

VIA ZAMBONI, 13 - 40126 BOLOGNA  
C. F. 80022230371 - P. IVA 03026170377

**LABORATORIO PROV.LE PROVE MATERIALI  
DA COSTRUZIONE (art. 20 Legge 1086/71)**  
Autorizzato con D.M. n. 17490 del 04-04-78

VIA SALICETO, 19 - 40013 CASTEL MAGGIORE  
TEL. 051/712325 - FAX 051/715529  
C/C POSTALE 12613402

**LABORATORIO LATERIZI**

**CERTIFICATO N. 0628/11-01R**

**VERBALE ACC. dal N. 28822 al N. 28822**

**Data emissione : 21/07/2011**

**PROVE DI COMPRESSIONE SU PROVINI DI LATERIZIO**

Intestatario : ARCH. MARIO BONAGURA  
Indirizzo : VIA VICOLO ALTO N.1 - CESENATICO (FC)  
Data richiesta : 18/07/2011 Numero provini : 3

**D A T I D I C H I A R A T I**

Provenienza materiali : PONTE CLEMENTE DI CESENA  
Opera/struttura : PROVE DIAGNOSTICHE PER LA DETERMINAZIONE DELLE  
CARATTERISTICHE MECCANICHE DELLA MURATURA  
Direttore dei Lavori : Richiesta prove non sottoscritta  
Descrizione campioni : Porzioni di mattoni di laterizio pieno ricavati  
da muratura esistente (data prelievo 08/07/2011).

**CERTIFICATO DI PROVA**

n	contrassegno dichiarato	massa g	dimensioni provino mm sez.res. alt.	data prova	resist compr. N/mm <sup>2</sup>
1.1	M1 P.CLEMENTE	264,6	55,0x57,0 56,3	19/07/2011	19,3
1.2	M2 P.CLEMENTE	290,5	57,0x59,5 59,1	19/07/2011	21,4
1.3	M3 P.CLEMENTE	214,2	48,5x48,8 50,2	19/07/2011	34,0

Le prove sono state eseguite secondo D.M. 14/01/2008 e secondo la norma UNI EN 772-1.

Note : DAI CAMPIONI SONO STATI RICAVATI PROVINI DELLE DIMENSIONI SOPRA  
RIPORTATE MEDIANTE TAGLIO. LE FACCE SOTTOPOSTE A CARICO DI PROVA  
SONO STATE RETTIFICATE MEDIANTE SPIANATURA.  
IL CONDIZIONAMENTO E' STATO EFFETTUATO PER ESSICCAZIONE ALL'ARIA.

N.D = non dichiarato

LO SPERIMENTATORE  
Geom. Emanuele Pintori



IL DIRETTORE DEL LABORATORIO  
Dott. Ing. Pietro Luminasi

E' vietata la copia anche parziale del presente certificato  
se non su esplicita autorizzazione del Laboratorio

Pagina 1/2


**PROVINCIA DI BOLOGNA**

 VIA ZAMBONI, 13 - 40126 BOLOGNA  
 C. F. 80022230371 - P. IVA 03026170377

**LABORATORIO PROV. LE PROVE MATERIALI  
 DA COSTRUZIONE (art. 20 Legge 1086/71)**  
 Autorizzato con D.M. n. 17490 del 04-04-78

 VIA SALICETO, 19 - 40013 CASTEL MAGGIORE  
 TEL. 051/712325 - FAX 051/715529  
 C/C POSTALE 12613402

**LABORATORIO LEGANTI IDRAULICI**
**CERTIFICATO N. 0628/11-01D**
**VERBALE ACC. dal N. 28822 al N. 28822**
**Data emissione : 21/07/2011**
**PROVE DI COMPRESSIONE SU PROVINI DI LATERIZIO**

 Intestatario : ARCH. MARIO BONAGURA  
 Indirizzo : VIA VICOLO ALTO N.1 - CESENATICO (FC)  
 Data richiesta : 18/07/2011 Numero provini : 2

**D A T I D I C H I A R A T I**

 Provenienza materiali : PONTE CLEMENTE DI CESENA  
 Opera/struttura : PROVE DIAGNOSTICHE PER LA DETERMINAZIONE DELLE  
 CARATTERISTICHE MECCANICHE DELLA MURATURA  
 Direttore dei Lavori : Richiesta prove non sottoscritta  
 Descrizione campioni : Fogli di malta ricavati da muratura esistente  
 (data prelievo 08/07/2011).

**CERTIFICATO DI PROVA**

n	contrassegno dichiarato	massa g	dimensioni provino mm sez.res/alt	sezione resist. mmq	massa volum. kg/mc	data confezion.	data prova	gg di mat	resist punz. N/mmq	res. media N/mmq
2.1	Mal P.CLEMENTE	41,5	20(*) 9,9	314	---	----	19/07/2011	---	10,20	---
2.2	Ma2 P.CLEMENTE	39,1	20(*) 14,9	314	---	----	19/07/2011	---	6,30	---

Le prove sono state eseguite secondo il metodo J.Henzel-S.Karl, Darmstadt Concrete, 1987, Vol.2, pp.123-136.

 Note : (\*) NON E' STATO POSSIBILE RICAVARE UN PROVINO DI SEZ.50x50 mm IN  
 QUANTO IL PROVINO SI SPEZZAVA IN MANIERA IRREGOLARE ALL'ATTO DEL TAGLIO;  
 E' QUINDI STATA ESEGUITA LA PROVA SUL PROVINO DETERMINANDO LA RESISTENZA  
 A PUNZONAMENTO COME RAPPORTO TRA IL CARICO DI ROTTURA E LA SEZIONE  
 RESISTENTE DI mmq 314 (SEZIONE DEL PUNZONE).

 Stagionatura campioni in laboratorio: temp. amb. 20±2 gradi C, umid. relat. 50%  
 N.D = non dichiarato

 LO SPERIMENTATORE  
 Geom. Emanuele Pintori



 IL DIRETTORE DEL LABORATORIO  
 Dott. Ing. Pietro Luminasi

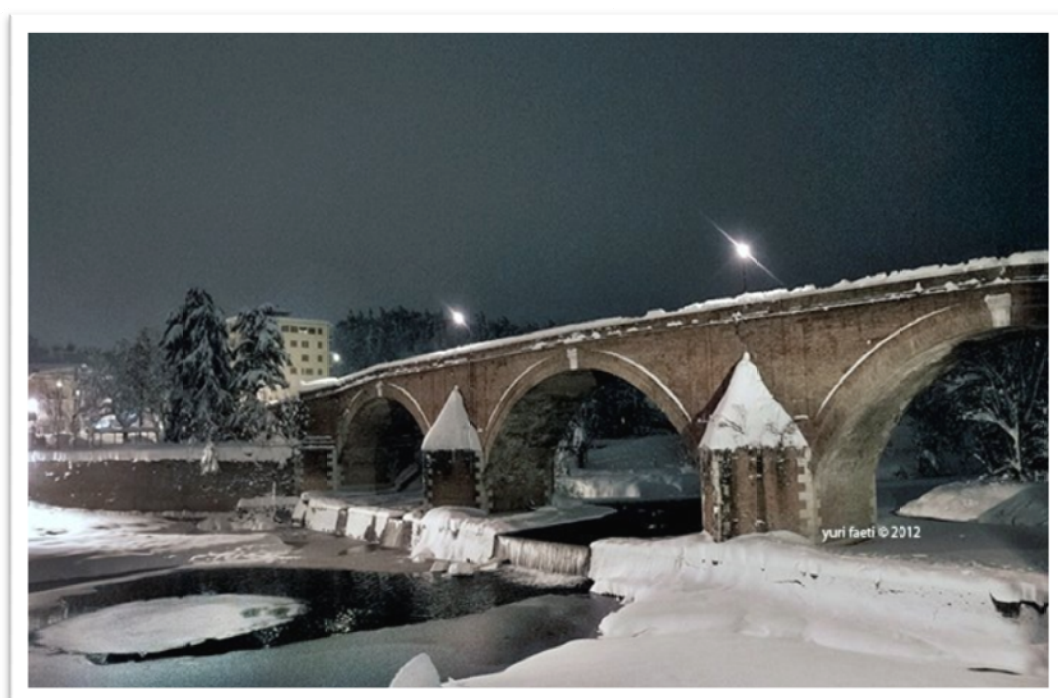


 E' vietata la copia anche parziale del presente certificato  
 se non su esplicita autorizzazione del Laboratorio

Pagina 2/2

## Conclusions

---





## CONCLUSIONS

Nowadays existing masonry arch bridges are very important to study because they represent a very significant part of National road and rail network, both in terms of numerical quantity and for the quality of their structural response. In fact the masonry arch bridges continue to be used today without any evident change to their original shape, even if the majority of them was built between 17th and 19th century. This is possible thanks to the high self-weight together with masonry mechanical characteristics, that allow these bridges to have a relevant strength regarding the loads which they are subjected. Maybe this is one of the most important aspects of the masonry arch bridges, that permits these ancient structures to keep in good health nowadays. However it can't be forgotten that weight, speed and traffic are increased during the last 100 years and these new elements will eventually lead to the deterioration of the bridge's structure. This is the reason why is important check the existing masonry bridges. Several strategies have been developed during the time to simulate the response of this type of structures, although even today there is no generally accepted standard one for assessment of masonry arch bridges.

In this thesis, the principal analytical and numerical methods existing in literature have been compared with each other. The methods taken in exam are mainly three: i) the Thrust Line Analysis Method; ii) the Mechanism Method; iii) the Finite Element Methods. As explained in chapter two, the Thrust Line Analysis Method and the Mechanism Method are analytical methods and are derived from two of the fundamental theorems of the Plastic Analysis, while the Finite Element Method is a numerical method, that uses different strategies of discretization to analyze the structure. Every method is applied to the case study through computer-based representations, that allow a friendly-use application of the principles explained: i) Archie-M; ii) Ring; iii) Abaqus. A particular closed-form approach based on an elasto-plastic material model is also studied.

To compare the three methods, two different case study have been presented: i) a generic masonry arch bridge with a single span; ii) a real masonry arch bridge, built on Savio River in Cesena. All the models presented are two-dimensional in order to have results comparable between the different methods taken in exam. In fact finite element models can be two-dimensional or three-dimensional, while the other methods allow to study only two dimensional models. This is the same for the analytical approach based on the elasto-plastic model.

In the case of the generic masonry arch bridge, there are applied all the methods presented. Concerning the hinge positions, Ring, Archie-M and the elasto-plastic model have shown similar results. Small differences are found near the point of application of concentrated load and near the right support, probably due to the different live load distributions. Concerning the finite element model, there is a good correspondence with the other models for the first hinge and the fourth hinge, while the positions of the other hinges are different. The differences can be explained, thinking to the different conceptual bases: Archie-M, Ring and the Elasto-Plastic model derive from the principles of limit state analysis, while the Finite Element Model comes from a completely different approach. However the results indicate that the a priori assumption regarding the occurrence of two hinges in the two support points which is frequently made is approximately true.

Concerning the collapse load, elasto-plastic model and Archie-M have shown a comparable behavior. The Ring collapse load is significantly higher than the others because the rigid-plastic model neglects the elasticity of the masonry, that is a very important factor when the thickness of the arch is big as in the bridge in exam. The differences in the collapse load can be summarized as follows: Elasto-Plastic collapse load  $\leq$  Archie-M collapse load  $\leq$  Finite Element collapse load  $\leq$  Ring collapse load.

The other case study taken in exam has been the Clemente Bridge, built over the River Savio at Cesena. Material samples have been taken from the bridge to estimate the masonry compressive strength. Besides, three different hypotheses regards to the vault thickness have been formulated in absence of reliable data. In this case, Ring e Archie-M have reproduced almost the same mode of collapse. In both cases, the critical position of the load is identified on the first span. Obviously as the structure is symmetrical, there is a mirror-like collapse condition also on the third span. The collapse load of Archie-M is resulted slightly smaller than Ring's one. Concerning the hinge location, there are small differences between Ring and Archie-M because the critical position of the live load is close to the supports. As there are no certainties on the constructive modes and the arch thickness is very high, with Ring it is also supposed that every vault may be made by two multi-ring arches superimposed: obviously, in this hypothesis the load is resulted the lowest of all the others. Future developments will regard the application of the finite element model and the elasto-plastic model also to the case of the Clemente Bridge.

In general, it can be concluded that every method and every its computational application has own advantages and disadvantages, depending on the input, on the purpose and on the researched results. The Thrust Line Analysis Method is the most ancient method and allows to



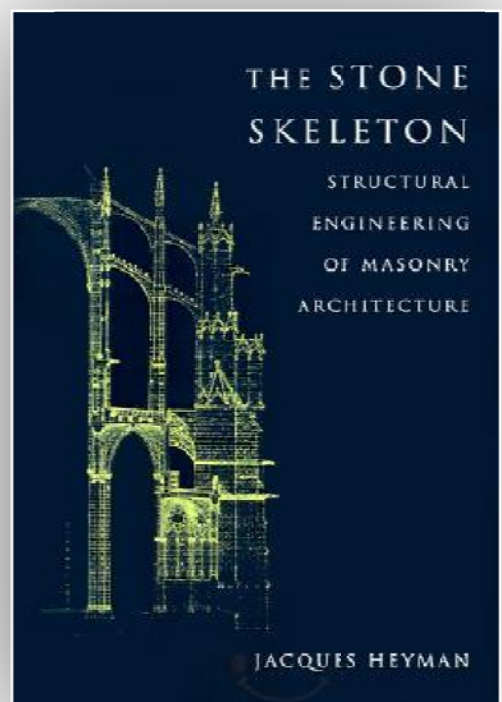
draw immediately the thrust line to test the arch safety, even if it doesn't give directly the critical load factor. Different attempts have to be made in order to achieve the correct result. The Mechanism Method allows to determine easily the collapse load factor. However, the rigid-plastic model neglects the elasticity of the masonry and that leads to overestimate the collapse load in the case of arches with a very big thickness. The Finite Element Method represents even now the most versatile tool for the numerical analysis of structural problems. However, it requires an elevate number of material characteristics, that are not always easy to determine in the historical constructions. In the case of masonry, the peculiar nature of material leads to pay particular attention to the application of this method. The analyses carried out have highlined that perhaps micro-modeling can be more appropriate than macro-modeling, even if the second one requires a lower computational effort. Finally, the elastic-plastic model gives a realistic view of the arch behavior, providing the hinge evolutions. At the same time, it provides a collapse load lower than the other methods.

All the two-dimensional models presented have the advantage to be easily constructible and analyzable, but generally focus on the arc behavior and don't quantify the stress in the section. To have a more detailed assessment of local phenomena, it is therefore important also to use three-dimensional models.



## References

---





- A.A.V.V. (2005)**, *Proceedings of the 4th International Seminar on Structural Analysis of Historical Constructions*, 10-13 November 2004, Padova-Italy, edited by Balkema Publishers, Leiden, The Netherlands, pp. 1323-1333
- Audenaert A. (2004)**, *Elasto-plastisch model ter bepaling van de statische bezwijklast van bogen in metselwerk*, PhD Thesis, Vrije University, Brussel
- Audenaert A., Peremans H. and De Wilde W.P. (2004)**, *Static determination of the internal forces and displacement in arch bridges*, The masonry society Journal, 22 (1), pp. 97-109
- Audenaert A., Peremans H., Reniers G. (2007)**, *An analytical model to determine the ultimate load on masonry arch bridges*, J Eng Math (2007)
- Benvenuto E. (1981)**, *La scienza delle costruzioni e il suo sviluppo storico*, Sansoni, Firenze
- Block P. (2005)**, *Equilibrium systems. Studies in Masonry Structure, Thesis of master of Science in Architecture Studies*, MIT, Boston
- Block P., Ciblac, T. and Ochsendorf, J. (2006)**, *Real-time limit analysis of vaulted masonry buildings*, Computers & Structures, 84 (29-30), p. 1841-1852.
- Boothby T. E. and B. J. Roberts (2001)**, *Transverse behavior of masonry arch bridges*, The Structure Engineer Volume 79(9): 21-26.
- Brasile S. , Casciaro R. , Formica G. (2007)**, *Multilevel approach for brick masonry walls*, Computer methods in applied mechanics and engineering, Vol. 196
- Brencich A., De Francesco U. (2004b)**, *Assessment of Multi-Span Masonry Arch Bridges. Part II: Examples and Applications*, J. of Bridge Eng.ng, ASCE, 9, pp.591-598.
- Bresse M. (1859)**, *Cours de Mècanique Appliquèe*, Paris, Imprimerie de Gauthier-Villar, 1859
- Breymann G.A. (1849)**, *Allgemeine Bau-Constructions-Lehre. I. Constructionen in Stein*, Hoffmann'sche Verlagsbuchhandlung, Stuttgart, 1849
- Cantori C. (2010)**, *Alla ricerca delle pietre perdute : il restauro delle parti lapidee del ponte Clemente di Cesena*, Il Ponte Vecchio, Cesena
- Chen W. F. (1985)**, *Constitutive Relations for Concrete, Rock and Soils: Discussor's Report*. Mechanics of Geomaterials. Z. Bazant, John Wiley & Sons Ltd.: 65-73

**Chen, W. F. a. E. M. (1990)**, *Non-linear Analysis in Soil Mechanics - Theory and Implementation*, The Netherlands, Elsevier Science Publishers B.V.

**Coulomb C. A (1773)**, *Essai sur une application des règles de maximis et minimis à quelques problèmes de statique, relatifs à l'architecture*, "Mémoires de mathématique & de physique, présentés à l'Académie Royale des Sciences par divers savans", vol. 7, pp. 343-382

**D'Altri Darderi S. (1996)**, *Il Ponte Vecchio di Cesena: le vicende costruttive del ponte Clemente : un caso emblematico del rapporto tra teoria e prassi*, Il Ponte Vecchio, Cesena

**De La Hire P. (1730)**, *Traité de Mécanique*, Acts of Académie des Sciences, Paris

**Drucker D. C. and Prager, W. (1952)**, *Soil mechanics and plastic analysis for limit design*, Quarterly of Applied Mathematics, vol. 10, no. 2, pp. 157–165

**Drucker D. C. (1953)**, *Limit analysis of cylindrical shells under axially-symmetric loading*, Proc. 1st Midwest Conf. Sol. Mech., I11

**Fanning P. J., and Boothby T. E. (2001)**, *Three-dimensional modeling and full-scale testing of stone arch bridges*, Computer and Structures, 79, 2645–2662

**Ford T.E., Augarde C.E., Tuxford S.S. (2003)**, *Modelling masonry arch bridges using commercial finite element software*. 9th International Conference on Civil and Structural Engineering Computing, Egmond aan Zee, The Netherlands.

**Gerstner F.J. von (1831-1834)**, *Handbuch der Mechanik*, J. Spurny, Prague

**Gilbert M. (1998)**, *On the analysis of multi-ring brickwork arch bridges*. Proceedings 2<sup>nd</sup> International Arch Bridges Conference, Venice, pp. 109-118.

**Gilbert M. (2001)**, RING home page, <http://www.shef.ac.uk/ring>

**Gilbert M. (2007)**. *Limit Analysis Applied to Masonry Arch Bridges: State of the art and Recent Developments*. Paper presented at the ARCH'07 - 5th International Conference on Arch Bridges.

**Gregory D. (1698)**, *Catenaria*,. *Philosophical Transactions of the Royal Society*, vol. 19, pp. 637-652

- Harvey W. J. (1988)**, *Application of the mechanism analysis to masonry arches*, The Structural Engineer, 77 - 84.
- Hendry A.W., Davies S.R. and Royles R. (1985)**, *Test on a Stone, Masonry Arch at Bridgemill-Girvan*, Transport and Road Research Lab, Contractor Report 7, UK
- Heyman J. (1966)**, *The stone skeleton. Structural Engineering of Masonry Architecture*, University of Cambridge, Cambridge
- Heyman J. (1980)**, *The estimation of the strength of masonry arches*, Proceedings ICE
- Heyman J. (1981)**, *The masonry arch*, Ellis Horwood
- Horne M.R. (1979)**, *Plastic theory of structures*, 2nd edition, Oxford: Pergamon Press
- Hooke, R. (1675)**, *A Description of Helioscopes, and Some Other Instruments*, John & Martin Printer to the Royal Society, London, 1675
- Huerta S. (2005)**, *The use of simple models in the teaching of the essentials of masonry arch behaviour, Theory and practice of constructions: knowledge, means and models. Didactic and research experiences*, Fondazione Flaminia, Ravenna, pp.747-771, 2005
- Italian Technical Standards** promulgated with Ministerial Decree of 14 January 2008 (NTC 2008)
- Kooharian A. (1953)**, *Limit analysis of voussoir (segmental) and concrete arches*, Proc. Am. Concr. Inst., Vol. 49
- Livesley R.K. (1978)**, *Limit analysis of structures formed from rigid blocks*, International Journal for Numerical Method in Engineering, 12, pp. 1853-1871.
- Livesley R.K. (1992)**, *A computational model for the limit analysis of three-dimensional masonry structures*, Meccanica 27, pp. 161–172
- Lourenco P. B. (1996)**, *Computational Strategies for Masonry Structures*, PhD thesis, Delft University of Technology
- Moseley H. (1833)**, *On a new principle in statics, called the Principle of least pressure*, The London and Edinburgh Philosophical Magazine and Journal of Science, vol. 3, pp. 285-288

**Navier C.L. (1826)**, *Résumé des Leçons données à L'École des Ponts et Chaussées, sur l'application de la mécanique à l'établissement des constructions et des machines*, Paris.

**Ng K., Fairfield C., Sibbad A. (1999)**, *Finite-element analysis of masonry arch bridges*, Proceedings of the Institution of Civil Engineers: Structures and Buildings, Vol. 134, pp. 119-127

**Nobile L., Gentilini C., Bartolomeo V., Bonagura M. (2010)**, *Destructive Tests for the Determination of Masonry Performance*, in Key Engineering Materials Vols. 417-418, Trans Tech Publications, Switzerland, pp. 753-756;

**Nobile L., Gentilini C., Bartolomeo V., Bonagura M. (2010)**, *Micro-Destructive Flat-Jack Test for the Diagnosis of Historic Masonry*, in Key Engineering Materials Vols. 417-418, Trans Tech Publications, Switzerland, pp. 741-744.

**Nobile L., Bartolomeo V., Bonagura M., Gentilini C. (2010)**, *Cracks are not dangerous in masonry arches*, Proceedings of 12th International Congress on Mesomechanics, Taipei, Taiwan

**Nobile L., Bartolomeo V., Bonagura M. (2011)**, *Structural Analysis of Historical Masonry Arches Bridges: Case Study of Clemente Bridge on Savio River*, Proceedings of 10th International Conference on Fracture and Damage Mechanics, Dubrovnik, Croazia

**Ochsendorf J.A., Hernando J.I., Huerta S. (2004)**, *Collapse of Masonry Buttresses*, Journal of Architectural Engineering, Vol. 10, pp. 88-97

**Ochsendorf J.A., De Lorenzis L. (2008)**, *Failure of rectangular masonry buttresses under concentrated loading*, Structure & Buildings, Vol. 161 (2008)

**Onat E.T. and Prager W. (1953)**, *Limit Analysis of Arches*, Journal of Mechanics and Physics of Solids, Volume 1

**Persy N. (1825)**, *Cours sur la stabilité des constructions, à l'usage des élèves de l'école royale de l'Artillerie et du Génie*, Lithographie de l'École Royale de l'Artillerie et du Génie, Metz

**Pippard A.J.S., Ashby R.J. (1939)**, *An experimental study of the voussoir arch*, Inst.n Civ. Eng., 10



**Pippard A.J.S. (1948)**, *The approximate estimation of safe loads on masonry bridges*, Civil engineer in war, 1, 365, Inst.n Civ. Eng.rs.

**Rankine W. J. M. (1858)**, *A Manual of Applied Mechanics*, Charles Griffin, London

**Timoshenko S. P. (1953)**, *History of Strength of Materials*, New York, McGraw-Hill Book Co.

**UNI EN 1996-1-1**: *Eurocode 6. Design of masonry structures. General rules for reinforced and unreinforced masonry structures*

**Young T. (1817)**, *Supplement to the fourth edition of the Encyclopaedia Britannica*

**William K. J., Warnke E. D. (1975)**, *Constitutive Model for the Triaxial Behavior of Concrete*, Proceedings, International Association for Bridge and Structural Engineering, ISMES. Bergamo, Italy, ISMES. Vol. 19: 174.

**Winkler E. (1867)**, *Die Lehre von der Elastizitat und Festigkeit*, Dominicus, Prague